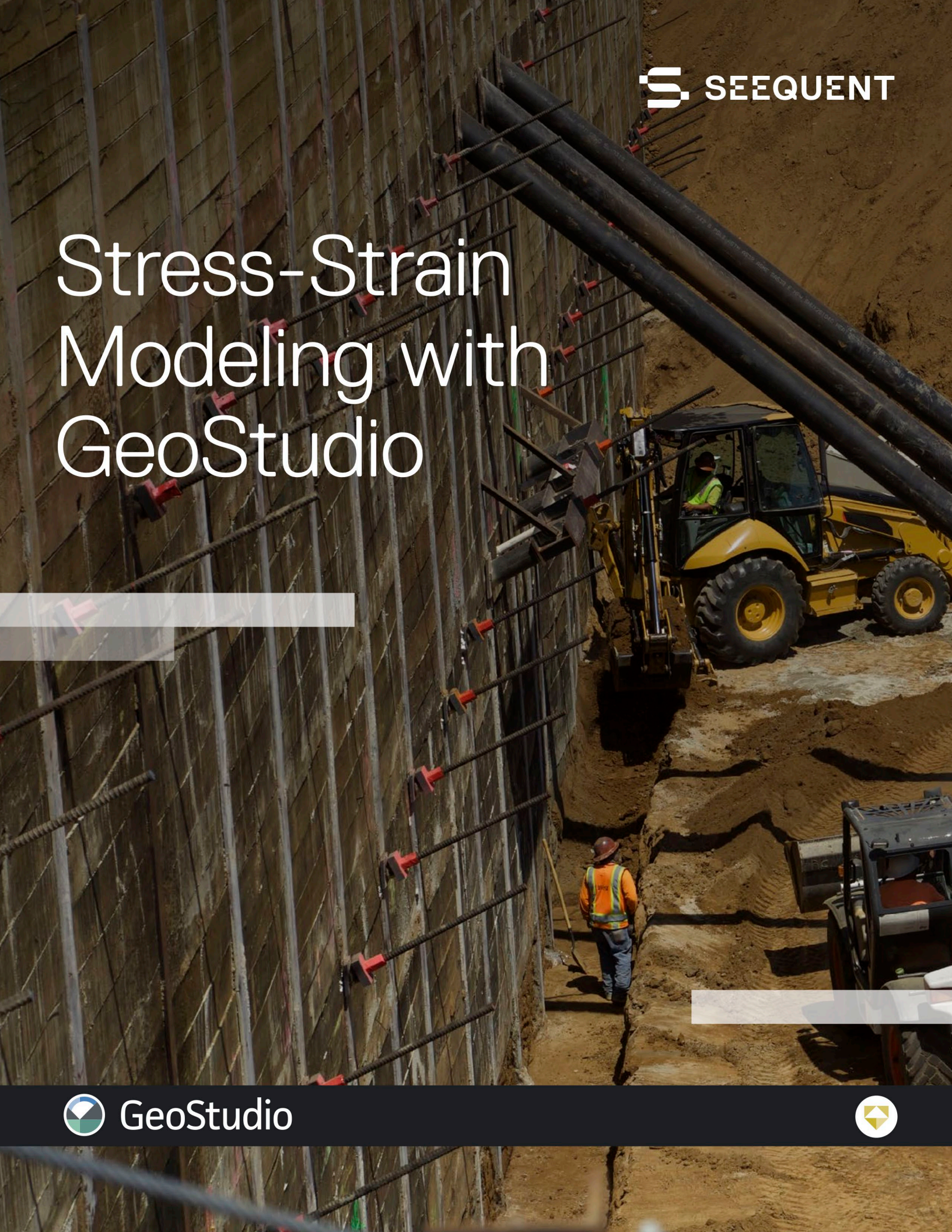

SEEQUENT

Stress-Strain Modeling with GeoStudio

GeoStudio

Email: sales@geoslope.com

Contents

Symbols

$\boldsymbol{\beta}$ Compressibility, /kPa
of the soil structure $\boldsymbol{\beta}$
of the solid soil particles $\boldsymbol{\beta_s}$

$\boldsymbol{\beta_w}$ Isothermal compressibility of water, 4.8×10^{-10} /kPa at 10 °C

$\boldsymbol{\gamma}$ Engineering shear strain
engineering shear strains γ_{xy}, γ_{yz}, γ_{zx}

$\boldsymbol{\delta}$ Small increment

$\boldsymbol{\varepsilon}$ Strain
axial strain ε_a
horizontal strain ε_h
vertical strain ε_v
volumetric strain ε_p
deviatoric strain ε_q
normal strains ε_{xx}, ε_{yy}, ε_{zz}
Cartesian shear strains ε_{xy}, ε_{yz}, ε_{zx}
principal strains ε_1, ε_2, ε_3

$\boldsymbol{\eta}$ Stress ratio $= q/p'$

$\boldsymbol{\theta}$ Volumetric content, m^3/m^3
water content, θ_w
saturated water content, θ_{sat}
residual water content, θ_{res}
air content, θ_a
ice content, θ_{ice}

$\boldsymbol{\kappa}$ Slope of the unloading-reloading line in $V - \ln p'$ plane

$\boldsymbol{\lambda}$ Slope of the normal compression line in $V - \ln p'$ plane

$\boldsymbol{\Lambda}$ Scalar multiplier

$\boldsymbol{\nu'}$ Poisson's ratio in terms of effective stress

$\boldsymbol{\rho}$ Mass density, g/ m^3
soil dry bulk density, ρ_d
of air, ρ_a
of water, ρ_w
of solids particles, ρ_s
of snow, ρ_{snow}
of ice, ρ_{ice}

$\boldsymbol{\sigma'}$ Effective stress, N/m^2
axial effective stress σ'_a
horizontal effective stress σ'_h
vertical effective stress σ'_v
volumetric effective stress σ'_p
deviatoric effective stress σ'_q
normal effective stresses σ'_{xx}, σ'_{yy}, σ'
shear stresses σ'_{xy}, σ'_{yz}, σ'_{zx}
principal effective stress σ'_1, σ'_2, σ'_3

$\boldsymbol{\sigma}$ Total stress, N/m^2

$\boldsymbol{\tau}$ Shear stress, N/m^2

$\boldsymbol{\phi'}$ Effective angle of shear resistance

$\boldsymbol{\psi}$ Angle of dilation

$\boldsymbol{c'}$ Effective cohesion, N/m^2

$\boldsymbol{C_c}$ Compression index

$\boldsymbol{C_s}$ Swelling index

$\boldsymbol{e}$ Void ratio

$\boldsymbol{E'}$ Effective stress elastic modulus

$\boldsymbol{E'^{ref}_{ur}}$ Reference unloading-reloading stiffness, N/m^2

$\boldsymbol{E'^{ref}_{oed}}$ Reference tangent stiffness

$\boldsymbol{G}$ Shear modulus

$\boldsymbol{K'}$ Effective stress bulk modulus, N/m^2

$\boldsymbol{K}$ Hydraulic conductivity, m/s
of isothermal liquid water, K_w
of a fluid, K_f
of dry air, K_a
of an unfrozen soil, K_u
of a frozen soil, K_f
of a partially frozen soil, K_{pf}
of a saturated soil, K_{sat}
of a dry soil, K_{dry}
of soil at a given water content, K'
in the x direction, K_x
in the y direction, K_y

$\boldsymbol{K'_y/K'_x}$ Hydraulic conductivity anisotropy ratio

$\boldsymbol{K_0}$ Earth pressure coefficient at rest

$\boldsymbol{K_a}$ Earth pressure coefficient for the active condition

$\boldsymbol{K_p}$ Earth pressure coefficient for the passive condition

$\boldsymbol{K_0^{nc}}$ Earth pressure coefficeint for normally compressed soil

$\boldsymbol{K_0^{oc}}$ Earth pressure coefficeint for overconsolidated soil

$\boldsymbol{K^{(m)}}$ Element characteristic matrix for FEM

$\boldsymbol{m_v}$ coefficient of volume compressibility, m^2/N

$\boldsymbol{M}$ Slope of the critical state line the $p' - q$ stress plane

$\boldsymbol{M^{(m)}}$ FEM element mass matrix

$\boldsymbol{p'}$ Mean effective stress, N/m^2

$\boldsymbol{p^{ref}}$ Reference confining stress, N/m^2

$\boldsymbol{q}$ Deviator stress, N/m^2

$\boldsymbol{q}$ Volumetric flux, $m^3/s/m^2$
of air, q_a
of liquid water, q_w

$\boldsymbol{S}$	Degree of saturation
$\boldsymbol{t}$	Time, s
$\boldsymbol{U^{(m)}}$	FEM matrix of nodal unknowns
$\boldsymbol{u}$	Primary variable anywhere within a finite element at nodal points, u_i
$\boldsymbol{u_w}$	Pore-water pressure, N/m^2
$\boldsymbol{V}$	Specific volume

Preface

GeoStudio is an integrated, multi-physics, multi-dimensional, platform of numerical analysis tools for geo-engineers and earth scientists. The multi-disciplinary nature of GeoStudio is reflected in its range of products: four finite element flow products (heat and mass transfer); two finite element stress-strain products; and a slope stability product that employs limit equilibrium and stress-based strategies for calculating margins of safety. The focus of this book is on the stress-strain products.

Countless textbooks provide a thorough treatment of the finite element method and its implementation, both in a general and subject-specific manner. Similarly, there are numerous comprehensive presentations of the mechanics of soils, both from a classical and critical state perspective. Journal articles and conference papers abound on specific aspects of soil stress-strain behaviour, formulation and implementation of constitutive models, and numerical strategies for coping with material non-linearity.

It follows, then, that the idea of writing a book on static stress-strain finite element modelling with GeoStudio is not only daunting, but also rather presumptuous, given the breadth of material already available to the reader. Nonetheless, we feel that a review of the foundational principles associated with both the physics and the numerical approaches used by GeoStudio will have value to the reader and will assist in the effective use of the models.

It is important to note that the purpose of this 'book' is not to provide detailed instructions for operating the software. The primary vehicle for that information is the learning section for GeoStudio on the Seequent website (www.seequent.com), where the user can access example files, tutorial movies, technical webinars and our online learning platform. In addition, help topics are available during operation of the software in the Help menu (accessed by pressing F1). These resources provide valuable information for those learning how to use GeoStudio.

The first two sections of this book include a general overview of GeoStudio and the finite element method as applied to static stress-strain problems. Sections 3 provides a summary of the underlying theory describing the stress-strain behavior of soils. Section 4 then outlines the various types of analyses that can be undertaken using GeoStudio. The formulations utilized within GeoStudio to describe specific material models is then summarized within Section 5. Similarly, Section 6 summarizes the formulation used within GeoStudio to incorporate various forms of structural elements. The final section provides a brief description of how boundary conditions applied to the finite model can be utilized to define external applied loading or deflections. A comprehensive reference list is provided to enable readers to develop a deeper understanding of a particular topics by exploring the archival literature. The appendices provide more detailed descriptions of several formulations described in a more general way within the body of the text.

1 GeoStudio Overview

GeoStudio comprises several products (Table 1). The first four products listed in Table 1 simulate the flow of energy or mass while the following three products are used to simulate a wide range of soil mechanical behavior. Integration of many of the products within GeoStudio provides a single platform for analyzing a wide range of geotechnical and geoscience problems.

Table 1. Summary of GeoStudio applications.

Product	Simulation Objective
TEMP/W & TEMP3D	Heat (thermal energy) transfer through porous media
SEEP/W & SEEP3D	Water (Liquid water and vapor) transfer through saturated and unsaturated porous media
CTRAN/W &CTRAN3D	Solute or gas transfer by advection and diffusion
AIR/W & AIR3D	Air transfer in response to pressure gradients
SIGMA/W	Static stress-strain response and stability of geotechnical structures
QUAKE/W	Dynamic stress-strain response of geotechnical structures
SLOPE/W & SLOPE3D	Static or pseudo-dynamic slope stability using limit equilibrium or stress-based methods

Many physical processes are coupled; that is, a change in the state variable governing one process alters the state variable governing another. For example, time-dependent deformation of a soil in response to an applied load represents a two-way, coupled process. During consolidation, the rate of water flow controls the dissipation of excess pore-water pressures and causes deformation, while the generation of excess pore-water pressures is linked to the resistance of the soil skeleton to deformation. Thus, the water transfer and equilibrium equations must be solved in a coupled manner using the SIGMA/W coupled consolidation formulation.

Water and air flow through porous media provides another example of a coupled process. The flow of water and air flow depend on their respective fluid pressures while the storage of water and air depend on the differential pressure between these two phases. A similar coupling occurs during the simulation of density dependent water flow. The simulation of heat (TEMP/W) or mass transport (CTRAN/W) can utilize water flows generated in a seepage analysis (SEEP/W); however, the water flow, in turn, can be affected by variations in water density created by the distribution of heat or mass within the domain. The same type of coupling also occurs in a density-dependent air flow analysis (i.e., AIR/W and

TEMP/W). Table 2 summarizes some of the processes that can be coupled in GeoStudio. Additional coupling can also be simulated using the Add-in functionality within GeoStudio. One example of this includes the use of oxygen transport and consumption within a waste rock dump (CTRAN/W) to create heating (TEMP/W), which then results in air flow (AIR/W) that drives oxygen transport (CTRAN/W).

A single GeoStudio Project file (*.GSZ) can contain multiple geometries and multiple analyses. Each analysis may contain a single set of physics (i.e., one product) or may integrate more than one set of physics (i.e., multiple products) with various levels of dependency (i.e., coupled or uncoupled analyses). For certain scenarios involving one-way coupling, it is often convenient to simulate the independent process in a separate analysis and direct the subsequent dependent analysis to the results from the independent analysis. For example, a CTRAN/W analysis could refer to water contents and water flow rates from an independent SEEP/W analysis. This simple method of product integration is the same functionality that allows a SLOPE/W or SIGMA/W analysis, for example, to obtain pore-water pressure information from a SEEP/W analysis. However, for two-way coupling, the coupled sets of physics must be contained within a single analysis.

Table 2. Summary of the coupled formulations.

Product	Coupled Processes
SEEP/W AIR/W	Coupled water and air transfer for modelling the effect of air pressure changes on water transfer and vice versa
SEEP/W TEMP/W	Forced convection of heat with water and/or vapor transfer, free convection of liquid water caused by thermally-induced density variations, and thermally-driven vapor transfer
AIR/W TEMP/W	Forced convection of heat with air transfer and free convection of air caused by thermally-induced density variations
CTRAN/W SEEP/W	Advection of dissolved solutes with water transfer and free convection of liquid water caused by density variations due to dissolved solutes
CTRAN/W AIR/W	Advection of gaseous solutes with air transfer and free convection of air caused by density variations due to differential gas pressures
SIGMA/W	Coupled water transfer and stress-strain behavior to simulate the transient pore-water pressure and deformation response (i.e. consolidation) due to loading and/or unloading and/or changes in hydraulic conditions.

The various analyses within a project file are organized in an Analysis Tree, as illustrated in many of the example files. The Analysis Tree provides a visual structure of the analyses and identifies the 'Parent-Child' relationships. For example, a CTRAN/W analysis might be the child of a SEEP/W analysis and,

consequently, the integration and dependency relationships are visible in the parent-child Analysis Tree structure. The Analysis Tree also encourages the user to adopt a workflow pattern that is consistent with the modelling methodology advocated for GeoStudio (Appendix II).

The heat and mass transfer products support one-dimensional, two-dimensional, three-dimensional, plan view, and axisymmetric analysis. The formulation and finite element procedures are the same regardless of dimensionality. The selected dimensionality is incorporated during assembly of the element characteristic matrices and mass matrices (Appendix I.4). Assembly of these matrices involves numerical integration over the volume of the element, which requires the area and out-of-plane thickness for elements that are not three-dimensional. For a conventional two-dimensional analysis, the element thickness defaults to a unit length (1.0). The element thickness and width for a one-dimensional analysis are implicitly one unit length. A cylindrical coordinate system is adopted for axisymmetric analyses, with the conventional x axis representing a radial dimension, r. The thickness of the domain at any point in space is the arc length, which is calculated from the specified central angle and radius r. The element thickness for a plan view analysis is the vertical distance between the upper and lower surfaces.

2 Finite Element Approach to Stress-Strain Analyses

In geotechnical engineering, there are fundamentally two design requirements that must be satisfied: the serviceability limit state (SLS) and the ultimate limit state (ULS). The primary focus of SLS is the levels of deformation (and accompanying stress) within the soil and any associated structures interacting with the soil. The primary focus of ULS is the overall stability of the system. A classic method such as limit equilibrium can address issues related to overall stability, but provides little insight into the actual stresses/strains within the system. In contrast, a rigorous numerical analysis of a soil-structure interaction problem can be used to address both the ULS (e.g. limiting stresses/strains at failure) and the SLS (e.g. stress/strains during safe operation) design requirements.

The finite element method (FEM) is a numerical approach to solving partial differential equations (PDEs) that describe the distribution of a variable (e.g. strain or pressure) across space and/or time as a function of specified material properties. The PDE are generally derived from fundamental considerations of conservation of mass or energy applied to a representative elementary volume (REV) which represents a finite volume of the physical domain for which unique material properties can be described. Mathematical solutions to these PDEs can be found for relatively simple geometries and material properties by finding an analytical solution to the PDE from which the value of the variable can be calculated as a function of space and/or time, subject to specified boundary conditions.

Analytical solutions are not obtainable for more complex domains (e.g. geometry) or material properties. In these cases a numerical solution is developed based on the principle of discretization in which the domain is subdivided into a number of 'finite elements' which have a defined geometry and material properties. The general 'shape' of the distribution of the dependent variable across these finite elements is prescribed and consequently the value of a dependent variable at the nodes can be used to represent the PDE description of the variable and the material properties across the element. This discretization enables the representation of the PDE in a semi-continuous way across the entire domain. The final result is a series of simultaneous equations of the value of a dependent variable or its derivative at each of the nodes. Boundary conditions (i.e. known values of the variable or its derivative) are used to constrain this set of simultaneous equations sufficiently to allow the equations to be solved using algebra.

The key components of the FEM are:

1. Discretization of the domain into finite elements;
2. Selection of a function to describe how the primary variables vary within an element;
3. Definition of the governing partial differential equation (PDE);
4. Derivation of linear equations that satisfy the PDE within each element (element equations);
5. Assembly of the element equations into a global set of equations, modified for boundary conditions; and,
6. Solution of the global equations.

Appendix I provides a detailed description of the FEM.

3 Theory

This chapter introduces some basic theoretical considerations for the stress-strain analysis of geomaterials and/or structures. The equations governing a stress-strain analysis are those of a static equilibrium (Section 3.1). The additional requirement of compatibility (Section 3.1.2) introduces strain quantities, which are linked to stress increments through a constitutive relationship (3.1.3). Stress and strain invariants (Section 3.2) are commonly used in the formulation of constitutive relationships; accordingly, some common invariants are described before presenting the elastic and elastic-plastic constitutive relationships (Sections 3.3 and Section 3.4). Section 3.5 recasts some of these relationships for geometric idealizations used in geotechnical analysis such as plane strain and axisymmetry.

In GeoStudio, each material within a stress-strain analysis must be designated as having a pore-water pressure response type (Section 3.6). All of these response types can be used in a coupled stress-strain and water flow simulation (Section 3.7), however, at least one of the materials must be designated 'Consolidating'. Geomaterials often interact with structures, so a general overview of structural elements and the associated failure criteria is provided in Section 3.8. Section 3.9 briefly explains how the classical elastic-plastic formulation can be revised for completing a stress redistribution type of analysis. This generalized formulation is used to complete two types of analyses in SIGMA/W: 1) Stress Correction (Section 4.4.1); and, 2) Strength Reduction Stability (Section 4.4.2).

3.1 General Requirements

The displacement based finite element method satisfies the requirements of equilibrium and compatibility. The relation between equilibrium and compatibility is governed by a constitutive model.

3.1.1 Equilibrium

The state of stress at any point within the domain is defined by a second order tensor comprising nine components in Cartesian coordinates (Figure 1):

$$[\sigma] = \begin{bmatrix} \sigma_{11} & \sigma_{12} & \sigma_{13} \\ \sigma_{21} & \sigma_{22} & \sigma_{23} \\ \sigma_{31} & \sigma_{32} & \sigma_{33} \end{bmatrix} \equiv \begin{bmatrix} \sigma_{xx} & \sigma_{xy} & \sigma_{xz} \\ \sigma_{yx} & \sigma_{yy} & \sigma_{yz} \\ \sigma_{zx} & \sigma_{zy} & \sigma_{zz} \end{bmatrix} \equiv \begin{bmatrix} \sigma_{xx} & \tau_{xy} & \tau_{xz} \\ \tau_{yx} & \sigma_{yy} & \tau_{yz} \\ \tau_{zx} & \tau_{zy} & \sigma_{zz} \end{bmatrix} \quad \text{Equation 1}$$

where the first subscript indicates the direction of the normal to the surface and the second subscript indicates the direction of the stress. Symmetry in a three-dimensional stress field requires that $\sigma_{xy} = \sigma_{yx}$, $\sigma_{yz} = \sigma_{zy}$, $\sigma_{zx} = \sigma_{xz}$, which allows the stress state to be defined by a tensor with 6 unique components:

$$\{\sigma\}^T = \{\sigma_{xx} \;\; \sigma_{yy} \;\; \sigma_{zz} \;\; \sigma_{xy} \;\; \sigma_{yz} \;\; \sigma_{zx}\} \quad \text{Equation 2}$$

Assuming the y Cartesian coordinate aligned with the direction of gravity and a compression positive notation, equilibrium of the static control volume subject to the stress field must satisfy the following three equations:

$$\left(\frac{\partial \sigma_{xx}}{\partial x}+\frac{\partial \sigma_{yx}}{\partial y}+\frac{\partial \sigma_{zx}}{\partial z}\right)dxdydz=0$$

$$\left(\frac{\partial \sigma_{xy}}{\partial x}+\frac{\partial \sigma_{yy}}{\partial y}+\frac{\partial \sigma_{zy}}{\partial z}+\rho g\right)dxdydz=0 \qquad \text{Equation 3}$$

$$\left(\frac{\partial \sigma_{xz}}{\partial x}+\frac{\partial \sigma_{yz}}{\partial y}+\frac{\partial \sigma_{zz}}{\partial z}\right)dxdydz=0$$

where the body (gravity) load ρg acts only in the vertical coordinate direction and inertia effects have been neglected. Equation 3 is written in terms of total normal stresses and assuming that compressive normal stresses are positive.

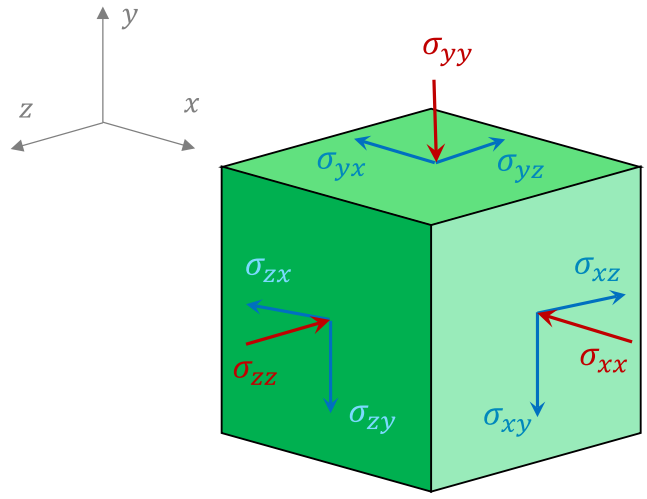

Figure 1. Components of the Cauchy stress tensor in Cartesian coordinates. The stress state depicted is for a compression positive notation.

3.1.2 Compatibility

A spatially continuous domain can be assumed to deform in a compatible manner. The deformations u, v, and w in the x, y and z directions, respectively, must therefore be defined by differentiable functions. The requirement for compatibility is expressed mathematically by the definition of the strain components. Assuming small strain theory and a compression positive sign convention, the strain field associated with the displacement field is defined with respect to the Cartesian coordinate system by a second order tensor comprising nine components:

$$[\varepsilon]=\begin{bmatrix}\varepsilon_{xx} & \varepsilon_{xy} & \varepsilon_{xz}\\ \varepsilon_{yx} & \varepsilon_{yy} & \varepsilon_{yz}\\ \varepsilon_{zx} & \varepsilon_{zy} & \varepsilon_{zz}\end{bmatrix}=\begin{bmatrix}\varepsilon_{xx} & \frac{1}{2}\gamma_{xy} & \frac{1}{2}\gamma_{xz}\\ \frac{1}{2}\gamma_{yx} & \varepsilon_{yy} & \frac{1}{2}\gamma_{yz}\\ \frac{1}{2}\gamma_{zx} & \frac{1}{2}\gamma_{zy} & \varepsilon_{zz}\end{bmatrix} \qquad \text{Equation 4}$$

where the Cartesian shear strain components of the strain tensor were expressed using the engineering shear strain quantity γ because it causes shear stress. In small strain theory, $\gamma_{ij} = \gamma_{ji}$ and the six engineering strain components comprise three normal strains and three shear strains that are defined as:

$$\varepsilon_{xx} = -\frac{\partial u}{\partial x} \quad \varepsilon_{yy} = -\frac{\partial v}{\partial y} \quad \varepsilon_{zz} = -\frac{\partial w}{\partial z} \qquad \text{Equation 5}$$

$$\gamma_{xy} = -\varepsilon_{yx} - \varepsilon_{xy} = -\frac{\partial v}{\partial x} - \frac{\partial u}{\partial y} \qquad \text{Equation 6}$$

$$\gamma_{yz} = -\varepsilon_{zy} - \varepsilon_{yz} = -\frac{\partial w}{\partial y} - \frac{\partial v}{\partial z} \qquad \text{Equation 7}$$

$$\gamma_{zx} = -\varepsilon_{zx} - \varepsilon_{xz} = -\frac{\partial w}{\partial x} - \frac{\partial u}{\partial z} \qquad \text{Equation 8}$$

which can be compactly written as a vector of six unique strain components:

$$\{\varepsilon\}^T = \{\varepsilon_{xx} \quad \varepsilon_{yy} \quad \varepsilon_{zz} \quad \gamma_{xy} \quad \gamma_{yz} \quad \gamma_{zx}\} \qquad \text{Equation 9}$$

3.1.3 Constitutive Relationship

The 3 equilibrium and 6 compatibility equations (i.e. 9 equations in total) comprise 15 unknown quantities: 6 stresses, 6 strains, and 3 displacements. Six additional equations are required to obtain a mathematical solution. The link between the equilibrium and compatibility equations takes the form of a relation between infinitesimal increments (δ) of stress and strain, which is expressed by a constitutive law:

$$\{\delta\sigma\} = [D]\{\delta\varepsilon\} \qquad \text{Equation 10}$$

where $\{\delta\sigma\}$ and $\{\delta\varepsilon\}$ are vectors comprising six stress and six strain increments, respectively:

$$\{\delta\sigma\}^T = \{\delta\sigma_{xx} \quad \delta\sigma_{yy} \quad \delta\sigma_{zz} \quad \delta\sigma_{xy} \quad \delta\sigma_{yz} \quad \delta\sigma_{zx}\} \qquad \text{Equation 11}$$

$$\{\delta\varepsilon\}^T = \{\delta\varepsilon_{xx} \quad \delta\varepsilon_{yy} \quad \delta\varepsilon_{zz} \quad \delta\gamma_{xy} \quad \delta\gamma_{yz} \quad \delta\gamma_{zx}\} \qquad \text{Equation 12}$$

and $[D]$ is a constitutive matrix relating increments of stress and strain. The constitutive matrix $[D]$ can be expressed in terms of effective or total stress parameters. This being the case, all onstitutive models in SIGMA/W are formulated in terms of effective stress parameters; consequently, additional theoretical considerations are required if an undrained response is to be simulated (Section 3.6.2). Alternatively, an undrained response can be simulated using an effective stress constitutive model via a coupled stress-strain and water transfer analysis (Section 3.7).

The relation between increments of stress and strain is normally nonlinear; consequently, the stiffness matrix $[D]$ is dependent on the current and past state of the material. The more complex constitutive models in Section 5 vary in both strength and stiffness with stress and strain levels.

3.2 Invariants

The formulation of stress-strain constitutive models, and sometimes the interpretation of numerical results, are often more conveniently accomplished by using invariants; that is, quantities with a magnitude independent of the chosen coordinate system. For example, the state of stress can be fully described using the six independent stress quantities corresponding to a fixed Cartesian coordinate system or three principal stresses and their corresponding normal unit vectors. Principal stresses are a convenient measure of the maximum and minimum normal stresses in the material. There are other invariants that are mathematically convenient and provide insight into the deformation response of a material. Specifically, these invariants indicate the amounts of volume and shear deformations, where the latter is particularly important given that changes in shape (i.e. shearing) can lead to failure.

Cauchy's stress theorem can be used to determine a traction (i.e. stress) vector for a known stress state on a plane defined by a normal unit vector defined with respect to the Cartesian coordinate system (Figure 1). The normal and shear stress on the plane can subsequently be determined from the traction vector. For the special case where the traction comprises a normal stress but no shear stress, then Cauchy's stress theorem becomes a standard eigenvalue problem, from which the principal stresses σ'_3, σ'_2, and σ'_1 and the associated normal unit vectors can be determined. Assuming a compression positive sign convention, the principal stresses are always ordered as:

$$\sigma'_1 \geq \sigma'_2 \geq \sigma'_3 \qquad \text{Equation 13}$$

Consideration can be given to the amount of work input per unit volume of a material undergoing normal and shear strain increments (Equation 12). The work equation can be decomposed into increments of volumetric work and increments of distortional work, from which the corresponding stress and strain invariants can be derived (Wood, 1990). Two stress invariants that provide insight into the deformation response are the mean effective stress:

$$p' = \frac{\sigma'_{xx} + \sigma'_{yy} + \sigma'_{zz}}{3} \qquad \text{Equation 14}$$

and the deviatoric stress:

$$q = \left[\frac{(\sigma'_{yy} - \sigma'_{zz})^2 + (\sigma'_{zz} - \sigma'_{xx})^2 + (\sigma'_{xx} - \sigma'_{yy})^2}{2} + 3(\sigma_{yz}^2 + \sigma_{zx}^2 + \sigma_{xy}^2)\right]^{1/2} \qquad \text{Equation 15}$$

The use of stress increments (e.g. $\delta\sigma'_{xx}$) in Equation 14 and Equation 15 instead of accumulated values results in corresponding increments of mean effective $\delta p'$ and deviatoric stress δq. The corresponding work-conjugate strain invariants are the volumetric strain increment:

$$\delta\varepsilon_p = \delta\varepsilon_{xx} + \delta\varepsilon_{yy} + \delta\varepsilon_{zz} \qquad \text{Equation 16}$$

and the deviatoric strain increment:

$$\delta\varepsilon_q = \frac{1}{3}\left\{2\left[\left(\delta\varepsilon_{yy} - \delta\varepsilon_{zz}\right)^2 + \left(\delta\varepsilon_{zz} - \delta\varepsilon_{xx}\right)^2 + \left(\delta\varepsilon_{xx} - \delta\varepsilon_{yy}\right)^2\right] + 3\left(\gamma_{yz}^2 + \gamma_{zx}^2 + \gamma_{xy}^2\right)\right\}^{1/2} \quad \text{Equation 17}$$

where the subscripts p and q indicate pairing with a stress invariant (Section 3.3). The accumulated strain invariants are calculated as:

$$\varepsilon_p = \sum \delta\varepsilon_p \quad \text{Equation 18}$$

$$\varepsilon_q = \sum \delta\varepsilon_q \quad \text{Equation 19}$$

The principal effective stresses can be calculated from the invariants as:

$$\begin{Bmatrix} \sigma'_1 \\ \sigma'_2 \\ \sigma'_3 \end{Bmatrix} = p' \begin{Bmatrix} 1 \\ 1 \\ 1 \end{Bmatrix} + \frac{2}{3} q \begin{Bmatrix} \sin\left(\theta + \frac{2\pi}{3}\right) \\ \sin\theta \\ \sin\left(\theta - \frac{2\pi}{3}\right) \end{Bmatrix} \quad \text{Equation 20}$$

where θ is another invariant referred to as Lode's angle:

$$\theta = \frac{1}{3}\operatorname{asin}\left(\frac{27}{2}\frac{\det \boldsymbol{s}}{q^3}\right) \quad \text{Equation 21}$$

where $\det \boldsymbol{s}$ is the determinant of the deviatoric stress tensor:

$$\det \boldsymbol{s} = \begin{vmatrix} \sigma_{xx} - p' & \sigma_{xy} & \sigma_{xz} \\ \sigma_{yx} & \sigma_{yy} - p' & \sigma_{yz} \\ \sigma_{zx} & \sigma_{zy} & \sigma_{zz} - p' \end{vmatrix} \quad \text{Equation 22}$$

The Lode angle is a measure of loading type and is bounded by:

$$-\frac{\pi}{6} \leq \theta \leq \frac{\pi}{6} \quad \text{Equation 23}$$

where the lower bound corresponds to a triaxial compression ($\sigma'_1 \geq \sigma'_2 = \sigma'_3$) and the upper bound to triaxial extension ($\sigma'_1 = \sigma'_2 \geq \sigma'_3$).

The mean effective stress influences volume change as quantified by the volumetric strain increment. The deviatoric stress influences a change in shape as quantified by the deviatoric strain increment. In principal stress space, a space diagonal, or hydrostatic axis, can be drawn where $\sigma'_1 = \sigma'_2 = \sigma'_3$ (Figure 2). A state of stress in principal space can be described by the distance along the space diagonal $\xi = p'\sqrt{3}$, the orthogonal distance from the diagonal $s = q\sqrt{2}/\sqrt{3}$, and the angle θ in the deviatoric plane that is the Lode angle (Figure 2).

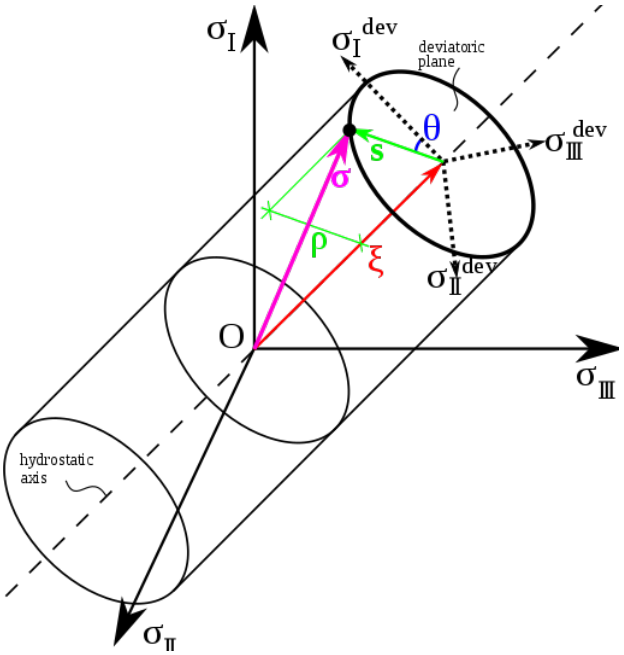

Figure 2. Visualisation of a Cauchy stress tensor σ in the Haight-Westergaard stress space by JoKalliauer is in the Public Domain.

3.3 Elastic Behaviour

The simplest definition of $[D]$ required by Equation 10 is obtained by assuming isotropic linear elastic behaviour. Although this assumption is often not completely representative of real soil behaviour, the isotropic linear elastic constitutive model is fundamental to the formulation and implementation of all constitutive models. In addition, isotropic linear elasticity provides the basis for understanding stress-strain behaviour and pore-water pressure response in undrained conditions (Section 3.6.2). The elastic stiffness matrix takes the following form (note: elements of the matrix that are not shown are zeros):

$$[D] = \frac{E'(1-\nu')}{(1+\nu')(1-2\nu')} \begin{bmatrix} 1 & \frac{\nu'}{1-\nu'} & \frac{\nu'}{1-\nu'} & & & & & & \\ \frac{\nu'}{1-\nu'} & 1 & \frac{\nu'}{1-\nu'} & & & & & & \\ \frac{\nu'}{1-\nu'} & \frac{\nu'}{1-\nu'} & 1 & & & & & & \\ & & & \frac{1-2\nu'}{2(1-\nu')} & & & & & \\ & & & & \frac{1-2\nu'}{2(1-\nu')} & & & & \\ & & & & & \frac{1-2\nu'}{2(1-\nu')} & & & \end{bmatrix} \quad \text{Equation 24}$$

where E' is the effective elastic modulus and ν' effective Poisson's ratio.

The stiffness form of the elastic stress-strain law (Equation 10 with Equation 24) can be inverted to obtain the compliance form of the relation:

$$\begin{Bmatrix} \delta\varepsilon_{xx} \\ \delta\varepsilon_{yy} \\ \delta\varepsilon_{zz} \\ \delta\gamma_{xy} \\ \delta\gamma_{yz} \\ \delta\gamma_{zx} \end{Bmatrix} = \frac{1}{E'} \begin{bmatrix} 1 & -\nu' & -\nu' & & & \\ -\nu' & 1 & -\nu' & & & \\ -\nu' & -\nu' & 1 & & & \\ & & & 2(1+\nu') & & \\ & & & & 2(1+\nu') & \\ & & & & & 2(1+\nu') \end{bmatrix} \begin{Bmatrix} \delta\sigma'_{xx} \\ \delta\sigma'_{yy} \\ \delta\sigma'_{zz} \\ \delta\sigma'_{xy} \\ \delta\sigma'_{yz} \\ \delta\sigma'_{zx} \end{Bmatrix} \qquad \text{Equation 25}$$

where the property by which shear stress is calculated from strain increments is recognizable as the shear modulus:

$$G = \frac{E'}{2(1+\nu')} \qquad \text{Equation 26}$$

Substitution of the normal strain increments from Equation 25 into Equation 16 and subsequent regrouping of the stress increments to obtain Equation 14 gives:

$$\delta\varepsilon_p^e = \frac{\delta p'}{K'} \qquad \text{Equation 27}$$

where the superscript e indicates elastic and K' is the effective bulk modulus given by:

$$K' = \frac{E'}{3(1-2\nu')} \qquad \text{Equation 28}$$

Similarly, substitution of the strain increments from Equation 25 into Equation 17 and subsequent regrouping of the stress increments to obtain Equation 15 gives:

$$\delta\varepsilon_q^e = \frac{\delta q}{3G} \qquad \text{Equation 29}$$

Having defined the shear modulus and bulk modulus, the stiffness matrix (Equation 24) can also be cast in a form that is convenient for the implementation of some constitutive models (Section 5.7):

$$[D] = \begin{bmatrix} K' + {}^4/_3\,G' & K' - {}^2/_3\,G' & K' - {}^2/_3\,G' & & & \\ K' - {}^2/_3\,G' & K' + {}^4/_3\,G' & K' - {}^2/_3\,G' & & & \\ K' - {}^2/_3\,G' & K' - {}^2/_3\,G' & K' + {}^4/_3\,G' & & & \\ & & & G & & \\ & & & & G & \\ & & & & & G \end{bmatrix} \qquad \text{Equation 30}$$

3.4 Elastic-Plastic Behaviour

An elastic-plastic framework can be used to formulate constitutive models that describe various aspects of the stress-strain behaviour of soils. The formulation of elastic-plastic constitutive models is summarized herein to facilitate subsequent discussions. A full discourse on elastic-plastic behaviour and the formulation of constitutive models is given by Potts and Zdravković (1990). The key elements of an elastic-plastic constitutive model are (Wood, 1990) the following:

1. Elastic model – a constitutive model that links elastic, recoverable, deformations (strains) with changes in effective stresses.
2. Yield surface – a function that describes a boundary in general stress space within which the deformations are elastic.
3. Plastic potential – a function that describes the relative magnitudes of the plastic strains;
4. Hardening/softening law – a relationship that links the changing size of the yield surface with the absolute magnitude of plastic strains.

It is also worthwhile to note the following:

- The elastic properties can be linear or nonlinear.
- The failure law (e.g. Mohr-Coulomb failure law) is often implicit in the yield function.
- The failure law describes a surface in effective stress space outside of which the stress state cannot exist (Wood, 1990).
- Elastic-plastic constitutive models manifest one or more types of plastic behaviour: perfect plasticity, strain hardening plasticity, and strain softening plasticity.

Elastic-plastic constitutive models recast the constitutive law (Equation 10) as:

$$\{\delta\sigma'\} = [D^{ep}]\{\delta\varepsilon\} \qquad \text{Equation 31}$$

where $[D^{ep}]$ is used to indicate that the constitutive matrix is elastic-plastic instead of purely elastic. The total strain increments are decomposed into elastic and plastic parts:

$$\{\delta\varepsilon\} = \{\delta\varepsilon^e\} + \{\delta\varepsilon^p\} \qquad \text{Equation 32}$$

where the superscripts e and p indicate elastic and plastic, respectively. The incremental stresses are related to the incremental elastic strains by

$$\{\delta\sigma'\} = [D]\{\delta\varepsilon^e\} \qquad \text{Equation 33}$$

The matrix $[D]$ has been retained to represent the elastic constitutive matrix, which could be linear elastic (Equation 25) or non-linear. Combining Equation 32 and Equation 33 gives:

$$\{\delta\sigma'\} = [D](\{\delta\varepsilon\} - \{\delta\varepsilon^p\}) \qquad \text{Equation 34}$$

Plastic, irrecoverable strains, are calculated by means of a flow rule, which can be expressed as:

$$\{\delta\varepsilon^p\} = \Lambda\left\{\frac{\partial P(\{\sigma'\},\{m\})}{\partial\sigma'}\right\} \quad \text{Equation 35}$$

where Λ is a scalar multiplier and $P(\{\delta\sigma'\},\{m\})$ is the plastic potential function of the form:

$$P(\{\sigma'\},\{m\}) = 0 \quad \text{Equation 36}$$

where $\{m\}$ is a vector of state parameters that are immaterial because only the differentials of P with respect to the stress components are needed in Equation 35. The differentials of P with respect to the stress components define the relative magnitudes of the plastic strains. Substitution of Equation 35 into Equation 34 gives:

$$\{\delta\sigma'\} = [D]\{\delta\varepsilon\} - \Lambda[D]\left\{\frac{P(\{\sigma'\},\{m\})}{\partial\sigma'}\right\} \quad \text{Equation 37}$$

A yield function is a scalar function that can be expressed in terms of either principal stresses, or stress invariants, and state parameters. The yield function must evaluate to zero when plastic strains are developing:

$$F(\{\sigma'\},\{k\}) = 0 \quad \text{Equation 38}$$

where $\{k\}$ is a vector of state parameters.

The stress state must also remain on the yield function when plastic strains are occurring, which requires:

$$\delta F(\{\sigma'\},\{k\}) = \left\{\frac{\partial F(\{\sigma'\},\{k\})}{\partial\sigma'}\right\}\{\delta\sigma'\} + \left\{\frac{\partial F(\{\sigma'\},\{k\})}{\partial k}\right\}\{\delta k\} = 0 \quad \text{Equation 39}$$

Equation 39 is referred to as the consistency condition. Equation 39 can be rearranged to give $\{\delta\sigma'\}$, which can in turn be set equal to Equation 37 to obtain Λ, which can subsequently be substituted into Equation 37 to determine the elastic-plastic constitutive matrix as:

$$[D^{ep}] = [D] - \frac{[D]\left\{\frac{\partial P(\{\sigma'\},\{m\})}{\partial\sigma'}\right\}\left\{\frac{\partial F(\{\sigma'\},\{k\})}{\partial\sigma'}\right\}^T[D]}{\left\{\frac{\partial F(\{\sigma'\},\{k\})}{\partial\sigma'}\right\}^T[D]\left\{\frac{\partial P(\{\sigma'\},\{m\})}{\partial\sigma'}\right\} + A} \quad \text{Equation 40}$$

where A is given by

$$A = -\frac{1}{\Lambda}\left\{\frac{\partial F(\{\sigma'\},\{k\})}{\partial k}\right\}^T\{\delta k\} \quad \text{Equation 41}$$

The parameter A has a form that is dependent on the type of plasticity: perfect plasticity, strain hardening/softening plasticity, or work hardening/softening plasticity.

3.5 Geometric Idealizations

In a 2D plane strain idealization of a stress-strain problem, the out-of-plane displacement is null (i.e. $w = 0$) and the strain increments are defined as:

$$\delta\varepsilon_{xx} = -\frac{\partial u}{\partial x} \quad \delta\varepsilon_{yy} = -\frac{\partial v}{\partial y} \quad \delta\varepsilon_{zz} = 0 \tag{Equation 42}$$

$$\delta\gamma_{xy} = -\frac{\partial v}{\partial x} - \frac{\partial u}{\partial y} \quad \delta\gamma_{yz} = 0 \quad \delta\gamma_{zx} = 0$$

There are four corresponding non-zero stress increments given by:

$$\{\delta\sigma\}^T = \{\delta\sigma_{xx} \quad \delta\sigma_{yy} \quad \delta\sigma_{zz} \quad \delta\sigma_{xy}\} \tag{Equation 43}$$

In a 2D axisymmetric idealization of a stress-strain problem the domain has symmetry about a central, rotational axis and the subsequent coordinate system is cylindrical, with the x coordinate representing the radial coordinate r, and the out-of-plane z coordinate representing the arc length for an assumed (i.e. specified) interior angle θ. As with the 2D plane strain idealization, there is no displacement in the out-of-plane direction. The strain increments are defined as:

$$\delta\varepsilon_r = -\frac{\partial u}{\partial r} \quad \delta\varepsilon_{yy} = -\frac{\partial v}{\partial y} \quad \delta\varepsilon_\theta = -\frac{u}{r} \tag{Equation 44}$$

$$\delta\gamma_{ry} = -\frac{\partial v}{\partial r} - \frac{\partial u}{\partial y} \quad \delta\gamma_{y\theta} = \delta\gamma_{r\theta} = 0$$

There are four corresponding non-zero stress increments given by:

$$\{\delta\sigma\}^T = \{\delta\sigma_r \quad \delta\sigma_{yy} \quad \delta\sigma_\theta \quad \delta\sigma_{ry}\} \tag{Equation 45}$$

A particular example of an axisymmetric stress-strain problem is that of a conventional triaxial compression test. The generalized invariants described in Section 3.2 can be simplified for the axisymmetric condition of conventional triaxial compression as:

$$p' = \frac{\sigma'_a + 2\sigma'_r}{3} \tag{Equation 46}$$

$$q = \sigma'_a - \sigma'_r \tag{Equation 47}$$

$$\delta\varepsilon_p = \delta\varepsilon_a + 2\delta\varepsilon_r \tag{Equation 48}$$

$$\delta\varepsilon_q = \frac{2(\delta\varepsilon_a - \delta\varepsilon_r)}{3} \tag{Equation 49}$$

where the axial stress $\sigma'_a = \sigma'_{yy}$.

3.6 Pore-water Pressure Response

Material models used in a Load-Deformation analysis must be assigned a pore-water pressure response type. The selection of the response type governs the nature of the constitutive matrix $[D]$ used to assemble the finite element equations and the calculation of changes in pore-water pressure. SIGMA/W supports two response types including Drained (3.6.1) and Undrained (Section 3.6.2). The following sections discuss the theoretical implications of each type.

3.6.1 Drained Response

The constitutive matrix $[D]$ required by Equation 10 can be expressed in terms of effective stress parameters to simulate a drained response to loading. All constitutive models in SIGMA/W are formulated in terms of effective stress stiffness parameters. The principle of effective stress requires that the total stresses be equivalent to the summation of the effective stresses and pore-water pressures. The principle of effective stress applies also to stress increments:

$$\{\delta\sigma\} = \{\delta\sigma'\} + \{\delta\sigma_w\} \qquad \text{Equation 50}$$

where the prime denotes effective stress and the vector of changes in pore-water pressure ($\delta\sigma_w$) is given by:

$$\{\delta\sigma_w\}^T = \{\delta u_w\ \delta u_w\ \delta u_w\ 0\ 0\ 0\} \qquad \text{Equation 51}$$

where u_w is pore-water pressure. Solving Equation 50 for the effective stress increments gives:

$$\{\delta\sigma'\} = [D']\{\delta\varepsilon\} = \{\delta\sigma\} - \{\delta\sigma_w\} \qquad \text{Equation 52}$$

which reveals that materials with a drained response type respond instantaneously to changes in pore-water pressure (Section 7.4).

3.6.2 Undrained Response

An undrained response to loading can be simulated without resorting to a coupled stress-strain and water transfer formulation (Section 3.7) if the material response type is set to undrained. The material is still considered to be responding to changes in effective stress (Equation 50); however, unlike the presumption of fully drained conditions (e.g. Section 3.6.1), the changes in pore-water pressure (δu_w) are non-zero as both the solid and fluid phases undergo deformation in response to the applied load (Naylor, 1974). The strains in each phase must be the same in a macroscopic sense. As such, the stress changes in both the solid and fluid phases are related to the incremental strain components by:

$$\{\delta\sigma'\} = [D']\{\delta\varepsilon\} \qquad \text{Equation 53}$$

and

$$\{\delta\sigma_f\} = [D_f]\{\delta\varepsilon\} \qquad \text{Equation 54}$$

where $[D']$ and $[D_f]$ are the effective stress stiffness and the bulk pore fluid stiffness matrices, respectively. Substitution of Equation 53 and Equation 54 into Equation 50 gives:

$$[D] = [D'] + [D_f] \qquad \text{Equation 55}$$

Equation 55, which is required in the equilibrium equations (i.e. Equation 3 via Equation 10), makes it possible to complete an undrained analysis using an effective stress constitutive model. The pore-fluid stiffness matrix is given by:

$$[D_f] = K_e \begin{bmatrix} 1_3 & 0_3 \\ 0_3 & 0_3 \end{bmatrix} \qquad \text{Equation 56}$$

where K_e is the equivalent bulk modulus of the pore-fluid, 1_3 and 0_3 are 3 x 3 matrices of ones and zero, respectively. Naylor (1974) demonstrated that the equivalent bulk modulus of the pore fluid, K_e, is related to the bulk modulus of the pore-fluid K_f. The formulation of Naylor (1974) can be expanded for partial saturation by considering the water-air mixture as a single phase. The isothermal compressibility of fluid is defined as the volume change of a fixed mass with respect to a pressure change per unit volume at constant temperature. The compressibility of an air-water mixture can be derived using the direct proportion of the compressibility of each fluid (Fredlund and Rahardjo, 1993). Ignoring the effects of matric suction and assuming the percentage of dissolved air negligible, the compressibility of the pore fluid is given by:

$$\beta_f = \frac{1}{V_f}\frac{\delta V_f}{\delta u_f} = S\beta_w + (1-S)\beta_{air} \qquad \text{Equation 57}$$

where the isothermal compressibility of air (β_{air}) is equal to the inverse of the of the absolute air pressure (e.g. $\sim 1/101.325$ m^2/kN), β_w is the isothermal compressibility of water (~4.8E-10 m^2/N at 10°C), and S is the degree of saturation. Recall that compressibility is the inverse of the bulk modulus.

In the undrained compression of an element of soil, the strains in each phase are the same at the macroscopic level, and if the solid and fluid phases deform together, the relative movement between the two phases is negligible. An increment in the pore-fluid pressure causes expansion or contraction of both the pore-fluid and the solid soil particles. The pore-fluid occupies a dimensionless volume equal to the porosity (n) and the soil solid particles volume $(1-n)$. The total volume change per unit volume of soil, $\delta\varepsilon_p$, is equal to the summation of the volume change of the pore-fluid and solid particles:

$$\delta\varepsilon_p = n\beta_f\delta u_f + (1-n)\beta_s\delta u_f \qquad \text{Equation 58}$$

where β_s is the compressibility of the solid soil particles. Substitution of Equation 56 into Equation 54 gives three identical equations that take the form:

$$\delta u_f = K_e\left(\delta\varepsilon_x + \delta\varepsilon_y + \delta\varepsilon_z\right) = K_e\left(\delta\varepsilon_p\right) \qquad \text{Equation 59}$$

Solving Equation 59 for the volumetric strain increment and setting it equal to Equation 58 gives:

$$K_e = \frac{1}{n\beta_f + (1-n)\beta_s}$$ Equation 60

Equation 60 can be simplified by assuming the bulk modulus of the solid particles is much greater than that of the soil structure and the pore-fluid. Using this assumption along with substitution of Equation 57 gives:

$$K_e = \frac{1}{n(S\beta_w + (1-S)\beta_{air})} = \frac{1}{\theta_w\beta_w + \theta_{air}\beta_{air}}$$ Equation 61

where θ_w is the volumetric water content and θ_{air} is the volumetric air content. The value of $1/K_e$ varies between β_w and β_{air} in a mixture of air and water (Figure 3). The maximum and minimum bulk fluid compressibility decrease when the air-water mixture exists within soil (Figure 3).

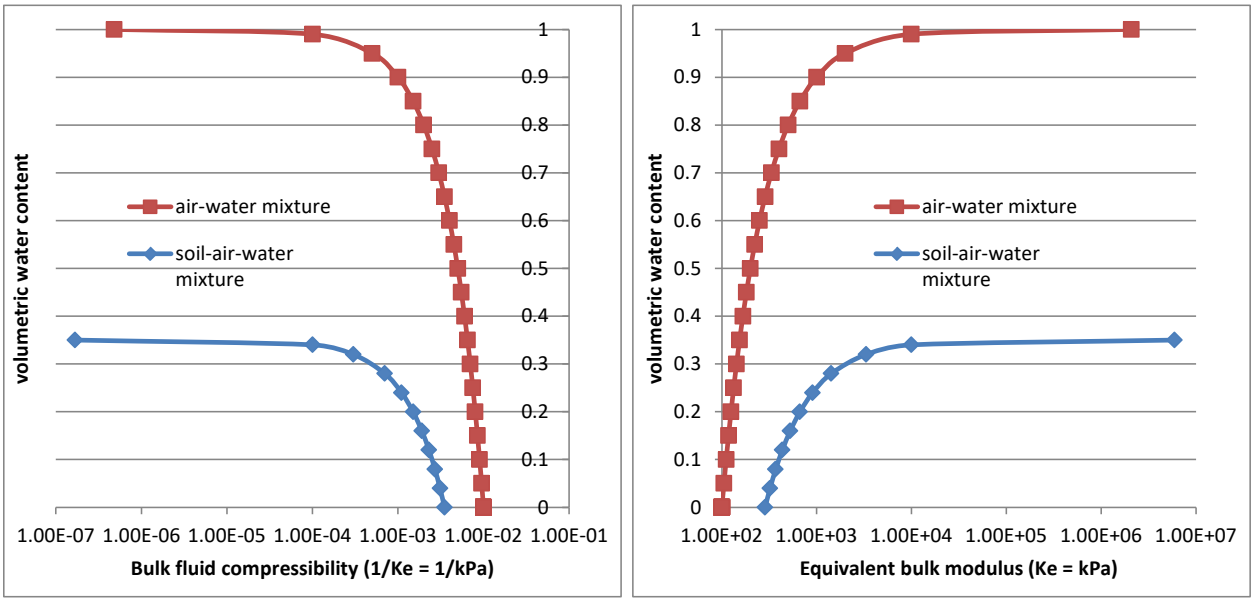

Figure 3. Bulk compressibility (left) and equivalent bulk modulus of an air-water mixture and an air-water mixture in a porous medium with a porosity of 0.35.

In summary, an undrained pore-water pressure increment can be computed by Equation 59 from the strain increments obtained from a finite element analysis in which the stiffness matrices are assembled using a total stress stiffness matrix $([D] = [D'] + [D_f])$. The effective stress stiffness matrix $[D']$ is obtained from the constitutive model (Section 5) while the stiffness matrix $[D_f]$ is calculated internally. For a saturated, isotropic, linear elastic material, the total stress stiffness matrix $[D]$ from Equation 55 can be shown to correspond to an equivalent undrained total stress elastic modulus E and Poisson's ratio ν (Section 3.6.2.1).

3.6.2.1 Pore-water Pressure Coefficients

The undrained response of porous media is often interpreted in the context of a pore-water pressure parameter. A rigorous Bishop pore-water pressure coefficient for both the saturated and unsaturated conditions is obtained by substitution of Equation 61 into Equation 59:

$$(\theta_w \beta_w + \theta_{air} \beta_{air}) \delta u_f = \delta \varepsilon_p \quad \text{Equation 62}$$

The volumetric strain of an undrained control volume can also be calculated from the change in mean total stress δp as:

$$\delta \varepsilon_p = \beta_u \delta p \quad \text{Equation 63}$$

where β_u is the undrained compressibility that embodies the compressibility of the soil structure and pore fluid. The pore-fluid pressure coefficient for a partially saturated porous media is therefore given as:

$$B = \frac{\delta u_f}{\delta p} = \frac{\beta_u}{(\theta_w \beta_w + \theta_{air} \beta_{air})} \quad \text{Equation 64}$$

Assuming the control volume to be saturated and comprising an isotropic linear elastic material, the undrained compressibility is given by:

$$\frac{1}{\beta_u} = K = \frac{E}{3(1 - 2\nu)} \quad \text{Equation 65}$$

where K is the inverse of the undrained bulk modulus and E and ν are the total stress (undrained) elastic modulus and Poisson ratio as indicated by the omission of the prime notation. The undrained parameters are related to the effective stress moduli and K_e (Equation 61) by (Naylor, 1974):

$$\frac{E}{E'} = \frac{3(1 - 2\nu') + E'/K_e}{2(1 - 2\nu')(1 + \nu') + E'/K_e} \quad \text{Equation 66}$$

and

$$\nu = \frac{(1 - 2\nu')(1 + \nu') + E'\nu'/K_e}{2(1 - 2\nu')(1 + \nu') + E'/K_e} \quad \text{Equation 67}$$

Assuming water incompressible (i.e. $K_e = \infty$), although theoretically incorrect, causes Equation 66 and Equation 67 to revert to the expressions commonly presented in soil mechanics textbooks:

$$E = \frac{3E'}{2(1 + \nu')} \quad \text{Equation 68}$$

and

$$\nu = 0.5 \quad \text{Equation 69}$$

Equation 64 through Equation 69 reveals that the undrained response of a saturated, isotropic, linear elastic porous medium will always be characterized by $B < 1$. The pore-fluid, having finite compressibility (i.e. $K_e < \infty$), will always volumetrically compress and therefore so too will the soil structure. The undrained response will be characterized by $B \to 1$, and therefore $\nu \to 0.5$ if the soil structure is much more compressible than that of water. Numerical instability can occur; however, if the total stress Poisson's ratio ν approaches 0.5. The equivalent total stress Poisson's ratio in GeoStudio is limited to 0.499 by recalculating the equivalent bulk modulus of the pore-fluid K_e via Equation 67.

3.7 Consolidation (Coupled Formulation)

Biot (1941) proposed a general theory of consolidation assuming isotropy, linear elasticity, small strains, incompressible pore-fluid, and Darcian flow. The formulation of Biot (1941) has been widely accepted and expanded to account for other physical processes such soil grain compressibility. Biot (1941) derived the general equations of consolidation by making the assumption that the water may contain air bubbles. Fredlund and Morgenstern (1979) later showed that the constitutive equation for an unsaturated soil with a continuous air phase has the same form as that for a discontinuous air phase. Dakshanamurthy et al. (1984) provided a more rigorous coupled formulation for an unsaturated soil based on the work of Fredlund and Morgenstern (1979). Wong et al. (1988) solved the coupled equations of Dakshanamurthy et al. (1984) using the finite element method.

A by-product of the formulation procedure used by Biot (1941) is that stress-strain constitutive properties were contained within the terms of the water transfer equation describing changes in volumetric water content. This in-turn restricted the use of different types of constitutive models and makes implementation within a finite element program cumbersome. The coupled consolidation formulation presented herein is similar to that of Biot (1941); however, the material property characterizations follow more closely that of Fredlund and Rahardjo (1993). In addition, consideration is given to the compressibility of water. The derivation of an alternative continuity equation was motivated by the needs for more transparent material property definitions and the flexibility to implement different stress-strain constitutive models.

The partial differential equation governing groundwater flow through porous media is presented in the book Heat and Mass Transfer Modeling with GeoStudio. The conservation of mass statement requires that the difference in the rate of mass flow into and out of a control volume must be equal to the rate of change in mass within the REV, as follows:

$$\dot{M}_{st} \equiv \frac{dM_{st}}{dt} = \dot{m}_{in} - \dot{m}_{out} + \dot{M}_S \qquad \text{Equation 70}$$

where M_{st} is the stored mass, the inflow and outflow terms, m_{in} and m_{out}, represent the mass transported across the surface of the control volume, and M_S represents a mass source or sink within the REV. The over-dot indicates a time-derivative (rate) of these quantities.

The rate of change in the mass of water stored within the control volume is (ignoring changes in vapour content):

$$\dot{M}_{st} = \dot{M}_w \quad \text{Equation 71}$$

where $\dot{M}_w$ represents the rate of change of liquid water. The rate of change in the stored liquid water is given by:

$$\dot{M}_w = \frac{\partial(\rho_w \theta_w)}{\partial t} dx\, dy\, dz \quad \text{Equation 72}$$

which can be expanded to (ignoring thermal expansion of water):

$$\dot{M}_w = \rho_w \left(\theta_w \beta_w \frac{\partial u_w}{\partial t} + \frac{\partial \theta_w}{\partial t}\right) \quad \text{Equation 73}$$

where ρ_w is the density of water, θ_w is the volumetric water content, β_w is the isothermal compressibility of water (~4.8E-10 m^2/N at 10°C), u_w is the pore-water pressure. The time derivative of volumetric water content in is given by:

$$\frac{\partial \theta_w}{\partial t} = \frac{\partial (Sn)}{\partial t} = S\frac{\partial n}{\partial t} + n\frac{\partial S}{\partial t} \quad \text{Equation 74}$$

where S is degree of saturation and n is porosity. The first term in Equation 74 characterizes the change in volumetric water content associated with a change in porosity at constant saturation and is given by:

$$S\frac{\partial n}{\partial t} = -S\frac{\partial \varepsilon_p}{\partial t} \quad \text{Equation 75}$$

The leading negative sign links volumetric compression (positive) to expulsion of water from the pore-volume (negative) and is associated with an increase in mean effective stress or matric suction. The second term in Equation 74 characterizes the change in volumetric water content associated with a change in degree of saturation at constant porosity and is given by:

$$n\frac{\partial S}{\partial t} = m_w \frac{\partial \varphi}{\partial t} \quad \text{Equation 76}$$

where m_w is the slope of the volumetric water content function and the matric suction, φ, is the difference between pore-air pressure and pore-water pressure ($\varphi = u_a - u_w$). Assuming instantaneous equilibrium of the air pressures gives:

$$m_w \frac{\partial \varphi}{\partial t} = -\, m_w \frac{\partial u_w}{\partial t} \quad \text{Equation 77}$$

The total rate of change in the mass of water stored within the REV must be equal to the difference between the rate of mass inflow ($\dot{m}_{in}$) and the rate of mass outflow ($\dot{m}_{out}$). These rates of mass flow describe processes of water transport across the REV control surfaces. All flows occur in response to

energy gradients. In the case of liquid water, flow can occur due to mechanical (elastic potential, gravitational potential, kinetic), electrical, thermal, or chemical energy gradients; however, only mechanical energy gradients are considered. The mass flow rate of liquid water in response to mechanical energy gradients can be described using Darcy's Law for a variable density fluid (e.g., Bear, 1979; Bear, 1988):

$$\dot{m}_w = \rho_w q_w dxdz = \frac{-K_w}{g}\left(\frac{\partial u_w}{\partial y} + \rho_w g \frac{\partial y}{\partial y}\right) dxdz \qquad \text{Equation 78}$$

where q_w is the water flux, K_w is the isothermal liquid water hydraulic conductivity, and g is the acceleration due to gravity.

Substitution and expansion of the rate equations into the conservation statement and division by the dimensions of the control volume gives:

$$\rho_w\left(\theta_w \beta_w \frac{\partial u_w}{\partial t} - S\frac{\partial \varepsilon_p}{\partial t} - m_w \frac{\partial u_w}{\partial t}\right) = \frac{\partial}{\partial y}\left[\frac{K_w}{g}\left(\frac{\partial u_w}{\partial y} + \rho_w g \frac{\partial y}{\partial y}\right)\right] \qquad \text{Equation 79}$$

The second term of Equation 79 conveniently embodies the stress-strain response. For a fully saturated soil, the drainage term is omitted, and the degree of saturation is equal to 1, giving:

$$\theta_w \beta_w \frac{\partial u_w}{\partial t} - \frac{\partial \varepsilon_p}{\partial t} = n\beta_w \frac{\partial u_w}{\partial t} - \beta \frac{\partial p'}{\partial t} = \frac{\partial}{\partial y}\left[\frac{k_w}{\rho_w g}\left(\frac{\partial u_w}{\partial y} + \rho_w g \frac{\partial y}{\partial y}\right)\right] \qquad \text{Equation 80}$$

where p' is mean effective stress and β is equal to the inverse of the effective bulk modulus K' and taken as positive. Equation 80 clearly highlights that the time derivative of the volumetric strain is the coupling term. Additional insight is gained by considering the undrained loading condition, which simplifies Equation 80 to:

$$\left(\beta + n\beta_w\right)\frac{\partial u_w}{\partial t} = \beta \frac{\partial p}{\partial t} \qquad \text{Equation 81}$$

or:

$$\frac{\partial u_w}{\partial t} = \frac{\beta}{(\beta + n\beta_w)}\frac{\partial p}{\partial t} \qquad \text{Equation 82}$$

which indicates that the pore-water pressure response within a saturated geological unit will be some fraction of the mean total stress change when the response is undrained. The commonly cited Bishop (1954) pore-water pressure coefficient B is obtained from Equation 82 as:

$$B = \frac{\delta u_w}{\delta p} = \frac{\beta}{(\beta + n\beta_w)} = \frac{1}{1 + n\frac{\beta_w}{\beta}} = \frac{1}{1 + n\frac{K'}{K_w}}$$ Equation 83

For example, a perfectly rigid soil structure (i.e. $\beta = 0$) would not generate excess pore-water pressure upon loading. Conversely, a soft soil (i.e. $\beta \gg \beta_w$) would generate excess pore-water pressures that are approximately equal to the change in mean total stress.

The coupling term for the stress-strain equation is introduced by substitution of the constitutive law for the solid phase (Equation 53) into Equation 50:

$$\{\delta\sigma\} = [D']\{\delta\varepsilon\} + \{\delta\sigma_f\}$$ Equation 84

Equation 84 suggests that the total stresses are composed of two parts: one that is caused by hydrostatic pressure of water filling the pores, the other that is caused by the average stress in the soil skeleton. The stresses are carried partly by the water and partly by the solid (Biot, 1941). Equation 84 is invalid if a soil is unsaturated because the relationship between total stress and pore-water pressure is not linear. A more general relationship for saturated-unsaturated soil is given by:

$$\{\delta\sigma\} = [D']\{\delta\varepsilon\} + \{m\}\alpha\delta u_w$$ Equation 85

where

$$\{m\}^T = \{1 \quad 1 \quad 1 \quad 0 \quad 0 \quad 0\}$$ Equation 86

and α is a coefficient varying from 0 to 1.0. The matrix $\{m\}^T$ comprises ones in the first three positions because water pressure acts isotopically. The last three positions of $\{m\}^T$ are zero because water cannot sustain shear stress. Expansion of Equation 85 gives the six total stress increments, one of which is:

$$\delta\sigma_{xx} = \frac{E'}{(1+\nu')(1-2\nu')}\Big(\delta\varepsilon_{xx}(1-\nu') + \nu'\big(\delta\varepsilon_{yy} + \delta\varepsilon_{zz}\big)\Big) + \alpha\delta u_w$$ Equation 87

An increment in the pore-water pressure will cause an increase in total stress and therefore a decrease in effective stress. Similarly, a decrement in pore-water pressure will cause a decrease in total stress, or an increase in effective stress.

The coefficient α intuitively varies between 0 and 1 depending on the degree of saturation. The coefficient α is assumed equal to the effective saturation given as (van Genuchten, 1980):

$$\alpha = S_e = \frac{\theta_w - \theta_r}{\theta_s - \theta_r}$$ Equation 88

In a consolidation analysis, the primary degrees of freedom at each node are the incremental displacements and incremental pore fluid pressures. By solving the water flow equation and stress-strain equation in a mathematically coupled manner, equilibrium and mass conservation is achieved simultaneously. Consider for example the loading of a soft soil with a low hydraulic conductivity. The tendency for volumetric compression must be satisfied by an expulsion of water from the pore space (Equation 80), causing a gradient in pore-water pressures to be established. The incremental change in pore-water pressure will equal the change in stress if water is not expulsed from the pore-space, implying that the change in effective stress is near zero. Volumetric strain is induced as water is expulsed from the pore space.

3.8 Structural Elements

The use of structural support (e.g., beams, cables, geosynthetics) to stabilize a soil mass is an important aspect of geomechanical analysis. SIGMA/W can be used to model structures of arbitrary geometry and properties and the corresponding interaction with soil or rock.

Bathe (2006) provides a detailed description of the formulation of structural elements. Even though some structural elements do not resist bending (e.g., cables, geosynthetics) the basic concepts pertaining to structural elements are most effectively explored by considering an element with flexural stiffness. Figure 4 shows a point on the mid-plane of a beam element being displaced by $\tilde{v}$ normal to the mid-surface (neutral axis) in the direction of the $\tilde{y}$ local axis. The mid-plane is aligned with the local axis $\tilde{x}$ and the local $\tilde{z}$ axis is out-of-plane. A key assumption of the formulation, which corresponds to Timoshenko beam theory, is that a plane section originally normal to the neutral axis remains plane, but because of shear deformations, this section does not remain normal to the neutral axis (Bathe, 2006). The total rotation of the plane originally normal to the neutral axis of the beam is given by the rotation of the tangent to the neutral axis and the shear deformation (Figure 4a):

$$\beta = \frac{d\tilde{v}}{d\tilde{x}} - \gamma \qquad \text{Equation 89}$$

where γ is a constant shear strain across the section.

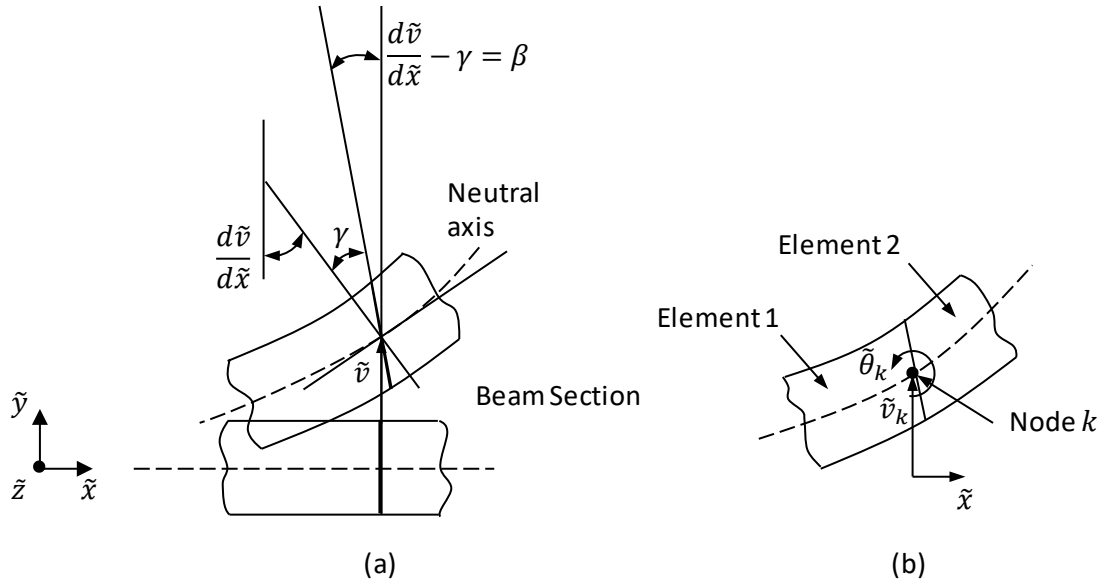

Figure 4. Beam deformations including shear effect (after Bathe, 2006): (a) deformation of cross section; (b) displacement and rotation at node k shared by element 1 and 2.

The transverse displacement $\tilde{v}$ and total rotation β at any location within an element can be interpolated from the nodal values $\tilde{v}_k$ and θ_k at node k (Figure 4b). The shear strain γ is therefore a secondary value calculated from the independent variables $\tilde{v}$ and β (note: the assumption of compression positive changes the sign in Equation 89):

$$\gamma = -\frac{d\tilde{v}}{d\tilde{x}} + \beta \qquad \text{Equation 90}$$

The bending strain is calculated as:

$$\kappa = \frac{d\beta}{d\tilde{x}} \qquad \text{Equation 91}$$

A point on the beam could also be displaced tangential to the mid-plane ($\tilde{u}$) in the direction of local axis $\tilde{x}$, resulting in an axial strain defined as:

$$\varepsilon = -\frac{d\tilde{u}}{d\tilde{x}} \qquad \text{Equation 92}$$

A transverse displacement $(\tilde{w})$ in the direction of the local axis $\tilde{z}$ generates additional shear and bending strains. The complete set of strain increments is summarized as:

$$\{\delta\varepsilon\}^T = \{\delta\varepsilon_1 \quad \delta\gamma_{12} \quad \delta\gamma_{13} \quad \delta\kappa_3 \quad \delta\kappa_2\} \qquad \text{Equation 93}$$

where the subscripts 1, 2, and 3 correspond to the local axis $\tilde{x}$, $\tilde{y}$ and $\tilde{z}$, respectively. The transverse displacements $\tilde{v}$ (2) and $\tilde{w}$ (3) produce rotation about the $\tilde{z}$ (κ_3) and $\tilde{y}$ (κ_2), respectively, and generate shear strains on the plane normal to the $\tilde{x}$ (1) axis in the $\tilde{y}$ (γ_{12}) and $\tilde{z}$ (γ_{13}), respectively. The corresponding force increments and bending moments are given by:

$$\{\delta\sigma\}^T = \{\delta N_1 \quad \delta S_{12} \quad \delta S_{13} \quad \delta M_3 \quad \delta M_2\} \qquad \text{Equation 94}$$

where N is an axial force, S a shear force, and M a bending moment. The strain increments are related to the force increments and bending moments constitutive law that is appropriate to the structural component. The structural elements available in SIGMA/W are discussed further in Section 6.

Plate and geosynthetic structural elements can be used in an axisymmetric analysis. The transverse displacement $\tilde{w}$ in the local axis $\tilde{z}$ direction (i.e. along the out-of-plane arc length) produces a circumferential strain:

$$\varepsilon_3 = -\frac{dr}{r_0} \qquad \text{Equation 95}$$

where r_0 is the circumferential radius and r the displacement in the radial direction, which can be calculated from the local displacements $\tilde{u}$ and $\tilde{v}$. In the case of the plate, which effectively becomes a shell in an axisymmetric analysis, the transverse displacement $\tilde{w}$ redefines κ_2 as the circumferential bending strain (Day, 1990). The circumferential bending strain would be relevant, for example, if modelling a cylinder under a non-uniform (e.g. parabolic) internal pressure distribution.

3.9 Stress Redistribution

Potts and Zdravković (2012) proposed a rigorous and consistent methodology for accounting for partial material factors in finite element analysis. The procedure is generalized and can be applied to any elastic-plastic constitutive model with varying degrees of complexity. The procedure can be adapted to perform three types of stress redistribution analyses:

1. Stress Correction (Section 4.4.1): to redistribute stresses within elements that violate the failure criteria and are therefore in illegal stress space;
2. Strength Reduction Stability (Section 4.4.2): to determine the factor by which the strength of all materials must be reduced to produce a global rupture zone (i.e. failure) and therefore determine the critical mode of failure (i.e. location of the rupture zone);

Potts and Zdravković (2012) developed the procedure by introducing a partial material factor γ_m as an additional state parameter in the yield function:

$$F(\{\sigma\},\{k\},\gamma_m) = 0 \qquad \text{Equation 96}$$

where the partial factor γ_m is the ratio of characteristic strength parameters to design strength parameters:

$$\gamma_m = \frac{\tan \phi'_c}{\tan \phi'_d} = \frac{c'_c}{c'_d} = \frac{S_{u,c}}{S_{u,d}} \qquad \text{Equation 97}$$

where the subscripts c and d indicate characteristic (unfactored) and design (factored) values, respectively. The consistency condition requires that the stress state remain on the yield function when plastic straining is occurring, which requires the function to be written as:

$$\delta F(\{\sigma'\},\{k\},\gamma_m) = \left\{\frac{\partial F(\{\sigma'\},\{k\})}{\partial \sigma'}\right\}\{\delta\sigma'\} + \left\{\frac{\partial F(\{\sigma'\},\{k\})}{\partial k}\right\}\{\delta k\} + \frac{\partial F(\{\sigma\},\{k\},\gamma_m)}{\partial \gamma_m}\delta\gamma_m = 0 \qquad \text{Equation 98}$$

Following the procedure outlined in Section 3.4 with Equation 98 (instead of Equation 39) produces a 'modified' elastic-plastic formulation. The essence of that formulation is intuitively summarized as:

$$\{\delta\sigma\} = [\boldsymbol{D}](\{\delta\varepsilon\} - \{\delta\varepsilon^p\}) - \{\delta\sigma_c\} \qquad \text{Equation 99}$$

where $\{\delta\sigma_c\}$ is the stress correction associated with incrementing the partial factor. As with a conventional elastic-plastic formulation, the elastic strain increments are calculated in Equation 99 as the difference between the total strain increments and plastic strain increments. The inclusion of the partial material factor produces additional plastic strains that result from incrementing the partial factor; that is, reducing the material strength parameters and therefore changing the size of the yield surface. These additional plastic strains result in the stress correction increment $\delta\sigma_c$. The stress path produced by the correction is controlled by the constitutive model, particularly the yield function and plastic potential.

A partial factor is calculated by the solver if a Stress Correction (Section 4.4.1) or Strength Reduction Stability analysis is being conducted (Section 4.4.2). The specialization of the procedures for these different analyses is discussed in the corresponding sections.

Figure 5 depicts a reduction in the strength parameter $g(\theta)$ (via a reduction in ϕ') that defines the slope of the Mohr-Coulomb failure surface in the $p' - q$ stress plane at a particular Lode angle θ (Section 5.8). The initial stress state is on the failure surface at the beginning of an increment $F(\{\sigma_0\},\{k\},\gamma_m) = 0$, but violates the yield condition at the end of the partial factor increment $F(\{\sigma_0\},\{k\},\gamma_m + \delta\gamma_m) > 0$ (i.e. using the initial stresses $\{\sigma_0\}$). The stress correction $\delta\sigma_c$ is calculated over the entire partial factor increment $\delta\gamma_m$. The direction of the stress correction is controlled partly by the outward normal to the plastic potential (not shown; refer to Section 5.8), which defines the relative magnitudes of the plastic

volumetric strain $\delta\varepsilon_p^p$ and the plastic deviatoric strain $\delta\varepsilon_q^p$ (Section 3.4). The outward normal is assumed vertically upwards in Figure 5 (i.e. $\delta\varepsilon_p^p = 0$ while $\delta\varepsilon_q^p > 0$), which corresponds to a horizontal plastic potential passing through the initial stress state $\{\sigma_0\}$. The stress correction, in this specific case (dilation angle = 0), therefore shows a decrease in the deviatoric stress at constant mean effective stress.

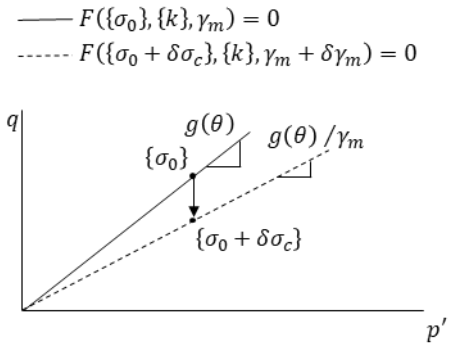

Figure 5. Stress correction associated with the increment in the partial factor.

4 Analysis Types

There are four analysis types in SIGMA/W including: 1) *In Situ*; 2) Load-Deformation; 3) Consolidation; and, 4) Stress Redistribution. An *In Situ* analysis is conducted using either the Gravity Activation or K_0 procedures to establish initial stresses. Load-Deformation analyses are used to analyze the stress-strain response of a geotechnical structure in which the pore-water pressures are not time-dependent. A Consolidation analysis solves the coupled stress-strain and water transfer equations and therefore simulates time-dependent changes in pore-water pressure and effective stress. The Stress Redistribution analysis type is concerned with ensuring that the simulated stresses adhere to a failure criteria and can be used to: i) correct stresses in illegal stress space (e.g. due to gravity activation); ii) perform a strength reduction stability analysis; and, iii) assess the safety factor in accordance with limit state design.

4.1 In Situ

4.1.1 Gravity Activation

Initial stresses can be generated by gravity activation and then optionally altered by the K_0 procedure (Section 4.1.2). The gravity activation procedure creates a vertical total stress σ_{yy} field, which is in equilibrium with the body forces, and a vertical effective stress $\sigma'_{yy} = \sigma_{yy} - u_w$ field, where u_w is the pore-water pressure. The simulated horizontal effective stresses σ'_{xx} are predominantly controlled by Poisson's ratio ν' and the geometry of the domain. The gravity activation procedure assumes the material response is isotropic and linear elastic, making consideration of past loading history impossible. The K_0 procedure can be used to overcome this limitation, but only if a rather strict set of criteria is obeyed (Section 4.1.2).

The gravity activation procedure may be used for cases involving a sloping ground surface (Table 3). Paradoxically, most problems involving a sloping ground surface (e.g. eroded valleys) comprise soils with

a stress history pertaining to overconsolidated soils. For such cases, neither the gravity activation nor the K_0 procedure is ideally suited for establishing the initial stresses (Table 3). Section 4.1.2 provides the necessary background information and procedures for such scenarios and clarifies the conditions placed on the K_0 procedure. Furthermore, Section 4.1.2 provides guidance on the selection of an appropriate Poisson's ratio for the establishment of initial stresses by gravity activation.

The following should be noted:

1. A gravity activation analysis ignores all non-zero stress and displacement boundary conditions except for the hydrostatic stress boundary condition that is used to represent ponding on the ground surface;
2. Poisson's ratio ν' is limited to 0.499 (maximum) to prevent numerical an ill-conditioned elastic constitutive matrix (Equation 24); and,
3. The gravity activation procedure can produce stresses that violate the failure condition. A stress correction analysis should be completed to return the stresses to legal stress space before completing additional stress-strain analyses (Section 4.4.1).

Table 3. Applicability of the gravity activation procedure and combined gravity activation with K_0 procedures.

State	Condition 1[1]		Condition 2[2]	
$OCR = 1.0$	Gravity Activation	Yes	Gravity Activation	Yes[4]
	+ $\boldsymbol{K_0}$ Procedure	Yes	+ $\boldsymbol{K_0}$ Procedure	No
$OCR \geq 1.0$	Gravity Activation	Yes[3]	Gravity Activation	No[5]
	+ $\boldsymbol{K_0}$ Procedure	Yes	+ $\boldsymbol{K_0}$ Procedure	No[5]

[1]One dimensional and axially symmetric stress history involving a horizontal ground surface with hydrostatic groundwater conditions and horizontal stratigraphic boundaries

[2]Sloping ground surface and/or groundwater flow and/or and sloping stratigraphic boundaries

[3]Horizontal effective stresses are controlled by Poisson's ratio if gravity activation is being applied; consequently, an artificial value of Poisson's ratio could be calculated from Equation 103 (Section 4.1.2) to achieve the desired response if $\nu' < 0.499$. The less ambiguous approach in this case is to apply the K_0 procedure.

[4]A sloping ground surface is often associated with erosional processes, which leads to overconsolidation. As such, the use of gravity activation procedures is assumes that all soils are 'nearly' normally compressed (i.e. only lightly overconsolidated).

[5]Simulation of the pseudo geological history is required (Section 4.1.2).

4.1.2 K_0 Procedure

The K_0 procedure makes it possible to capture the stress history for cases involving horizontal ground surface and stratigraphic layers and hydrostatic groundwater conditions (Table 3). The stress history of soils under these conditions is entirely one-dimensional and axially symmetric. The one-dimensional loading might have involved processes such as glacial advance or pore-water pressure decreases, while the unloading might have involved processes such as erosion, pore-water pressure increases, or glacial recession. The stress history of one-dimensional axisymmetric deformation can be characterized by ratio of horizontal to vertical effective stress:

$$K_0 = \frac{\sigma'_{xx}}{\sigma'_{yy}} = \frac{\sigma'_{zz}}{\sigma'_{yy}}$$ Equation 100

where K_0 is called the at-rest earth pressure coefficient. The K_0 procedure uses the specified K_0 to calculate the current initial horizontal effective stresses as:

$$\sigma'_{xx} = \sigma'_{zz} = K_0 \sigma'_{yy}$$ Equation 101

where σ'_{yy} is obtained via the gravity activation procedure (Section 4.1). The value of K_0 is dependent on the loading history of the soil. Soils that have been subjected to a monotonic one-dimensional normal compression (nc) stress history require $K_0 = K_0^{nc}$. Jâky (1946) deduced the following relationship between K_0^{nc} and the angle of shearing resistance ϕ' for one-dimensionally and normally compressed soils:

$$K_0^{nc} \approx 1 - \sin\phi'$$ Equation 102

Soils that have been subjected to subsequent one-dimensional unloading, and are therefore overconsolidated, require $K_0 = K_0^{oc}$. Assuming that the soil behaved isotropically and elastically immediately upon unloading implies a stress path given by:

$$\frac{\delta\sigma'_{xx}}{\delta\sigma'_{yy}} = \frac{v'}{1 - v'}$$ Equation 103

which can be converted into a relationship between K_0^{oc} and the overconsolidation ratio (OCR):

$$K_0^{oc} = (OCR)K_0^{nc} - (OCR - 1)\frac{v'}{1 - v'}$$ Equation 104

where the OCR is defined as:

$$OCR = \frac{\sigma'^{max}_{yy}}{\sigma'_{yy}}$$ Equation 105

and σ'^{max}_{yy} is the past maximum value of the vertical effective stress and σ'_{yy} is the current, or initial, vertical effective stress. Most soils exhibit a non-linear effective stress path (i.e. non-linear elasticity) on unloading, producing a stress history that is better approximated by a relationship of the form (Schmidt, 1966):

$$K_0^{oc} = K_0^{nc} OCR^a$$ Equation 106

where a is an exponent that is dependent on the plasticity of the soil and is generally about 0.5 (Meyerhof, 1976). Alternative approximations exist in the literature for both K_0^{nc} and K_0^{oc}.

The user-defined value of K_0 can produce stresses that violate the Mohr-Coulomb failure condition in the active or passive states. The theoretical limitations on the earth pressure coefficient for a soil without cohesion are:

$$\frac{1-\sin\phi'}{1+\sin\phi'} < K_0 < \frac{1+\sin\phi'}{1-\sin\phi'}$$ Equation 107

where the lower and upper bounds are the active K_a and passive K_p earth pressure coefficients, respectively.

The following should be noted:

1. The K_0 procedure is invalid if the principal stress directions are not aligned with the horizontal and vertical direction, which requires that the ground surface, stratigraphic layers, and phreatic surface are nearly horizontal (Table 3). A stress correction (Section 4.4.1) analysis might ensure that the stresses obey the failure criteria; however, the stress redistribution algorithms cannot ensure force equilibrium.
2. The pseudo-geological history can be modeled to establish the initial stresses for cases that violate the requirements of the K_0 procedure (Table 3). Consider an eroded river valley cut into horizontal and overconsolidated soil layers. Prior to the erosional down cutting, the soils may have been subjected to a one-dimensional axisymmetric stress history that involved loading and unloading via deposition, erosion, or other processes. In such cases, the K_0 procedure may be used to approximate the initial stress prior to downcutting (Figure 6a). The downcutting is then simulated via a plane strain Load-Deformation analyses involving excavation (Figure 6b).

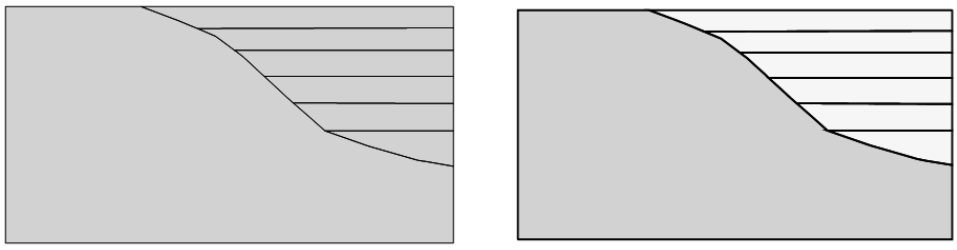

Figure 6. Geometry used to model erosional down cutting of an overconsolidated soil. a) Geometry for gravity activation analysis with K0 procedure; and, b) geometry after load-deformation analysis of 'excavation' sequence.

4.2 Load-Deformation Analysis

A Load-Deformation analysis is used to determine the response of a geotechnical structure subject to a force or displacement boundary condition. This analysis type can provide information on the displacements of the geotechnical structure and adjacent ground, the bending moments, axial forces, and shear forces in structural members, and the forces that develop in adjacent structures. A Load-Deformation analysis does not provide information on time-dependent pore-water pressure response, but can be used with material having an Undrained Response type to analyze the undrained pore-water pressure response to loading/unloading. A Load-Deformation analysis requires the following information:

1. Initial effectives stresses;
2. Final pore-water pressures;
3. Number of load steps;
4. Boundary conditions; and,
5. Material properties.

The initial and final pore-water pressures are used to automatically calculate an increment (or decrement) in the pore-water pressures, which is then imposed as an isotropic boundary condition (see Section 7.4). For example, this option can be used to model dewatering of an excavation. The pore-water pressure boundary condition will be null if the final and initial pore-water pressures are obtained from the same source and are therefore equivalent.

4.3 Consolidation (Coupled Formulation)

A Coupled Consolidation analysis is used to analyze the time dependent pore-water pressure response, and therefore time-dependent deformation, common to many geotechnical problems. The generation of excess pore-water pressure due to embankment loading is a typical example of this process. Similarly, the removal of soil for an excavation (i.e., unloading) can cause a reduction in pore-water pressure in soils with certain stiffness and hydraulic properties. A consolidation analysis is accomplished by combining and simultaneously solving the equation governing stress-strain response (Equation 85) with the equation governing pore fluid transfer through the soil matrix (Equation 79). The following components must be defined for a consolidation analysis:

1. Initial stresses and pore-water pressures.
2. Time duration and number of steps.
3. Hydraulic and stress-strain boundary conditions.
4. Hydraulic and stress-strain material properties.

The requirement for initial stress conditions is consistent with a Load-Deformation analysis (Section 4.2). The initial pore-water pressure conditions must be defined because the transient groundwater flow equation computes the change in pore-water pressure across a time step, making it necessary to know the conditions at the start of the time step. Naturally, it follows that a time increment must be defined, along with the total duration of the analysis.

A consolidation analysis requires the definition of both hydraulic and stress-strain boundary conditions. The stress-strain boundary conditions discussed in Section 7 are relevant to this analysis type. Many practical geotechnical engineering problems will specifically involve construction and/or excavation boundaries via material activation/deactivation. Most of the hydraulic boundary conditions available in SEEP/W can be used in a consolidation analysis. The most used hydraulic boundary conditions include total head, pressure head, water rate, water flux, and the potential seepage face.

All stress-strain material models discussed in Section 5 can be used in a consolidation analysis. The example files should be consulted to understand the anticipated response in a consolidation analysis. Similarly, the saturated-only and saturated-unsaturated material models from SEEP/W are available in SIGMA/W.

4.4 Stress Redistribution

Section 3.9 provides an overview of the theoretical considerations of a stress redistribution analysis, which involves the calculation of a stress correction $\delta\sigma_c$ that arises from an increment in a partial factor γ_m. The solver calculates the partial factor if the stress redistribution procedures is being used to complete a Stress Correction (Section 4.4.1) or a Strength Reduction Stability analysis (Section 4.4.2). The specialization of the procedures for these different analyses is discussed in the following sections.

4.4.1 Stress Correction

Analyses involving linear elastic material models and sloping ground, such as a Gravity Activation analysis, can result in stresses outside the yield surface (illegal stresses) when the elastic material is replaced with an elastic-plastic material. A Stress Correction analysis can be used to return stresses within a domain to legal stress space; that is, to a location in stress space that is on or below the yield surface. In a Stress Correction analysis, regions that require a stress correction must use an elastic-plastic constitutive model that invokes a Mohr-Coulomb failure law.

The calculation of a stress correction $\delta\sigma_c$ requires a partial factor γ_m (Equation 98), which in-turn requires design and characteristic strength parameters (Figure 7). The input strength parameters can be interpreted as the design parameters. The failure surface passing through the initial (illegal) stress state$\{\sigma_0\}$ can be described by pseudo, and unknown, characteristic strength properties. The relationship between the characteristic and design (i.e. input) strength parameters (Equation 98) can be substituted into the Mohr Coulomb yield function and the resulting expression solved for the partial material factor γ_m, allowing the strength correction $\delta\sigma_c$ to be calculated.

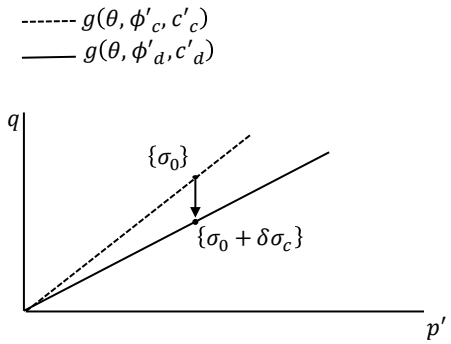

Figure 7. Strength reduction procedure used to complete a Stress Correction analysis: Mohr-Coulomb failure surfaces defined by pseudo-characteristic and design strengths passing through the initial (illegal) and corrected stress states, respectively.

The following should be noted:

1. An initial stress condition must be defined to complete a Stress Correction analysis;
2. The initial stresses can be obtained from an *In Situ*, Load-Deformation, or Consolidation Analysis.

4.4.2 Strength Reduction Stability

A Strength Reduction Stability (SRS) analysis involves a gradual increase in the partial material factor (i.e. reduction in strength) until failure in the soil is fully mobilized, which should correspond to a fully developed global rupture zone. A SRS analysis involves first completing a conventional stress-strain simulation such as a Gravity Activation or Load-Deformation analysis. The initial stresses within every element must start in legal stress space before completing a Strength Reduction Stability analysis. A Stress Correction analysis (Section 4.4.1) should first be completed if this condition is not met.

A SRS stability analysis can be added at any relevant stage of an analysis (e.g. after each construction stage) to determine the global factor of safety. The SRS analysis is advantageous because the simulation provides information about the global factor of safety and, unlike conventional limit equilibrium (LE) stability methods, reveals the mode of failure (i.e. location and shape of the rupture zone) in a natural manner. In addition, an SRS analysis can be used to assess both serviceability and ultimate limit states (i.e. collapse) of structures interacting with the soils. For example, an SRS analysis could be used to simulate the maximum stress transfer onto a pile wall being used to stabilize a slope. A noteworthy disadvantage of the SRS analysis is that it cannot be used to explore multiple modes of failure; that is, the procedure can only find a single global rupture zone. Fortunately, the Stress Based Stability and LE method in SLOPE/W can still be used to calculate the factor of safety for other potential modes of failure.

Advanced soil models are made to behave as a standard Mohr-Coulomb model when completing a strength reduction stability analysis. The input strength parameters are interpreted as the characteristic (i.e., unfactored) values. The final reduced strength parameters are interpreted as the design (i.e., factored) values. A strength reduction stability analysis successively, and incrementally, reduces the soil strength parameters by increasing the partial factor for all characteristic strength values until global

failure is detected (stress path A to F in Figure 8). At the point of collapse, the final partial factor is equivalent to the global factor of safety ($F.S.$):

$$F.S. = \gamma_m = \frac{\tan \phi'_c}{\tan \phi'_d} = \frac{c'_c}{c'_d} = \frac{S_{u,c}}{S_{u,d}} \qquad \text{Equation 108}$$

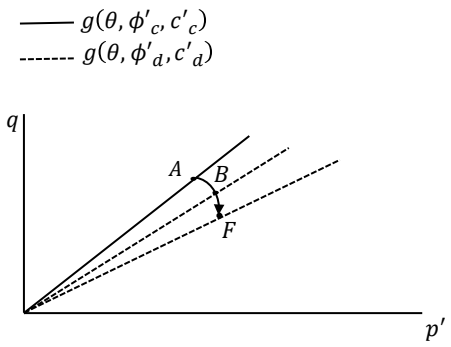

Figure 8. Procedure used to complete a Strength Reduction Stability analysis showing an incremental reduction in strength.

As noted in Section 3.9, the direction of the stress correction is partly controlled by the outward normal to the plastic potential, which defines the relative magnitudes of the plastic volumetric strain $\delta\varepsilon_p^p$ and the plastic deviatoric strain $\delta\varepsilon_q^p$ (Section 3.4). The dilation angle ψ of the Mohr-Coulomb material model controls the slope of the plastic potential in the $p' - q$ stress plane and therefore the direction of the outward normal (Section 5.8). Failure within a soil domain does not occur everywhere simultaneously as the strengths are reduced. As such, changes to the dilation angle ψ with increasing partial factor γ_m imposes a control on the deformation patterns – that is, the kinematics of the failure mechanism – and therefore the factor of safety. Tschuchnigg et al. (2015a, 2015b) simulate a case involving a soil with $\phi' = 45°$. The SRS factor of safety is 1.53 if associated plasticity is assumed (i.e. $\psi = \phi'$) and approximately 1.30 if non-associated plasticity is assumed with $\psi = 0$. Tschuchnigg et al. (2015a, 2015b) note, however, that the problem of non-associated flow in SRS analyses is generally insignificant until $\phi' > 35°$. Having stated this, the flow law is accommodated in a SRS analysis as follows:

1. Associated plasticity (i.e. $\psi = \phi'$): the dilatancy angle ψ is reduced incrementally in the same way as the friction angle ϕ',
2. Non-associated plasticity with $\psi < \phi'$: the dilation angle ψ is kept constant as long as the reduced value for ϕ' is larger than ψ . Once ϕ' falls to the value of ψ, both angles are reduced simultaneously.

The following points about a Strength Reduction Stability analysis should be observed:

1. Stress dependent changes in stiffness are not considered during the analysis; however, the stiffness values at the onset of the analysis are consistent with the state defined by the parent analysis.

2. Regions that are assigned an elastic material model participate in the stress-strain response of the system but do not undergo a stress-correction.
3. The strength characteristics of structural elements, including the axial capacity (tension/compression) or the bending capacity, are not reduced by the global partial factor.

5 Material Models

5.1 Synopsis

Many of the constitutive models presented in the following sections fit within the generalized framework for formulating elastic-plastic models (Section 3.4). The stress-strain response of each model arises from assumptions about the mathematical descriptions of the elastic properties, yield function (Equation 38), plastic potential (Equation 36) and the manner in which the changing size of the yield locus is linked to plastic straining (Equation 41). The mathematical descriptions generally provide little insight into the parameterization and expected response in a numerical simulation unless the reader is intimately familiar with elastic-plastic theory. As such, the 'Formulation' section for each constitutive model is purposefully restrained to the key, and basic, mathematical ingredients. A more enlightening approach to exploring the formulations, and the one adopted here, is quasi-graphical with reference to the progress of a conventional drained compression test. Wood (1990) cleverly used this approach to elucidate the behaviour of the Modified Cam Clay model in both drained and undrained triaxial compression. These sections are titled 'Conceptual Response' and occur immediately after the section summarizing the material properties. A similar approach is used to present the Hyperbolic $E - B$ model despite it not being formulated based on the generalized framework for elastic-plastic models.

It is worth noting that only the drained response is considered because: (a) it reveals the role of the central material properties; and, (b) further consideration to the undrained or (coupled) consolidation responses can be found in the example files. Lastly, the response to triaxial compression does not reveal the behaviour of a particular constitutive model to loading conditions in generalized three dimensional stress space, such as those involving excavation and construction. Again, the reader is directed to the example files and the literature for a more complete discourse on the assumptions and/or limitations of any particular constitutive model.

5.2 Basic Inputs

All material models require specification of unit weight and initial void ratio. The unit weight is used in the calculation of gravity loads (Section 4.1 and 7.3). The void ratio for each material is updated at the end of every load/time step based on the volumetric strain. The void ratio can be used to modify the hydraulic conductivity in a consolidation analysis (Section 5.4). In some material models, for example modified Cam clay, the void ratio is a state parameter that effects the stress-strain behaviour.

5.3 Pore-water Pressure Response Types

Every material model must be assigned a pore-water pressure response type of either Drained or Undrained (Section 3.6). The response type of a material is only relevant for Load-Deformation analyses. The following should be noted:

1. Drained response: the pore-water pressure remains unchanged throughout the analysis in response to loading/unloading. This response type is used to model well-drained materials in Load-Deformation analyses. Specification of a different initial and final pore-water pressure condition results in an automatic boundary condition that calculates an isotropic effective stress change that equals the pore-water pressure change (Section 7.4) for Drained materials, which in turn affects the general stress distribution in the domain.
2. Undrained response: the pore-water pressure response due to loading/unloading is calculated according to theory outlined in Section 3.6.2. This response type is used simulate an undrained response without resorting to a Consolidation analysis.
3. Materials with different pore-water pressure response types can be combined in a Load-Deformation analysis.
4. Response types are ignored in a Consolidation analysis.

5.4 Hydraulic Properties

The definition of hydraulic properties is optional for materials used in *In Situ*, Load-Deformation, and Stress Redistribution analyses, but is mandatory for Consolidation analyses. The Saturated Only or Saturated-Unsaturated hydraulic models can be used, where the later comprises the volumetric water content and hydraulic conductivity. The following should be noted:

1. An increment or decrement in negative pore-water pressures is an *In Situ* or Load-Deformation analysis is weighted by the effective degree of saturation if a volumetric water content function is defined (Section 7.4).
2. The coupled stress-strain and water transfer equation is solved for all regions/materials in a Consolidation analysis; consequently, the Response Type (Section 3.6) is ignored.
3. Selecting the option 'No change in water pressures due to volumetric strain' in the hydraulic properties definition implies that that a material will not respond to loading or unloading in a Consolidation analysis, although the material will still conduct water due to a gradient in total head.
4. Hydraulic conductivity K_w is required for a consolidation analysis. The conductivity can vary as a function of void ratio using a modifier factor $MF = K_w/K'_w$, where K'_w is the reference conductivity. The modifier factor is defined as a function of void ratio decrement/increment Δe (i.e. $MF = MF(\Delta e)$), where $\Delta e = e - e_0$ and e_0 is the initial void ratio. For example, the modifier function could be defined by curve fitting laboratory data using the relationship $MF = K_w/K'_w = 10^{(\Delta e/A)}$, where A is a constant that controls the non-linearity in the relationship (e.g. 0.2; Figure 9). Generally, the modifier function will be specified over a negative range in Δe (i.e. decrement) because the conductivity decreases with decreasing void ratio.

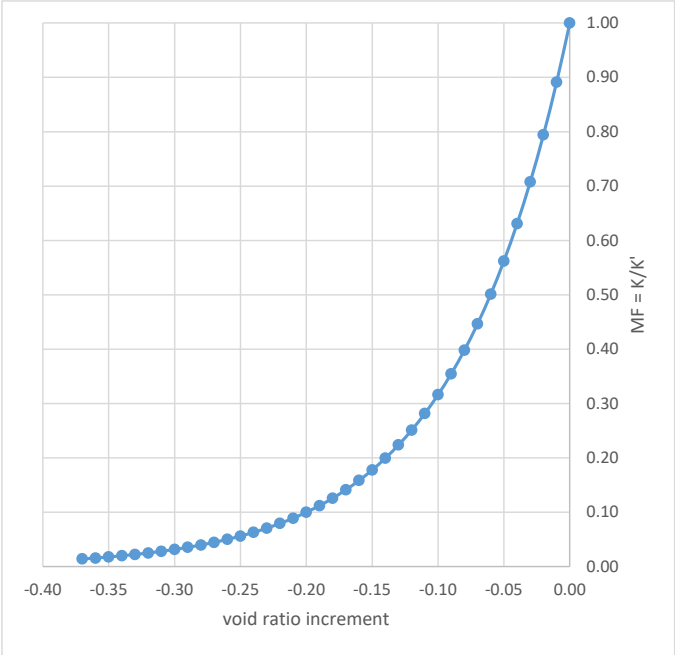

Figure 9. Example of the hydraulic conductivity modified factor function.

5.5 Isotropic Elastic Model

The simplest definition of $[D]$ required by Equation 10 is obtained by assuming isotropic elastic behaviour (Section 3.3). The elastic response is described by two independent elastic parameters: effective stiffness modulus E' and Poisson's ratio ν'. The modifying term 'linear' was purposefully excluded because the Isotropic Elastic model can accommodate non-linear elasticity. The effective elastic modulus E' can be made to vary with y-effective stress through use of a functional relationship (Section I.6.1) or by some other means using an Add-in (Section I.6.2).

5.6 Transverse Isotropic Elastic Model

Sedimentary depositional environments often produce soil layers that are parallel to a single plane of deposition ($x - z$ plane in Figure 12). An axis of symmetry exists in the depositional direction. The stress-strain characteristics are different in the depositional direction as compared to those in the plane of deposition; however, the characteristics do not change in the plane of symmetry. Figure 12 shows the direction of deposition aligned with the y-axis and the plane of deposition parallel to the x-z plane; however, the implementation allows for rotation of the plane of deposition about the z-axis (Figure 11). The rotated coordinated system is $x' - y' - z$; that is, the z-axis remains unchanged in the primed and unprimed coordinate systems.

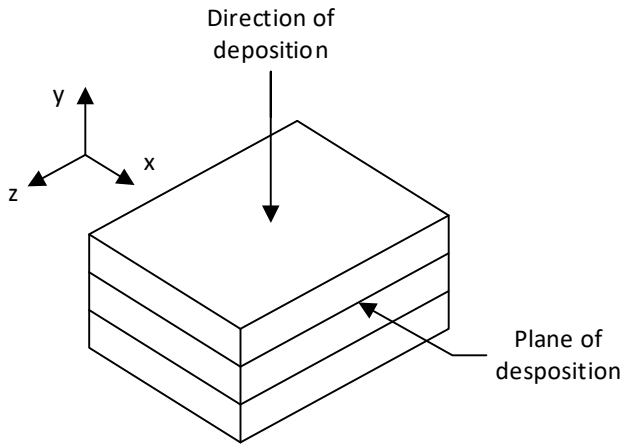

Figure 10. Axis orientations for transverse isotropy without rotation about the z-axis.

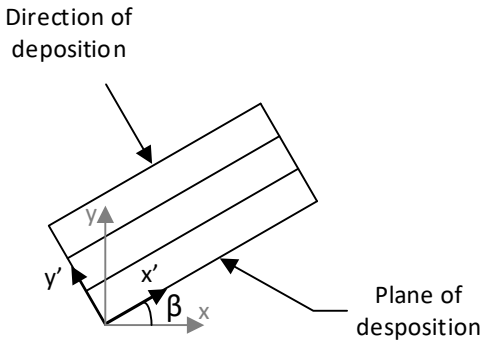

Figure 11. Axis orientations for transverse isotropy with rotation about the z-axis.

5.6.1 Formulation

The stiffness matrix $[D]$ for an anisotropic elastic material, with properties defined with respect to a local coordinate system $(x'y')$ rotated from the Cartesian x-axis by angle β (Figure 12), is given by:

$$\begin{bmatrix} A\left(1-\left(\nu'_{y'x'}\right)^2\frac{E'_{x'}}{E'_{y'}}\right)E'_{y'} & A\nu'_{y'x'}\left(1+\nu'_{x'z'}\right)E'_{y'} & A\left(\nu'_{x'z'}+\left(\nu'_{y'x'}\right)^2\frac{E'_{x'}}{E'_{y'}}\right)E'_{y'} & & & \\ \square & A\left(1-\left(\nu'_{x'z'}\right)^2\right)\left(\frac{E'_{y'}}{E'_{x'}}\right)E'_{y'} & A\nu'_{y'x'}\left(1+\nu'_{x'z'}\right)E'_{y'} & \multicolumn{3}{c}{\begin{matrix}0&0&0\\0&0&0\\0&0&0\end{matrix}} \\ \square & \square & A\left(1-\left(\nu'_{x'z'}\right)^2\frac{E'_{x'}}{E'_{y'}}\right)E'_{y'} & & & \\ \multicolumn{3}{c}{\begin{matrix}\square&\square&\square\\ \square & Symmetric & \square\\ \square&\square&\square\end{matrix}} & \multicolumn{3}{c}{\begin{matrix}G_{x'y'}&0&0\\ \square&G_{x'y'}&0\\ \square&\square&G_{x'}\end{matrix}} \end{bmatrix}$$

Equation 109

where

$$A = \frac{1}{\left(1 + \left(\nu'_{x'z'}\right)^2\right)\left[\frac{E'_{y'}}{E'_{x'}}\left(1 - \nu'_{x'z'}\right) - 2\left(\nu'_{y'x'}\right)^2\right]}$$ Equation 110

Equation 110 follows from symmetry requirements that produce these relationships:

$$\nu'_{x'y'} = \nu'_{y'x'}\frac{E'_{x'}}{E'_{y'}}$$ Equation 111

and

$$G_{x'z'} = \frac{E'_{x'}}{2(1 + \nu'_{x'z'})}$$ Equation 112

5.6.2 Material Parameters

Table 4 provides a summary of the user inputs and properties calculated by the solver.

Table 4. Parameters for the Anisotropic

Parameters	Symbol	Symbol (UI)	Note
Stiffness in the depositional direction	$E'_{y'}$	E'_2	Input
Stiffness in the plane of deposition	$E'_{x'}$	E'_1	Input
Poisson's ratio for staining in the plane of deposition due to stress changes in the direction of deposition	$\nu'_{y'x'}$	ν'_2	Input
Poisson's ratio for staining in the direction of deposition due to stress changes in the plane of deposition	$\nu'_{x'y'}$		Calculated
Poisson's ratio for staining in the plane of deposition due to stress changes in the same plane	$\nu'_{x'z'}$	ν'_1	Input
Shear modulus in the plane of the direction of deposition	$G_{x'y'}$	G_2	Input
Shear modulus in the plane of deposition	$G_{x'z'}$		Calculated
Angle between the x and x' axes (counterclockwise positive)	β	$Angle$	Input

The following restrictions must be applied to the inputs (Pickering, 1970):

1. $E'_{x'}$ $E'_{y'}$ and $G_{x'y'} > 0$
2. $-1 < \nu'_{x'z'} < 1$
3. $1 - \nu'_{x'z'} > 2\left(E'_{x'}/E'_{y'}\right)\nu'_{y'x'}$

5.7 Hyperbolic $E - B$ Model

The Hyperbolic model (Duncan et al., 1980) is sometimes referred to as the hyperbolic $E - B$ constitutive model because the bulk modulus (B) is constant during loading while the elastic modulus (E) varies according to a hyperbolic relationship (Duncan and Chang, 1970). The assumptions regarding the formulation result in non-linearity of the stress-strain response and volumetric response during primary loading. The elastic modulus, and therefore the elastic shear modulus, tend towards zero at failure, resulting in no additional stress changes with continued straining, and therefore no additional volume changes, despite the assumption of a constant bulk modulus. The tendency towards zero volume change at failure is in keeping with the concept of a critical state.

5.7.1 Formulation

The Hyperbolic model captures the non-linear response of a drained triaxial test for a normally compressed specimen (i.e. primary loading). Such a test produces a plot of triaxial deviator stress $q = \sigma'_1 - \sigma'_3$ versus axial strain ε_1 that is described by a hyperbolic relationship (Figure 12; Konder, 1963):

$$\varepsilon_a = \varepsilon_1 = \frac{1}{E'_i} \frac{q}{\left(1 - \frac{q}{q_a}\right)} \quad for \;\; q < q_f \qquad \text{Equation 113}$$

where q_a the asymptotic value of the triaxial shear strength, E_i the initial small strain tangent stiffness quantity, and q_f the ultimate triaxial deviatoric shear strength given by the Mohr-Coulomb failure law:

$$q_f = \frac{2 \sin \phi'}{1 - \sin \phi'} (c' \cot \phi' + \sigma'_3) \qquad \text{Equation 114}$$

where c' and ϕ' are the peak effective stress cohesion and friction angle. The asymptotic shear strength is related to the ultimate deviator stress at failure q_f by:

$$q_a = \frac{q_f}{R_f} \qquad \text{Equation 115}$$

where R_f is the failure ratio, which for most soils is about 0.9.

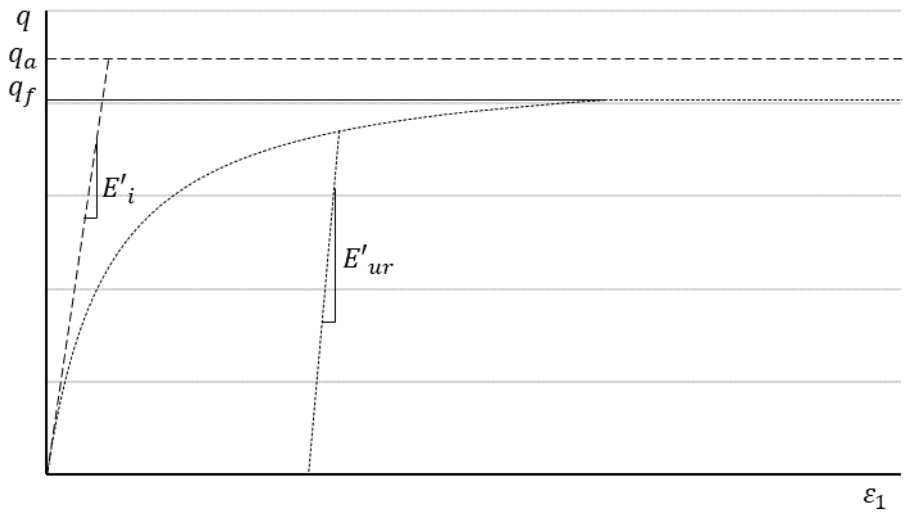

Figure 12. Conventional drained triaxial compression test on a soil described by the Hyperbolic $E-B$ model: $q-\varepsilon_1$ stress-strain plot.

Differentiating Equation 113 with respect to axial strain gives an expression for tangent stiffness E_t at any point on the $q-\varepsilon_1$ stress-strain curve (Duncan et al. 1980):

$$E'_t = \left(1 - \frac{q}{q_a}\right)^2 E'_i \qquad \text{Equation 116}$$

Substitution of Equation 114 and Equation 115 gives:

$$E'_t = \left(1 - \frac{R_f q(1-\sin\phi')}{2\sin\phi'\,(c'\cot\phi' + \sigma'_3)}\right)^2 E'_i \qquad \text{Equation 117}$$

Equation 117 can be used with a constant Poisson's ratio, ν', to calculate a tangent shear modulus (vis Equation 26):

$$G_t = \frac{E'_t}{2(1+\nu')} \qquad \text{Equation 118}$$

The initial, and constant, bulk modulus is calculated as:

$$K = \frac{E'_i}{3(1-2\nu')} \qquad \text{Equation 119}$$

Equation 118 and Equation 119 are in turn used to populate the elastic stiffness matrix (Equation 30), thereby completing the mathematical description of the Hyperbolic $E-B$ model, which, as noted, makes use of a constant bulk modulus (Equation 119) and a tangent stiffness modulus (Equation 118) that varies according to a hyperbolic relationship (Duncan and Chang, 1970). The Hyperbolic $E-B$ model also allows for the (indirect) specification of an unload-reload modulus E_{ur}.

5.7.2 Material Parameters

Table 5 summarizes the inputs required by the Hyperbolic $E-B$ model. The initial stiffness E_i can be assumed constant or made to vary spatially by means of an estimation technique. The unload-reload modulus E'_{ur}, which is depicted in Figure 12, is calculated by the software as:

$$E_{ur} = \frac{K_{ur}}{K_L} E_i \qquad \text{Equation 120}$$

where K_L is a modulus number. The ratio K_{ur}/K_L is a user input quantity. The value of K_{ur} is always larger than the value of K_L and may be 5 times greater than K_L for stiff soils such as dense sands and 3 times greater for soft soils, like loose sands (Duncan et al., 1980).

Table 5. Parameters for the Hyperbolic $E-B$ Model

Parameter	Symbol	Unit
Effective (peak) angle of shear resistance	ϕ'	
Effective cohesion	c'	
Initial stiffness (via drained triaxial)	E'_i	
Unload-reload stiffness ratio (via drained triaxial)	K_{ur}/K_L	
Unload-reload Poisson's ratio	ν'_{ur}	
Failure ratio q_f/q_a	R_f	

The initial modulus E'_i required by the Hyperbolic $E-B$ may vary considerably with the initial stresses. The stress dependency of the initial modulus can be estimated by (Janbu, 1963):

$$E'_i = K_L \left(\frac{\sigma'_{3i}}{p^{ref}} \right)^n p^{ref} \qquad \text{Equation 121}$$

where K_L is a modulus number, n an exponent that controls the degree of non-linearity, σ'_{3i} the initial minor principal effective stress, and p^{ref} the standard atmospheric air pressure, which is included in Equation 121 to make the expression independent of the unit system. A typical value of the modulus exponent is 0.5. The initial minor principal effective stress can be estimated from initial vertical effective stress and the at rest earth pressure coefficient as:

$$\sigma'^{i}_{3} \approx K_0 \sigma'^{i}_{y} \qquad \text{Equation 122}$$

5.7.3 Conceptual Response

Section 5.1 describes the approach being taken here to explore some of most important aspects of the Hyperbolic $E-B$ model. As noted, the reader is directed to the example files and the literature for a more complete discourse on the assumptions and/or limitations of any particular constitutive model.

The Hyperbolic $E-B$ model is not formulated based on elastic-plastic theory. Regardless, the basic idea of the Hyperbolic $E-B$ model is to manipulate the stiffness moduli to account for plastic, irrecoverable deformations. This is accomplished by reducing the stiffness as the deviatoric stress approaches the asymptotic value of the triaxial shear strength q_a (Equation 116). As such, the following discussion makes use of terminology often reserved for describing elastic-plastic constitutive models, such as 'yield' or 'plastic' straining', in order to identify the behaviour for what it is and to facilitate comparison with the other constitutive models.

Figure 13 depicts the conceptualized simulated results of a conventional drained triaxial test on a material represented by the Hyperbolic $E-B$ model. The results were generated assuming $K_{ur}/K_L > 1$ (Equation 120). It is assumed that the increments starts from stress state A lying on the p' axis and an arbitrary location in the $V-p'$ compression plane. The route by which point A in Figure 13 was reached in both the $p'-q$ effective stress plane and the $V-p'$ compression plane has been left vague. A numerical simulation could have been performed to isotopically compress the sample to a mean effective stress in excess of point A and then unloaded isotropically to A, leaving the soil theoretically overconsolidated. Regardless, the initial response would have been that of a normally compressed soil because the Hyperbolic material parameters do not contain an input to locate the 'yield surface' (i.e. maximum past deviator stress) in the $p'-q$ stress plane (e.g. through point B in Figure 13a) relative to the initial stress state, making it impossible to initiate (shear) loading in any form other than normal compression.

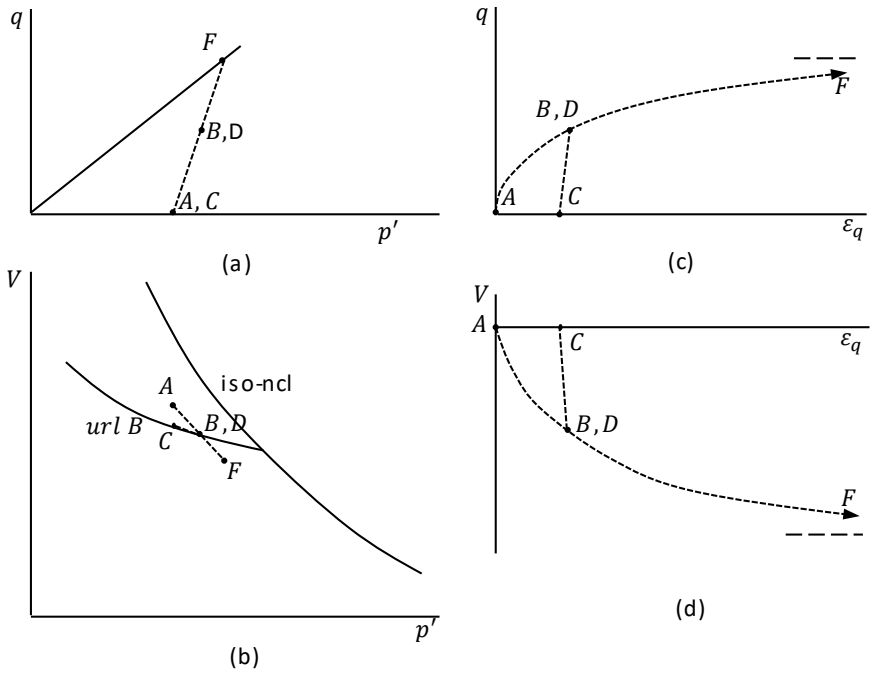

Figure 13. Conventional drained triaxial compression test on a soil described by the Hyperbolic $E-B$ model: $p'-q$ effective stress plane (with increments of plastic volumetric and deviatoric strain); (b) $V-p'$ compression plane; (c) $q-\varepsilon_q$ stress-strain plot; (d) $V-\varepsilon_q$ volume-strain plot.

The drained compression from A to B is associated with primary loading; that is, triaxial compression of a normally compressed specimen. Plastic strains develop from the onset of drained compression; therefore, the stress-strain plot $q-\varepsilon_q$ (Figure 13c) shows a continuous curve as the test proceeds. The tangent derivative at any point on the stress-strain curve $q-\varepsilon_q$ is equal to $3G_t$ (Equation 118). The slope would be equal to E'_t in Figure 13c had the deviatoric stress q been plotted against axial strain ε_a.

As already noted, Duncan et al. (1980) formulated the model using a constant bulk modulus to ensure that the volumetric strain goes to zero at failure. From the specific volume V of the soil at A and B, the change in volume can be converted into a volumetric strain increment:

$$\delta\varepsilon_{pAB} = \frac{-\delta V_{AB}}{V_A} \qquad \text{Equation 123}$$

allowing a bulk modulus to be calculated as:

$$K' = \frac{\delta p'_{AB}}{\delta\varepsilon_{pAB}} \qquad \text{Equation 124}$$

The result obtained from the simulated result via Equation 124 is equivalent to that obtained more directly from Equation 119 using E'_i and ν.

The soil is unloaded at B and both B and C lie on the unloading-reloading line url B. The bulk modulus can again be calculated from the simulated response between B and C, but this time the value is equivalent to (see Equation 119):

$$K = \frac{E'_{ur}}{3(1-2\nu')} \qquad \text{Equation 125}$$

The unloading-reloading line $url\ B$ is governed by the unload-reload modulus E'_{ur}. A comparison of the initial response (AB) to the unloading response (BC) in the $V-p'$ compression plane (Figure 13b) reveals a contradiction in the formulation of the Hyperbolic $E-B$ model: the assumption of a constant bulk modulus causes the response in the $V-p'$ compression plane to always be governed by E'_i or E'_{ur}, even when the soil is undergoing primary loading (AB). Primary loading implies the development of plastic irrecoverable volume changes, but this is not properly reflected in the $V-p'$ compression plane (Figure 13b), hence the initial response (AB) was not drawn on the isotropic normal compression line. Stated another way, the material model captures the $q-\varepsilon_q$ response for primary loading, while the $V-p'$ response is more consistent with linear elasticity.

The soil shows a stiff elastic response on reloading from C to D. The stress-strain curve $q-\varepsilon_q$ shows a sharp drop in stiffness when plastic strains start to develop as the soil yields at D and it rejoins the continuous curve (Figure 13c). Similarly, the volume change from C to D is elastic, recoverable, and controlled entirely by E'_{ur} (Figure 13b); and the volume-strain curve $V-\varepsilon_q$ (Figure 13d) shows a sharp break at D.

As further increments of drained compression are applied between B and F, the deviator stress approaches the ultimate triaxial deviatoric shear strength q_f and the modulus G_t (Equation 118) tends towards zero. As such, the slope of the stress-strain curve $q-\varepsilon_q$ steadily decreases towards zero:

$$\frac{\delta q}{\delta \varepsilon_q^p} = 0 \qquad \text{Equation 126}$$

The gradient of the volume change curve as F is approached (Figure 13d plotted in terms of volumetric strain) is given by Equation 27 and Equation 29 with $G_t = 0$:

$$\frac{\delta \varepsilon_p}{\delta \varepsilon_q} = \frac{3G_t}{K'}\frac{\delta p'}{\delta q} = 0 \qquad \text{Equation 127}$$

Plastic shearing continues at constant effective stress ($\delta p' = 0$), and the loading can proceed no further unless the test were strain controlled. The curvature of the volume-strain curve $V-\varepsilon_q$ (Figure 13d) during primary loading (loading increments AB and DF) is a by-product of the mathematical relationship between q and ε_q (Equation 118), not the result of the mathematical description of the volumetric response for primary loading.

5.8 Mohr-Coulomb Model

5.8.1 Formulation

The Mohr-Coulomb failure law, which is adopted as the yield function, can be written in terms of principal stresses as shown in Equation 128, where c' and ϕ' are the effective stress cohesion and friction angle. A non-associated flow rule, Equation 129, is used for shear failure where ψ is the angle of dilation.

$$f_s(\sigma) = (\sigma_1 - \sigma_3) - (\sigma_1 + \sigma_3)\sin\phi' - 2c'cos\phi' \qquad \text{Equation 128}$$

$$g_s(\sigma) = (\sigma_1 - \sigma_3) - (\sigma_1 + \sigma_3)\sin\psi \qquad \text{Equation 129}$$

An optional tension criterion and plastic potential are:

$$f_t(\sigma) = \sigma_t - \sigma_3 = 0 \qquad \text{Equation 130}$$

$$g_t(\sigma) = -\sigma_3 \qquad \text{Equation 131}$$

where σ_t is the tensile strength.

Figure 14 provides a view of the Mohr-Coulomb yield surface in 3D principal stress space for a compression positive sign convention (i.e. the adopted sign convention), which reveals a six-sided hexagonal pyramid. The failure surface has a hexagonal cross section in the deviatoric plane (Figure 15). The Mohr Coulomb yield function is fixed in stress space and does not change in size when plastic strains

are developing; consequently, the model is often described as elastic-perfectly plastic. The yield function is coincident with the failure surface, so reference to the yield surface implies failure surface and vice versa.

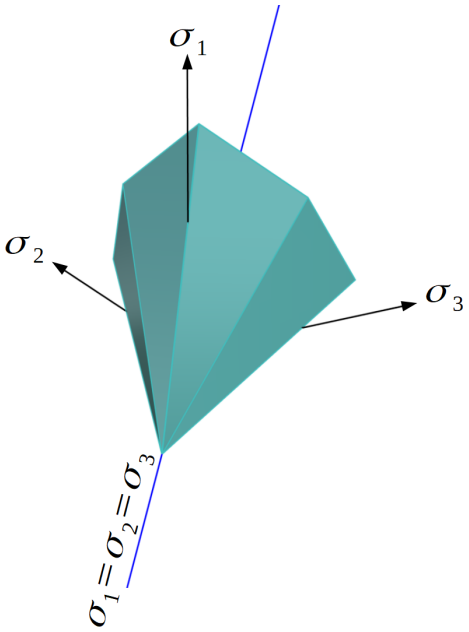

Figure 14 View of Mohr-Coulomb failure surface in 3D principal stress space (compression positive sign convention).

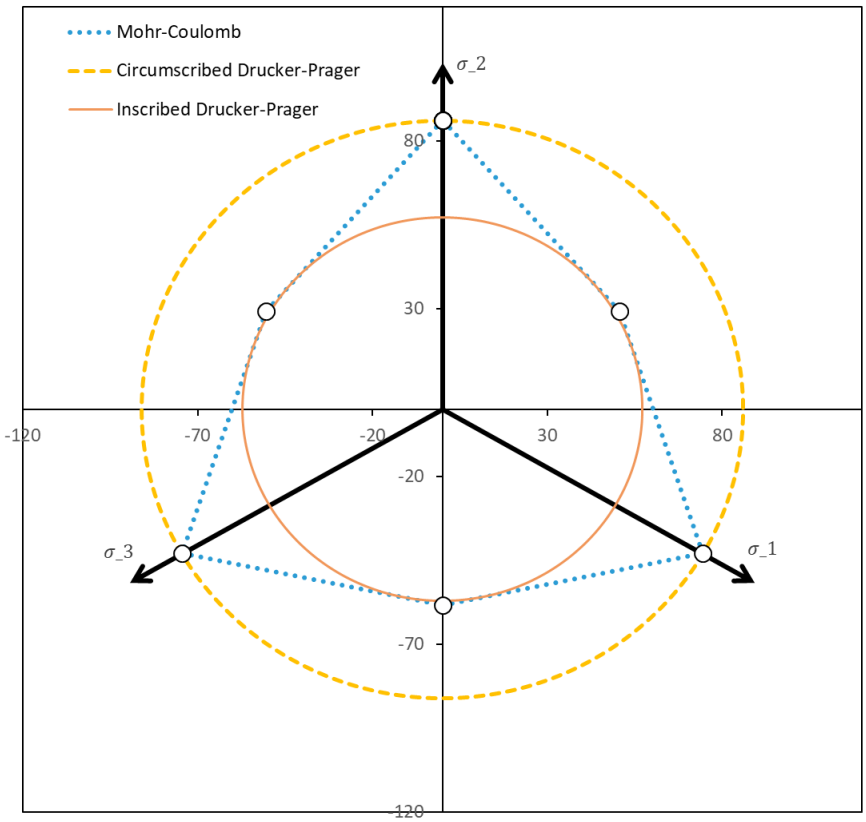

Figure 15. Mohr-Coulomb yield surface in the deviatoric plane with the Drucker-Prager yield surface circumscribed at $\theta = -\pi/6$ (compression) and fully inscribed.

The Mohr-Coulomb failure line in the $p' - q$ stress plane is essentially a cross-section along the space diagonal of the hexagonal pyramid (Figure 14). The orientation of the cross-sectional plane is defined by the Lode angle in the deviatoric plane (Figure 2). The relationship between p' and q and the corresponding stress invariants in principal stress space is given in Section 3.2. Only one side of the hexagonal pyramid is shown Figure 16 because q (Equation 15) is always positive.

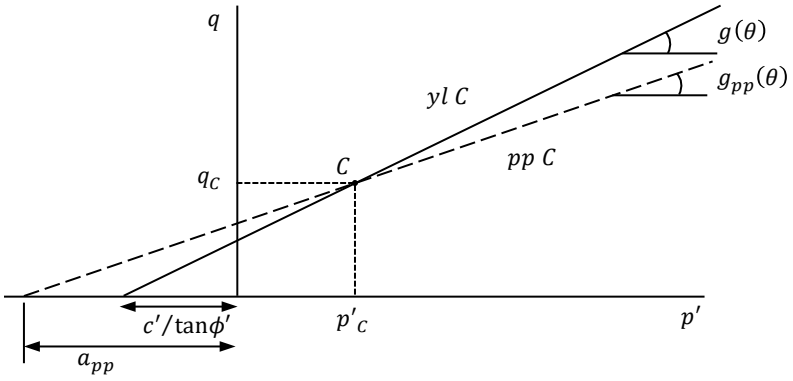

Figure 16. Mohr-Coulomb yield surface and plastic potential passing through the current stress state.

In addition to the six planes of the Mohr-Coulomb shear yield surface defined by Equation 128, Equation 130 defines three planes which truncate the Mohr-Coulomb hexagon at the tensile strength of the material (Figure 17). The tension criterion is optional in this model. If the tensile strength option is not used then the Mohr-Coulomb criterion is only used in the stress corrections. A similar behaviour occurs if the specified tensile strength is beyond the Mohr-Coulomb apex (where the Mohr-Coulomb surface meets the $\sigma_1 = \sigma_2 = \sigma_3$ line).

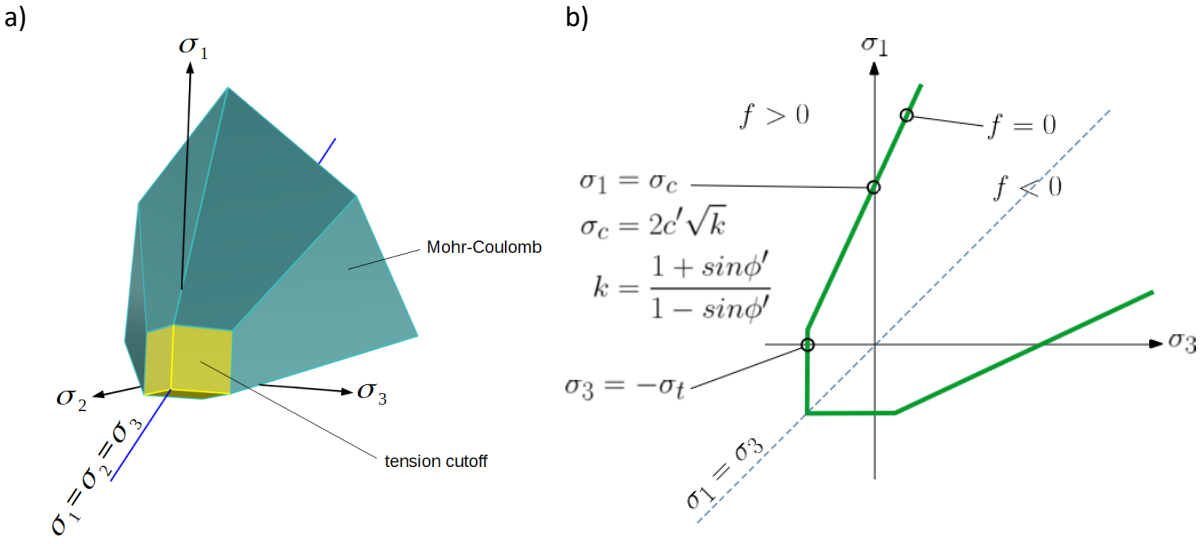

Figure 17 The Mohr-Coulomb and tensile yield surfaces (yellow) in a) principal stress space and b) a section through the $\sigma_1 - \sigma_3$ plane.

The following should be noted:

1. Application of the Mohr-Coulomb model to the simulation of an undrained response requires caution because the tendency for volume change is entirely elastic until the stress path intersects the yield surface. The pore-water pressure response can therefore be underestimated if the soil yields – transitions from elastic to elastic-plastic behaviour – prior to reaching failure. This being the case, and as already noted, the application of the Mohr-Coulomb model is generally understood to imply that the material is overconsolidated and that it will exhibit an abrupt transition from stiff (rigid) elastic to perfect plasticity behaviour when the stress state reaches the yield (i.e. failure) surface.
2. A critical state condition is defined by two requirements: $\delta\varepsilon_p^p/\delta\varepsilon_q^p = 0$ and $\delta q/\delta\varepsilon_q^p = 0$. Clearly the first of these conditions is not met if the dilation angle $\psi > 0$; that is, plastic volumetric strains continue to develop indefinitely with additional shearing. The Mohr-Coulomb Hardening/Softening model (Section 5.9) overcomes this deficiency.

5.8.2 Material Parameters

Table 6 summarizes the inputs required by the Mohr-Coulomb model. The elastic response is described by isotropic linear elasticity and therefore requires two independent elastic parameters: effective elastic modulus E' and Poisson's ratio ν'.

Table 6. Parameters for the Mohr-Coulomb Model

Parameter	Symbol	Unit
Effective angle of shear resistance	ϕ'	°
Effective cohesion	c'	kPa
Angle of dilation	ψ	°
Tensile strength (a positive value)	σ_t	kPa
Effective elastic stiffness	E'	kPa
Poisson's ratio	ν'	
Coefficient of earth pressure for the overconsolidated state*	K_0^{oc}	

*The coefficient of earth pressure for the over-consolidated state K_0^{oc} is an optional parameter for establishing the initial stresses by means of a Gravity Activation analysis in combination with the K_0-procedure (Section 4.1.2).

5.8.3 Conceptual Response

Section 5.1 describes the approach being taken here to explore some of most important aspects of the Mohr-Coulomb model. As noted, the reader is directed to the example files and the literature for a more complete discourse on the assumptions and/or limitations of any particular constitutive model. A comparative study of the stress-strain response of the Hardening/Softening Mohr-Coulomb (Section 5.9.3) is insightful because this constitutive model expands the basic functionality of the Mohr-Coulomb model.

Figure 18 depicts the conceptualized simulated results of a conventional drained triaxial test on a dilative material $(\psi > 0)$ represented by the Mohr-Coulomb model. It is assumed that the increments start from stress state P lying on the p' axis and at a point in the $V - p'$ compression plane associated with url Q. As noted in Section 5.7.3, the route by which the starting point (P) in Figure 13 was reached in both the $p' - q$ effective stress plane and the $V - p'$ compression plane has been left vague. The response of the Mohr-Coulomb model is independent of the initial state in the compression plane; consequently, it is rather paradoxical to display an unloading-reloading line and isotropic normal compression line in Figure 18b. Having stated this, the application of the Mohr-Coulomb model implies that the material will behave elastically until failure, at which point the behaviour transitions to perfect plasticity. This behaviour is generally associated with overconsolidated states, which implies an initial $V - p'$ state that is on an unload-reload line. This realization not does not preclude the use of the Mohr-Coulomb model to approximate the response of lightly to normally compressed (and likely non-dilative) soil; however, Figure 18b stands as a reminder of the generally accepted implicit assumption of an overconsolidated state when applying the elastic-perfectly plastic Mohr-Coulomb model.

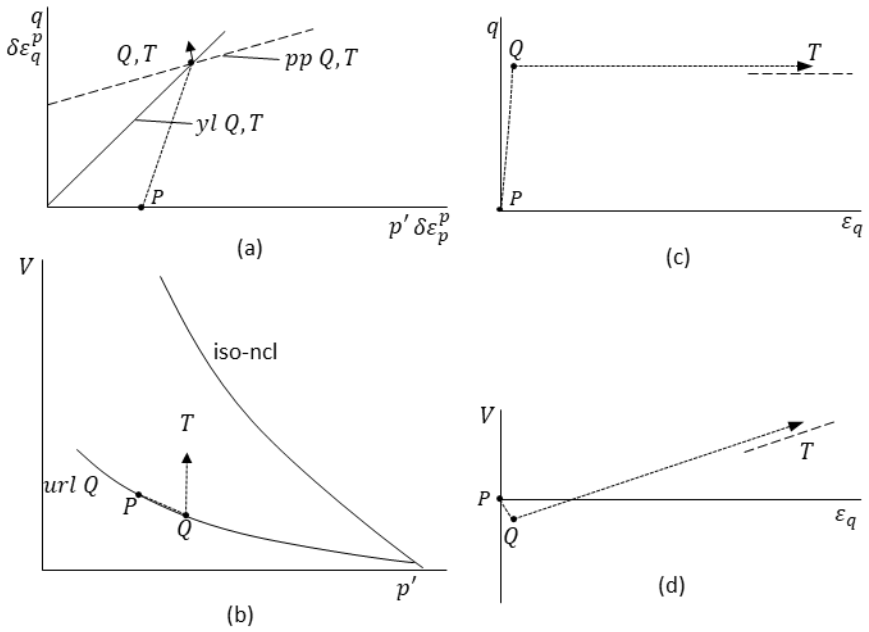

Figure 18. Conventional drained triaxial compression test on a soil described by the Mohr-Coulomb model: (a) $p' - q$ effective stress plane (with increments of plastic volumetric and deviatoric strain); (b) $V - p'$ compression plane; (c) $q - \varepsilon_q$ stress-strain plot; (d) $V - \varepsilon_q$ volume-strain plot.

The stress increment PQ represents changes in stress lying inside the yield locus. Point Q can be located in the compression plane by projection onto an unloading-reloading line url Q (Figure 18a). The change in volume from P to Q is purely elastic and associated with the a change in mean effective stress $\delta p'$. From the specific volume V of the soil at Q, the recoverable change in volume can be converted to an elastic volumetric strain:

$$\delta\varepsilon_{pPQ}^e = \frac{-\delta V_{PQ}^e}{V_P} \qquad \text{Equation 132}$$

allowing the elastic bulk modulus to be calculated:

$$K' = \frac{\delta p'_{PQ}}{\delta\varepsilon_{pPQ}^e} \qquad \text{Equation 133}$$

The result obtained from the simulated result via Equation 133 is equivalent to that obtained more directly from Equation 28 using E' and ν'. The slope of the dotted unloading-reloading line between P and Q is uncharacteristically linear because of the assumption of isotropic linear elasticity.

The yield locus remains fixed in size as further increments QT of drained compression are applied (Figure 18a). Perfect plasticity is achieved at Q and points Q and T lie in the same position on the yield surface (Figure 18a). From point Q onwards, the stress ratio $\eta = q/p'$ is constant and the slope of the

stress-strain curve $q - \varepsilon_q$ abruptly reduces to zero (Equation 126). Plastic shearing continues at constant effective stress ($\delta p' = 0$), and the loading can proceed no further unless the test was strain controlled.

Similarly, point Q marks an abrupt inflection point in the $V - p'$ compression plane (Figure 18b) and $V - \varepsilon_q$ volume-strain plot (Figure 18d). At Q, the plastic strain increment vector points to the left, indicating that continued increases in shear strain are going to be associated with negative plastic volumetric strains; that is, plastic volumetric expansion. The changing specific volume as the shear strain increases is controlled entirely by the irrecoverable plastic volumetric strain because the elastic contribution is zero (i.e. $\delta p' = 0$). The ratio of plastic shear strain to plastic volumetric strain remains constant because the outward normal to the plastic potential does not evolve with further loading (Figure 18a). Recall that the plastic potential is of fixed size but can move to pass through the current stress state (Section 5.8.1). The relative magnitudes of the plastic volumetric strain and plastic shear strain $\delta\varepsilon_p^p / \delta\varepsilon_q^p$ are governed entirely by the dilation angle.

5.9 Hardening/Softening Mohr-Coulomb Model

One of the drawbacks of the Mohr-Coulomb model (Section 5.8) is that it simulates continued dilation upon yielding. In reality, soil may dilate initially when a stress path encounters the yield surface, but will eventually reach a constant volume condition at larger strains. Furthermore, dilative soil often exhibits a rapid increase in shear stress up to a peak value over a small change in shear strain, and then a decrease in shear stress with increasing shear strain (i.e., strain softening), ultimately reaching a constant value referred to as the critical state (Figure 19a). The critical state shear stress corresponds to no further volume change with continued shearing (Figure 19b). Figure 19b depicts the calculation of the peak dilation angle from the results of a shear box test. Naturally other expressions exist for different testing procedures, such as that pertaining to the use of Mohr's circle of plastic strains from a drained triaxial compression test.

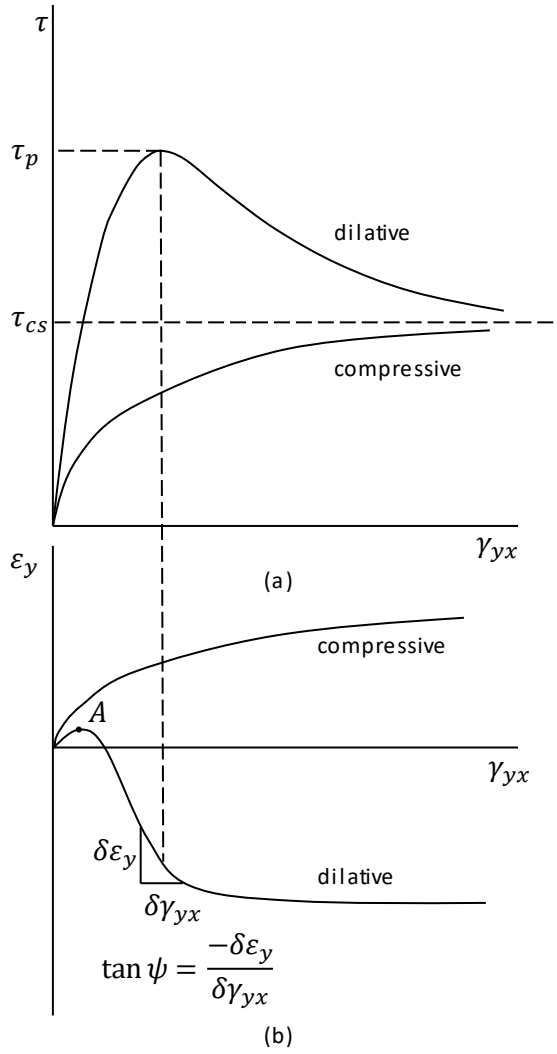

Figure 19. Response of soils to direct shearing.

5.9.1 Formulation

Consider a non-linear peak failure envelop corresponding to a dilative soil (Figure 20). Coulomb's failure law can be written as:

$$\tau_f = c' + \sigma'_n \tan\left(\phi'_m\right) \qquad \text{Equation 134}$$

where the mobilized effective friction angle is given by:

$$\phi'_m = \phi'_{cs} + \psi_m \qquad \text{Equation 135}$$

where ϕ'_{cs} is the critical state friction angle and ψ_m is the mobilized dilation angle. Equation 135 becomes a stress-dilatancy relationship linking the mobilized friction angle ϕ'_m with an angle of dilation ψ and an assumed constant critical state friction angle ϕ'_{cs} (Wood, 1990). The relationship between ϕ'_m and ψ_m has been deliberately left vague because the link between the two properties would be

revealed by means of lab testing. By way of contrast, the Hardening Soil model (Schanz et al. 1999) prescribes a stress-dilatancy relation that links the mobilized friction angle ϕ'_m to the mobilized dilation angle ψ_m (Rowe 1962, 1971).

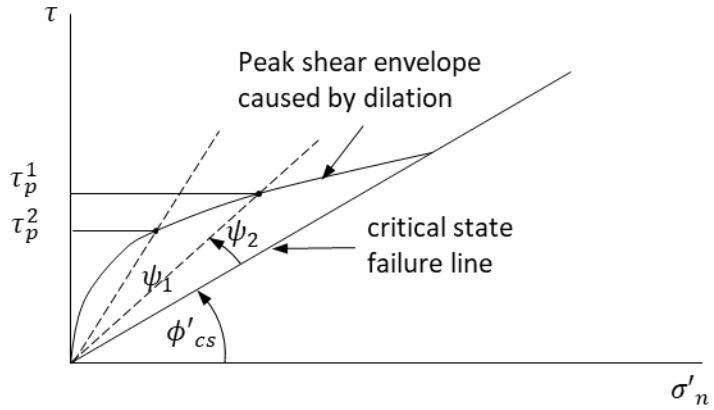

Figure 20. Effects of dilation on Coulomb's peak strength failure envelope.

Figure 20 can be viewed as compilation of test results – such as those shown in in Figure 19 – that depicts the role of dilation in effecting the shear strength of soil along with the suppression of dilative behaviour with increasing normal stress. The results of a specific test (e.g. Figure 19) could be used to determine the evolution of the dilation angle ψ_m with accumulated deviatoric plastic strain at a specific effective normal stress (Taylor, 1948). Equation 135 could then be used to deduce the relationship between ϕ'_m and accumulated deviatoric plastic strain. Various testing procedures (e.g. conventional triaxial compression), which are described in detail in a plethora of testing standards, textbooks, and journal articles, offer more sophisticated data interpretation strategies than a direct application of Equation 135.

Regardless of the testing and data interpretation procedures, the properties c', ϕ'_m, ψ_m can all be made to vary with accumulated plastic deviatoric strain ε_q^p defined by Equation 19 via Equation 17 or a simplified variant of Equation 17 for a particular testing procedure (e.g. Equation 49 for drained triaxial compression). It is important to note that the accumulated deviatoric strain quantity ε_q^p comprises only the plastic part; that is, the elastic part is subtracted from the (total) accumulated deviatoric strain at each stage of the test:

$$\varepsilon_q^p = \varepsilon_q - \varepsilon_q^e \qquad \text{Equation 136}$$

Again, the appropriate resources should be consulted to determine how to isolate the elastic component from the accumulated deviatoric strain at each stage of a test. In the case of a triaxial test, a simplified procedure might involve a single unloading-reloading stage to obtain the accumulated deviatoric elastic strain. Wood (1990) notes that for many materials, the contribution of elastic strains may be negligible when yielding is occurring, and the difference between a plastic strain increment and a total stain increment ratio may be small. Wood (1990) does, however, suggest caution, particularly if

the test is undrained, because the total stain increment $\delta\varepsilon_p^{\square}/\delta\varepsilon_q^{\square} = 0$ as the volume is constant, but the condition of constant volume requires the plastic strain increment $\delta\varepsilon_p^p/\delta\varepsilon_q^p \neq 0$.

Figure 21a shows an example with three distinct zones of behaviour described by linearized variations in the properties. The mobilized values of c', ϕ', ψ increase from their initial values (subscript i) linearly in zone 1 up to the peak values (subscript p), remain constant and equal to the peak values through zone 2, and finally decrease in zone 3 to a residual value (subscript r) or to zero in the case of ψ. The three zones are associated with hardening (i.e. expansion of the purely elastic zone define by the yield surface), perfect plasticity, and softening (i.e. contraction of the yield surface), respectively. Figure 21b shows only two distinct zones of behaviour associated with hardening and perfect plasticity, respectively, assuming a constant cohesion. The yield locus initiates on the p' axis in the $p' - q$ stress plane ($\phi'_i = 0$), which means that plastic straining initiates immediately with positive shear strains. The dilation angle is zero (i.e. zero plastic volumetric straining) until the mobilized friction angle reaches the critical state value, at which point the dilation angle increases steadily with the mobilized friction angle to the peak values. This type of behaviour is characteristic of the Hardening Soil model (Schanz et al. 1999).

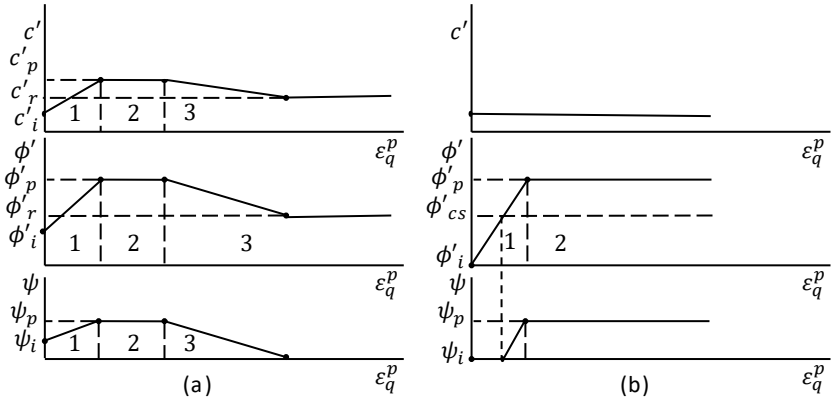

Figure 21. Examples of variations of c', ϕ', ψ with accumulated deviatoric plastic strain: a) hardening, perfect plasticity, and softening; b) hardening followed by perfect plasticity

The yield function of the H/S Mohr-Coulomb model retains its hexagonal cross section in the deviatoric plane (Figure 15); however, the slope of the yield locus in the $p' - q$ stress plane (Figure 16) changes in accordance with the mobilized friction angle ϕ'_m. In addition, the hexagonal pyramid slides along the space diagonal in accordance with the variations of cohesion c'. The plastic potential, which is also a hexagonal pyramid in 3D principal stress space, changes in a similar manner, but its slope in the $p' - q$ stress plane changes in accordance with the mobilized dilation angle ψ_m. The following should be noted:

1. The ability to specify c', ϕ', ψ, and σ_t as functions of the accumulated deviatoric plastic strain allows for a range of behaviours to be simulated by the H/S Mohr-Coulomb model. For example, the conventional elastic-perfectly plastic Mohr-Coulomb model (Section 5.8) is recovered if c', ϕ', and ψ are constant functions of accumulated deviatoric plastic strain ε_q^p. Alternatively, the

functions could be defined to simulate hardening followed by perfectly plasticity (zones 1 and 2 in Figure 21b), or softening-only behavior (Section 5.9.3) and so on.

2. By way of contrast, and as indicated by the material model name, the Hardening Soil model (Schanz et al. 1999) cannot simulate a reduction in strength from peak to critical state (or a residual state) that is associated with plastic softening.
3. The H/S Mohr-Coulomb and conventional Mohr-Coulomb model do not prescribe a surface bounding the elastic zone along the space diagonal in principal stress space. The Hardening Soil model (Schanz et al. 1999) addresses this deficiency via introduction of a 'cap' yield surface on the hexagonal cone.

5.9.2 Material Parameters

The elastic response is described by isotropic linear elasticity and therefore requires two independent elastic parameters: effective elastic modulus E' and Poisson's ratio ν'.

Table 7. Parameters for the Hardening/Softening Mohr-Coulomb Model

Parameter	Symbol	Unit
Effective angle of shear resistance as a function of ε_q^p	ϕ'	°
Effective cohesion as a function of ε_q^p	c'	kPa
Angle of dilation as a function of ε_q^p	ψ	°
Tensile strength (a positive value) as a function of $\left\|\varepsilon_3^p\right\|$	σ_t	kPa
Effective elastic stiffness	E'	kPa
Poisson's ratio	ν'	
Coefficient of earth pressure for the overconsolidated state*	K_0^{oc}	

*The coefficient of earth pressure for the over-consolidated state K_0^{oc} is an optional parameter for establishing the initial stresses by means of a Gravity Activation analysis in combination with the K_0-procedure (Section 4.1.2).

5.9.3 Conceptual Response

Section 5.1 describes the approach being taken here to explore some of most important aspects of the H/S Mohr-Coulomb model. As noted, the reader is directed to the example files and the literature for a more complete discourse on the assumptions and/or limitations of any constitutive model. The comparable explorations of the Hyperbolic $E-B$ model (Section 5.7.3) and Mohr-Coulomb model (Section 5.8.3) should be consulted before reading this section in order to gain additional insights into the stress-strain response of this model.

Figure 22 depicts the conceptualized simulated results of a conventional drained triaxial test on a material represented by the H/S Mohr-Coulomb model. The parameters ϕ' and ψ are assumed to vary with accumulated deviatoric plastic strain (Figure 23) while the effective cohesion c' was assumed zero. As with the drained triaxial test discussed in Section 5.8.3, it is assumed that the increments start from stress state P lying on the p' axis and at a point in the $V-p'$ compression plane associated with url Q. The apparent contradiction of displaying an unloading-reloading line and isotropic normal compression line in Figure 22b was discussed above.

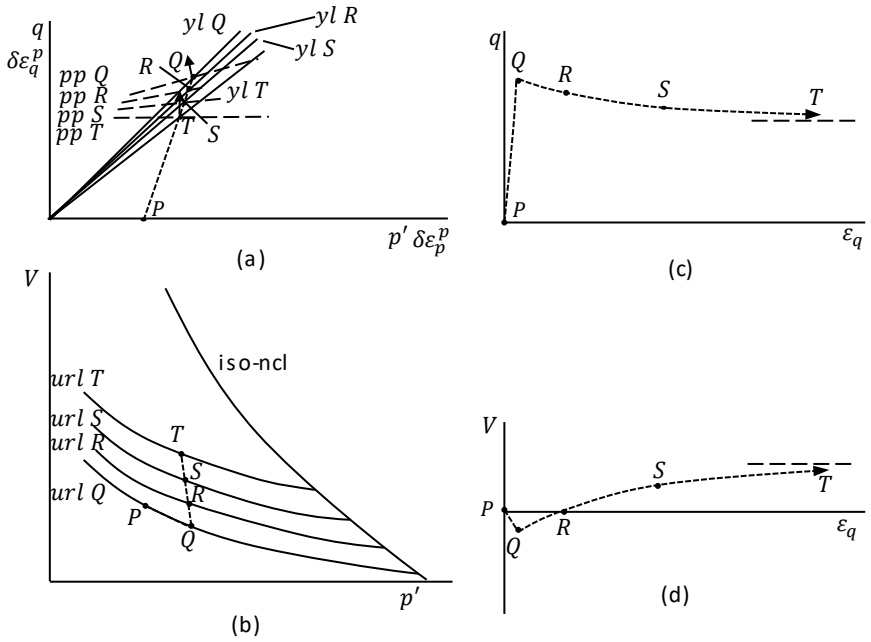

Figure 22. Conventional drained triaxial compression test on a soil described by the H/S Mohr-Coulomb model: $p' - q$ effective stress plane (with increments of plastic volumetric and deviatoric strain); (b) $V - p'$ compression plane; (c) $q - \varepsilon_q$ stress-strain plot; (d) $V - \varepsilon_q$ volume-strain plot.

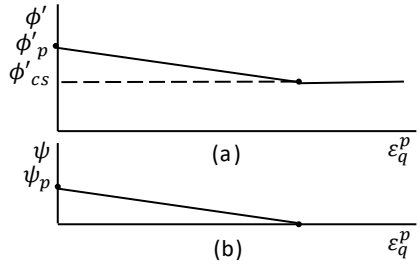

Figure 23. Variation of ϕ', ψ with accumulated deviatoric plastic strain for the triaxial compression test shown in Figure 22.

The drained compression from P to Q represents changes in stress lying inside the yield locus and are consequently purely elastic processes (Figure 22a). The soil exhibits a stiff elastic response on drained compression from P to Q that is clearly reflected in the $V - p'$ compression plane (Figure 22b), the stress-strain curve $q - \varepsilon_q$ (Figure 22c), and volume-strain curve $V - \varepsilon_q$ (Figure 22d). The simulated result thus far is in exact agreement with that presented in Section 5.8.3. Both P and Q lie on the unloading-reloading line url P and the total deviatoric strain comprises only an elastic component $\varepsilon_q = \varepsilon_q^e$.

The peak friction angle ϕ'_p (Figure 23a) controls the initial size of the yield locus yl Q. The drained compression from P to Q mobilized the maximum frictional resistance $\left(\phi'_m = \phi'_p\right)$. At Q, the plastic strain increment vector on the plastic potential pp Q points to the left, indicating that that if a continued increase in shear strain is to occur, with plastic shear strains of the same sign as the preceding elastic

shear strains (i.e. positive), then negative plastic volumetric strain must occur; that is, plastic volumetric expansion (Wood, 1990).

The development of deviatoric plastic strain ε_q^p is associated with a reduction in the effective friction angle ϕ' (Figure 23), which requires a contraction in the yield surface. As a result, the effective stress path must retreat back towards P, otherwise the stress state would exist in illegal stress space. The progress of the test is deduced in the compression plane (Figure 22b) by projecting the points R, S, and T in the stress plane (Figure 22a) from their yield loci yl R, yl S, and yl T downwards to the simulated specific volume.

As the yield locus contracts in accordance with ϕ' (Figure 23a), the plastic potential moves to pass through the current stress state and its slope evolves in accordance with the functional relationship in Figure 23b. The direction of the plastic strain increment vector gradually approaches the vertical until at T, plastic shear deformation can continue without plastic change in volume. The initial rise in q and decrease in volume (PQ) was followed by a drop in q and increase in V towards the limiting values at T. The sharpness of the break in the stress-strain curve $q - \varepsilon_q$ (Figure 22c) and volume-strain curve $V - \varepsilon_q$ (Figure 22d) at Q depends on the functional relationship between c', ϕ', ψ and the deviatoric plastic strain ε_q^p.

5.10 Hardening Soil Model

The Hardening Soil Model (Schanz et al. 1999) shares two key attributes with the H/S Mohr-Coulomb model described in Section 5.9: 1) it can simulate an increase in shear strength up to a peak value over a limited range of shear strain (i.e. shear hardening), ultimately reaching a constant, critical state, value; and, 2) it can simulate an evolving angle of dilation with shear straining. The Hardening Soil Model also differs from H/S Mohr-Coulomb model (Section 5.9) in a number of key respects: 1) it cannot simulate softening; 2) it can simulate plastic straining for stress paths that are predominately along the space diagonal in principal stress space (i.e. compression hardening); and, 3) it can simulate non-linear elastic behaviour.

The Hardening Soil model makes a distinction between shear hardening and compression hardening by means of two unique yield surfaces (Figure 24). These surfaces enclose the elastic domain. Consider an initial stress state P that is on both yield surfaces; that is, at the intersection of the surfaces in Figure 24. The behaviour of the soil will depend on the direction of the stress path. A stress path directed below both yield surfaces into zone 1 produces nonlinear elastic strains. A shear path directed into zone 2 produces elastic-plastic behaviour with the cap yield surface active and expanding (i.e. hardening). The shear yield surface remains stationary. A stress path directed into zone 3 produces elastic-plastic behaviour and expands both yield surfaces simultaneously. Lastly, a stress path directed into zone 4 activates and expands the shear yield surface while the cap surface remains stationary. The name of the constitutive model portends the increasing shear strength associated with hardening; that is, expansion of the purely elastic zone defined by the shear and cap yield surfaces.

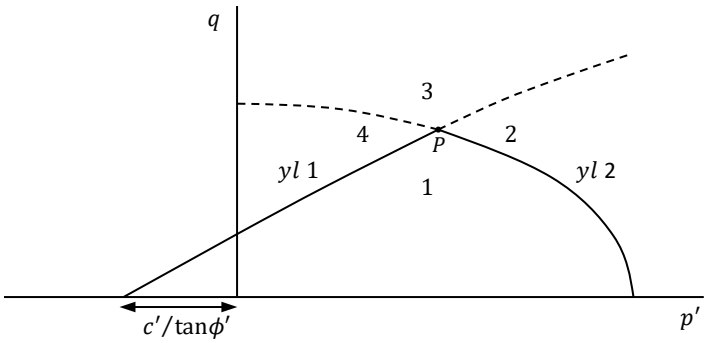

Figure 24. Yield surfaces for the Hardening Soil model.

5.10.1 Formulation

A key ingredient of the mathematical formulation of the Hardening Soil model is a stress dependent stiffness modulus, denoted E'_{50}, that can be measured in a drained triaxial test. Consider a plot of triaxial deviator stress $q = \sigma'_1 - \sigma'_3$ versus axial strain ε_a for a drained triaxial test of a normally compressed specimen (Figure 25). The primary loading stress-strain path can be described by the hyperbolic relationship given by Equation 113, which requires knowledge of an initial small strain tangent stiffness quantity E_i, the ultimate triaxial deviatoric shear strength q_f (Equation 114), and asymptotic value of the triaxial shear strength q_a (Equation 115).

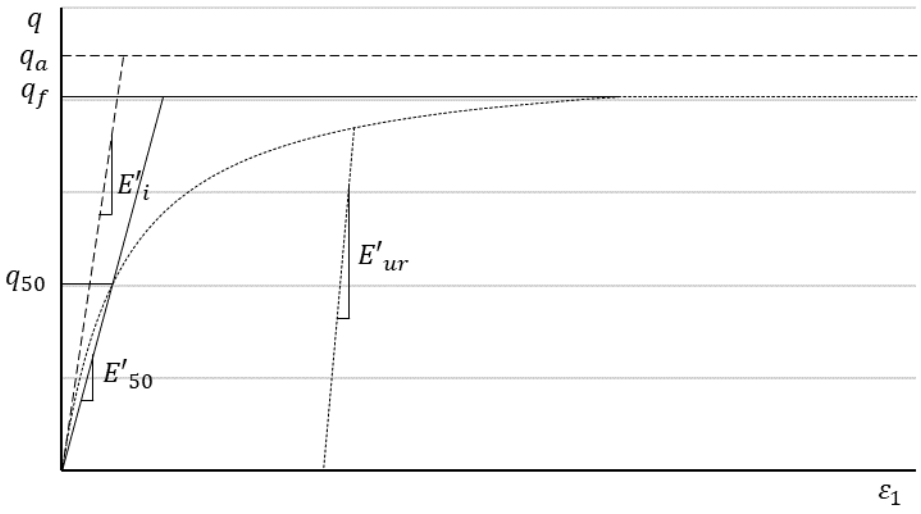

Figure 25. Simulation of a conventional drained triaxial test using the Hardening Soil model.

The stiffness E_i is a small strain tangent slope that is generally difficult to measure (Figure 25). A more easily measured value is the secant stiffness E'_{50}, corresponding to a line passing through the $q - \varepsilon_1$ stress-strain data at a deviator stress $q = 0.5(q_f)$. The stiffness E_i is related to E'_{50} by:

$$E'_i = \frac{2E'_{50}}{2 - R_f}$$ Equation 137

where E'_{50} is given:

$$E'_{50} = E'^{ref}_{50} \left(\frac{c' \cos\phi' + \sigma'_3 \sin\phi'}{c' \cos\phi' + p^{ref} \sin\phi'} \right)^m$$ Equation 138

and σ'_3 is the effective minor principal stress, which is equal to the confining stress in a triaxial test, p^{ref} a reference confining stress, and m an exponent that controls the amount of stress dependency. The reference stiffness E'^{ref}_{50} is generally measured at a reference confining stress p^{ref} of 100 kPa. A logarithmic $q - \varepsilon_1$ relationship, typical of soft clays, is obtained if $m = 1$. Norwegian sands and silts are represented by $0.5 < m < 1.0$ (Janbu, 1963 and von Soos, 1990).

It is important to note that the stiffness quantities E_i and E'_{50} are not elastic properties. The elastic response in zone 1 (Figure 24) is described by isotropic elasticity and therefore requires two independent elastic parameters. The Hardening soil model adopts a stress dependent effective elastic modulus determined from an unloading-reloading stress path, E'_{ur}, and a constant Poisson's ratio, ν'_{ur}, that is also specific to unloading-reloading (Figure 25). The expression for the modulus E'_{ur} has the same form as Equation 138:

$$E'_{ur} = E'^{ref}_{ur} \left(\frac{c' \cos\phi' + \sigma'_3 \sin\phi'}{c' \cos\phi' + p^{ref} \sin\phi'} \right)^m$$ Equation 139

The reference stiffness E'^{ref}_{ur} is measured at a reference confining stress p^{ref} (e.g. 100 kPa). Section 5.10.2 presents some typical relationships between E_i and E'_{ur}.

5.10.1.1 Shear Hardening

The Hardening Soil model adopts a shear yield function that comprises the hyperbolic relationship (Equation 113), which in turn comprises the Mohr-Coulomb failure law (Equation 114 and Equation 115):

$$F_1(\{\sigma'\}, \{k_1\}) = \bar{F}_1 - \gamma^p$$ Equation 140

where $\bar{F}_1$ is given by:

$$\bar{F}_1 = \frac{2}{E_i} \frac{q}{1 - \frac{q}{q_a}} - \frac{2q}{E_{ur}}$$ Equation 141

and γ^p is a frictional hardening parameter that is calculated from the accumulated plastic strain components as:

$$\gamma^p = 2\varepsilon_1^p - \varepsilon_p^p \qquad \text{Equation 142}$$

The yield surface retains a hexagonal cross section in the deviatoric plane (Figure 15) but can be slightly curved in the $p' - q$ stress plane (Figure 26). The nonlinearity of any particular yield loci in the $q - p'$ stress space arises from stress dependency of the stiffness properties (Equation 138 and Equation 139), which is controlled by the exponent m. Straight lines are obtained if $m = 1$ whereas the curvature is noticeable if $m = 0.5$, which is typical for stiff soils (Figure 26). As failure is approached, the yield function theoretically reverts to that of Mohr-Coulomb, becoming linear in the $p' - q$ stress plane even if $m \ll 1.0$ (Figure 26).

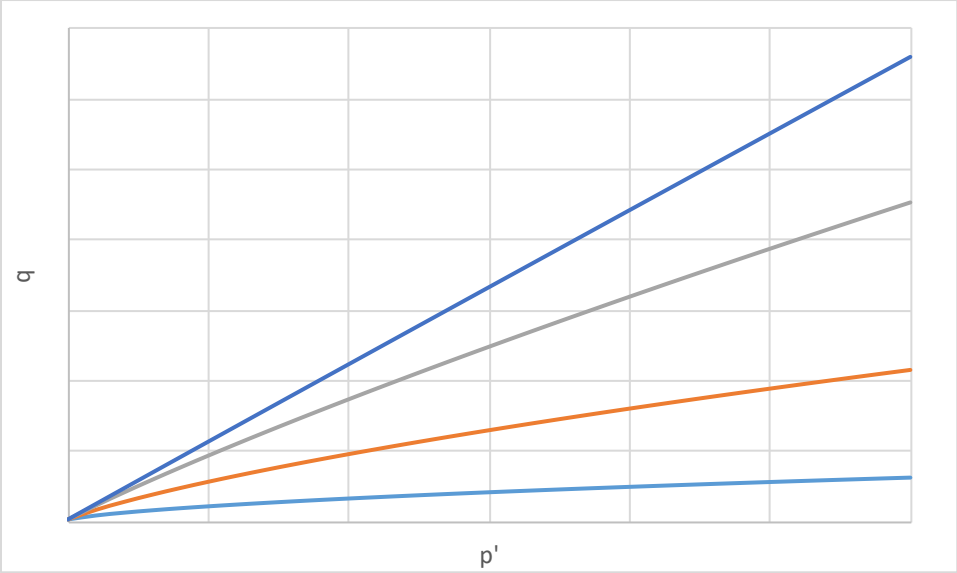

Figure 26. Successive yield loci for various values of the hardening parameter γ^p and $m = 0.5$.

The current size of the shear yield function is controlled by a measure of accumulated plastic shear strain γ^p ($\gamma^p \approx 2\varepsilon_q^p$), hence the successive yield loci in Figure 26 correspond to increasing values of γ^p. For a stress state on a particular yield locus in Figure 26, the mobilized friction angle ϕ'_m can be calculated as (Rowe, 1962):

$$\sin \phi'_m = \frac{\sigma'_1 - \sigma'_3}{\sigma'_1 + \sigma'_3 - 2c' \cot \phi'} \qquad \text{Equation 143}$$

which reveals that γ^p is implicitly linked to a mobilized friction angle ϕ'_m, which is not unlike the

accumulated plastic deviatoric strain ε_q^p being explicitly linked to the mobilized friction angle ϕ'_m in the H/S Mohr-Coulomb model (Figure 21b).

The plastic potential associated with shear yield surface is given by:

$$P_1(\{\sigma'\},\{m_1\}) = \frac{(\sigma'_1 - \sigma'_3)}{2} - \frac{(\sigma'_1 + \sigma'_3)}{2}\sin\psi_m \qquad \text{Equation 144}$$

where ψ_m is the mobilized dilation angle. The expression for the plastic potential is the same as that of the Mohr-Coulomb model, which is a hexagonal pyramid in 3D principal stress space and a straight line in the $p' - q$ stress plane (Figure 16). The dilation angle ψ controls the slope of the plastic potential in the $p' - q$ stress plane ($g_{pp}(\theta)$ in Figure 16), which controls the relative magnitude of dilative (expansive) or contractive (positive) plastic volumetric strain when the soil is yielded. The plastic potential adopted by the Hardening Soil model produces plastic strain increments that imply:

$$\delta\varepsilon_p^p = \sin\psi_m \, \delta\gamma^p \qquad \text{Equation 145}$$

when plastic deformations are occurring. The actual magnitude of the plastic strain increments is calculated from a flow rule of the form shown Equation 35.

The Hardening Soil model adopts the relationships between ψ_m and the mobilized friction angle ϕ'_m (Equation 143) that were established by Schanz and Vermeer (1996) based on the stress-dilatancy theory proposed by Rowe (1962). For a user specified peak friction angle, ϕ', and peak dilation angle, ψ, the mobilized dilation angle is given by:

$$\sin\phi'_m < (3/4)\sin\phi' \qquad \psi_m = 0 \qquad \text{Equation 146}$$

$$\sin\phi'_m \geq (3/4)\sin\phi' \;;\; \psi > 0 \qquad \sin\psi_m = \max\left(\frac{\sin\phi'_m - \sin\phi'_{cs}}{1 - \sin\phi'_m \sin\phi'_{cs}}, 0\right) \qquad \text{Equation 147}$$

$$\sin\phi'_m \geq (3/4)\sin\phi' \;;\; \psi \leq 0 \qquad \psi_m = \psi \qquad \text{Equation 148}$$

where ϕ'_{cs} is the critical state friction angle given by:

$$\sin\phi'_{cs} = \frac{\sin\phi' - \sin\psi}{1 - \sin\phi'\sin\psi} \qquad \text{Equation 149}$$

Notice that the maximum operator (max) ensures that the mobilized dilation angle (ψ_m) remains at zero until the mobilized friction angle ϕ'_m exceeds the critical state friction angle ϕ'_{cs} even if $\sin\phi'_m \geq (3/4)\sin\phi'$. The rules ensure that compression occurs for small stress ratios, characterized by $\phi'_m < \phi'_{cs}$, and that dilation occurs for high stress ratios characterized by $\phi'_m > \phi'_{cs}$. Figure 27 illustrates a

stress-dilatancy relationship generated by Equation 147 for assumed peak strength properties. The sharp break in the functional relationship occurs at the critical state friction angle ϕ'_{cs}. The Hardening Soil model implicitly links ψ_m to ϕ'_m (Equation 147), which is in turn linked to the current stress state and peak strength properties (Equation 143), which is in turn linked to the accumulated plastic shear strain $\gamma^p \approx 2\varepsilon_q^p$. The implicit relationships could therefore be elucidated by plotting a graph of the simulated ψ_m versus γ^p (or ε_q^p; refer to Section 5.10.3). Again, this is not unlike how the H/S Mohr-Coulomb model explicitly links the current slope of the plastic potential, characterized by ψ_m, to the accumulated plastic deviatoric strain ε_q^p via a user defined function (Figure 21b).

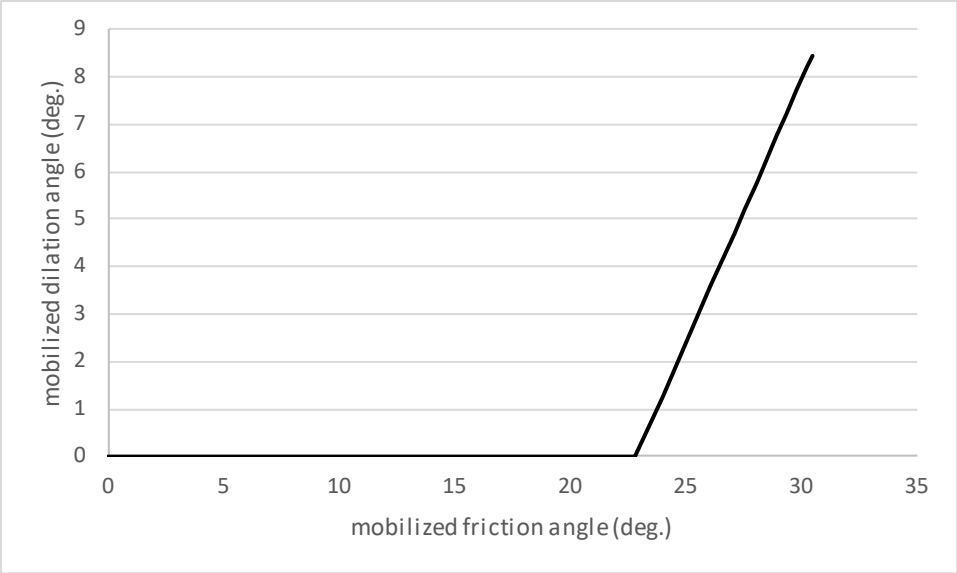

Figure 27. Mobilized dilation angle ψ_m versus mobilized friction angle ϕ'_m for peak friction and dilation angles of 30° and 8°, respectively, and cohesion of 8 kPa.

The following should be noted:

1. As indicated by the material model name, the Hardening Soil model cannot simulate a reduction in strength from peak to critical state (or a residual state) that is associated with plastic softening.
2. The mobilized dilation angle (Equation 147) remains at the peak value $\psi_m = \psi$ once the mobilized friction angle $\phi'_m = \phi'$, implying that plastic volumetric expansion will continue indefinitely with continued shearing. In actuality, the mobilized dilation angle should decrease to zero with continued shearing past the peak, causing the volumetric expansion to cease and the void ratio to reach a constant critical state value. Although the evolution of the dilation angle cannot be simulated post peak, the mobilized dilation angle can be toggled to $\psi_m = 0$ if the $e \geq e_{max}$, where the subscript max indicates the maximum. The specification of a maximum void ratio e_{max} is referred to as a dilatancy cut-off.

5.10.1.2 Compression Hardening

The plastic compression strains, which are generated by compression (p') dominant stress paths (zone 2 in Figure 24), are governed by another yield surface that caps the open end of the shear hardening surface (Cudny and Truty, 2020):

$$F_2(\{\sigma'\},\{k_2\}) = \frac{q^2}{M^2 g^2(\theta)} + {p'}^2 - {p_p}^2 \qquad \text{Equation 150}$$

where q and p' are generalized stress invariants (Section 3.2):

$$g(\theta) = \left(\frac{1-\beta\sin(3\theta)}{1+\beta}\right)^n \qquad \text{Equation 151}$$

$$\beta = \frac{1-k^{\frac{1}{n}}}{1+k^{\frac{1}{n}}} \qquad \text{Equation 152}$$

$$k = \frac{3-\sin\phi'}{3+\sin\phi'} \qquad \text{Equation 153}$$

and M is a secondary model parameter that is calculated from the earth pressure coefficient K_0^{nc} that is given by Jaky's relationship:

$$K_0^{nc} = 1 - \sin\phi' \qquad \text{Equation 154}$$

In principal stress space, the can be described as a rounded hexagonal ellipsoid (Figure 28). The cap yield locus is revealed as an ellipse in the $p' - q$ stress plane for any given Lode angle (Figure 24) and as a rounded hexagon in the deviatoric plane that wraps the original function proposed by Schanz and Vermeer (1996; Figure 29).

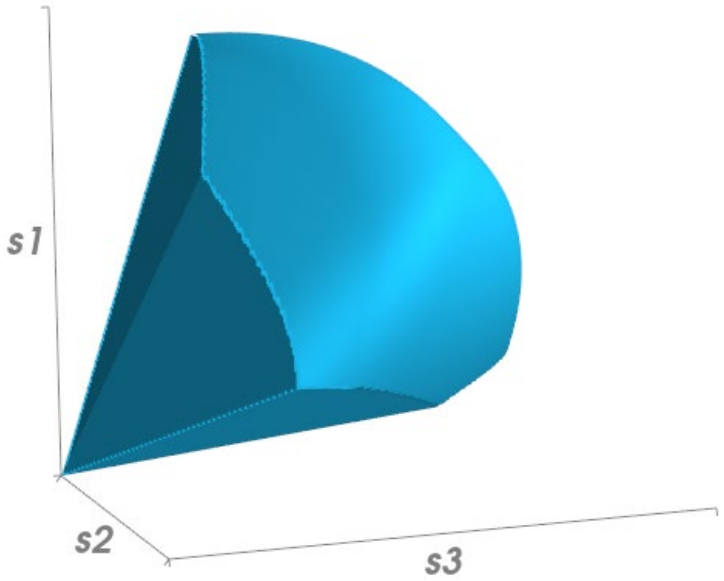

Figure 28. Representation of the complete yield surface of the Hardening Soil model in principal stress space for a soil without cohesion.

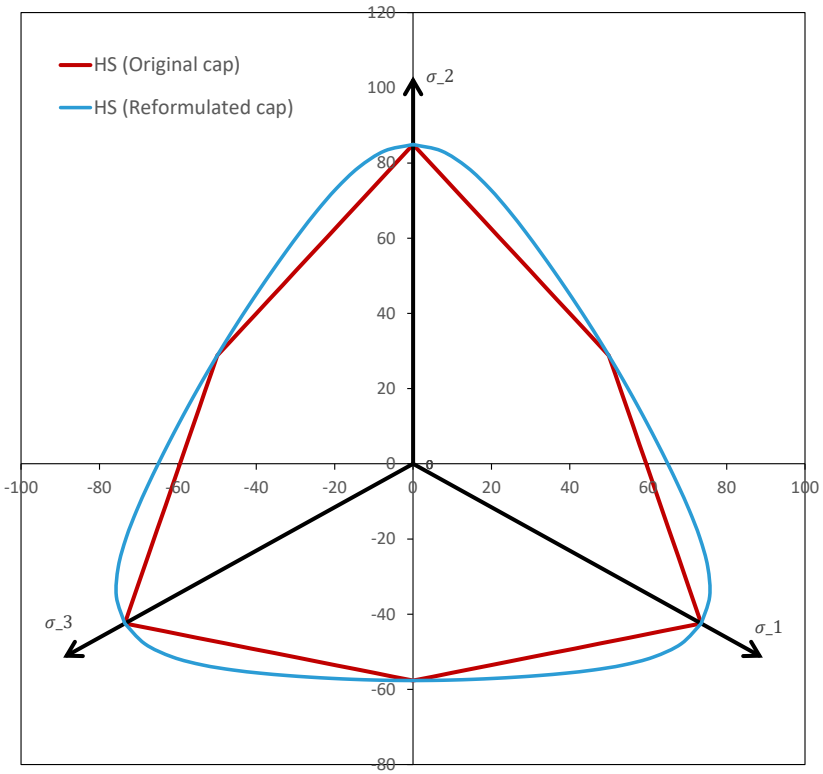

Figure 29. Reformulated and original cap yield surfaces in the deviatoric plane.

The plastic potential associated with the cap takes the form:

$$P_2(\{\sigma'\},\{k_2\}) = \frac{q^2}{M^2} + {p'}^2 \qquad \text{Equation 155}$$

The expression for the compression plastic potential (Equation 155) differs from the yield function Equation 150); an assumption referred to as non-associated plasticity. The Hardening Soil model is formulated on the assumption that the compression yield loci expand at constant shape, with the size being controlled by the tip stress ${p'}_p$, and that expansion of the yield loci – that is, the hardening of the soil – is linked with normal compression of the soil. The compression plastic potential produces plastic volumetric strain increments that can be calculated over a finite change in ${p'}_p$ as:

$$\delta\varepsilon_p^p = \frac{1}{H}\delta {p'}_p \qquad \text{Equation 156}$$

where H is referred to as the hardening modulus:

$$H = \left(\frac{{K'}_c}{{K'}_s - {K'}_c}\right){K'}_s \qquad \text{Equation 157}$$

where ${K'}_c$ and ${K'}_s$ are the bulk moduli in isotropic normal compression and swelling, respectively. The bulk modulus in isotropic swelling is given by:

$${K'}_s = {K'}_s^{ref}\left(\frac{c'\cot\phi' + {p'}_0}{c'\cot\phi' + p^{ref}}\right)^m \qquad \text{Equation 158}$$

The reference bulk modulus ${K'}_s^{ref}$ is calculated as:

$${K'}_s^{ref} = \frac{{E'}_{ur}^{ref}}{3(1-2{\nu'}_{ur})} \qquad \text{Equation 159}$$

The ratio of the bulk moduli ${K'}_s/{K'}_c$ for isotropic loading conditions can be approximated by the expression:

$$\frac{{K'}_s}{{K'}_c} \approx \frac{{E'}_{ur}^{ref}}{{E'}_{oed}^{ref}}\frac{K_0^{nc}}{(1+2K_0^{nc})(1-2{\nu'}_{ur})} \qquad \text{Equation 160}$$

where K_0^{nc} is the coefficient of earth pressure for the normally compressed state and ${E'}_{oed}^{ref}$ is a tangent stiffness obtained from an oedometer test at ${\sigma'}_1 = {\sigma'}_v = p^{ref}$; that is, the reference pressure for an

oedometer test is the vertical effective stress instead of the horizontal confining stress used for a triaxial tests.

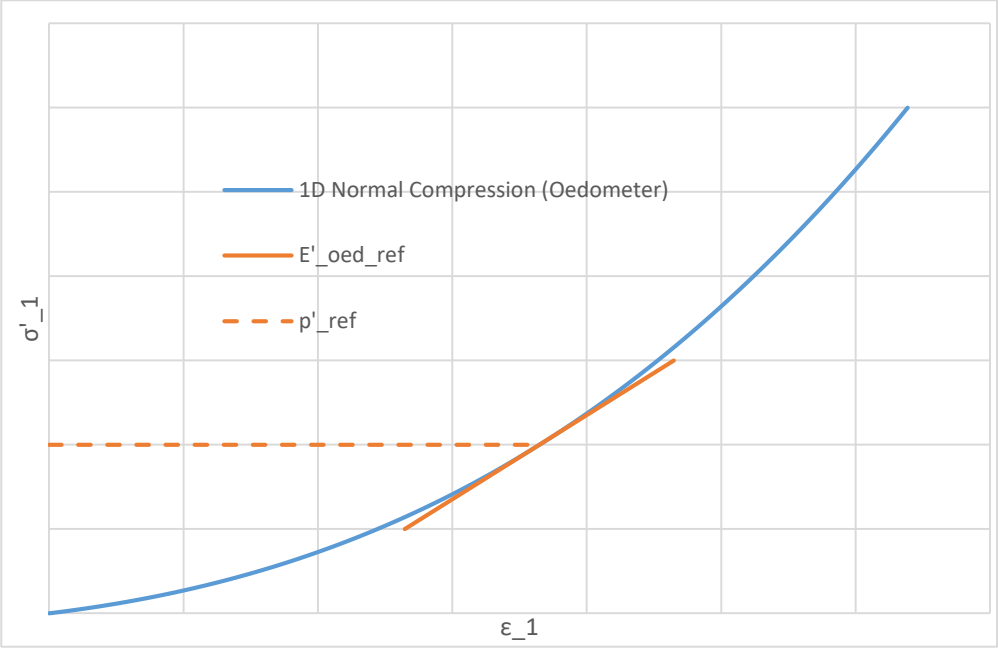

Figure 30. Reference tangent stiffness E'^{ref}_{oed} at the reference stress $\sigma'_1 = \sigma'_v = p^{ref}$.

The following should be noted:

1. As noted in the synopsis (Section 5.10), a stress path directed into zone 3 (Figure 24) produces elastic-plastic behaviour and expands both the shear and cap yield surfaces simultaneously. The elastic-plastic response is governed by the shear yield surface in this scenario. The elastic-plastic response is only controlled entirely by the cap yield surface if the stress path is not engaging the shear yield surface, which would require simulation of a stress path that expands the shear and cap yield surfaces, then retreats within the expanded elastic zone, and finally re-engages only the cap yield surface when reloaded in a compression dominated manner (zone 3; Figure 24).
2. The shear yield surface will always be engaged at the onset of loading regardless of the OCR state and initial stress conditions unless the stress history to create OCR conditions was modelled. Even if an initial stress analysis is conducted, Equation 143 would be used to compute the initial mobilized friction angle. The only way to create an initial stress state inside both the shear and cap yield surfaces would be to model stress history.

5.10.2 Material Parameters

Table 8 provides a summary of the required parameters. The elastic response in zone 1 (Figure 24) is described by isotropic elasticity and therefore requires two independent elastic parameters. The Hardening soil model adopts a stress dependent effective elastic modulus determined from an unloading-reloading stress path, E'_{ur}, and a constant Poisson's ratio, ν'_{ur}, that is specific to unloading-

reloading (Figure 25). The reference stiffness E'^{ref}_{ur} is measured at a reference confining stress p^{ref} of 100 kPa.

Table 8. Parameters for the Hardening Soil Model

Parameter	Symbol	Unit
Effective angle of shear resistance	ϕ'	°
Effective cohesion	c'	kPa
Angle of dilation	ψ	°
Reference unload-reload stiffness (via drained triaxial)	E'^{ref}_{ur}	kPa
Reference secant stiffness (via drained triaxial); $q = 0.5(q_f)$	E'^{ref}_{50}	kPa
Reference tangent stiffness in primary oedometer loading	E'^{ref}_{oed}	kPa
Unload-reload Poisson's ratio	ν'_{ur}	
Exponent controlling stiffness stress dependency	m	
Reference confining stress for stress dependent stiffness calculations	p^{ref}	kPa
Failure ratio q_f/q_a	R_f	
Isotropic over-consolidation ratio	$OCR = p'_{p,max}/p'_{p,i}$	
Coefficient of earth pressure for the normally compressed state	K_0^{nc}	
Coefficient of earth pressure for the overconsolidated state*	K_0^{oc}	
Initial void ratio	e	
Maximum void ratio (dilatancy cut-off)	e_{cs}	

*The coefficient of earth pressure for the over-consolidated state K_0^{oc} is an optional parameter for establishing the initial stresses by means of a Gravity Activation analysis in combination with the K_0-procedure (Section 4.1.2).

Table 9 provides a number of common relationships to assist with conversion between commonly measured material parameters and those required by the Hardening Soil model. Interpretation of Table 9 requires consideration of the following notes:

1. A compressibility parameter has a unit of inverse pressure (e.g. kPa^{-1}) while stiffness (e.g. E'^{ref}_{ur} and E'^{ref}_{50}) is the inverse of compressibility and has units of pressure (e.g. kPa).
2. The reference tangent stiffness E'^{ref}_{oed} is measured in an oedometer loading test during primary compression at a reference confining stress $\sigma'_1 = \sigma'_v = p^{ref}$ of 100 kPa. The stiffness E'^{ref}_{oed} is the inverse coefficient of volume compressibility m_v; that is, $E'^{ref}_{oed} = 1/m_v$.
3. Conversion between E'^{ref}_{ur} and a shear modulus G^{ref}_{ur} is possible because these are true elastic properties. In contrast, no such conversion is possible for the tangent stiffness E'^{ref}_{50}.
4. The parameter e_0 is the initial void ratio of the soil specimen and is only an approximation of the actual void ratio at which m_v is determined.

5. The approximation of $K_0^{nc} \approx 1 - \sin\emptyset'$ is only applicable for one-dimensional axially symmetric stress paths such as experienced in an oedometer and in some geological environments. For example, in the case of isotropic compression, $K_0^{nc} = 1.0$.
6. The parameter E'^{ref}_{50} is between about 1.25 and 2.0 times E'^{ref}_{oed} for stiff and soft soils respectively; however, large ratios of $E'^{ref}_{50} / E'^{ref}_{oed}$ can lead to numerical problems depending on the value of K_0^{nc}.

Table 9. Relationships between Hardening Soil material parameters and other commonly measured quantities.

Parameter	Relationship
E'^{ref}_{ur}	$E'^{ref}_{ur} \sim 3E'^{ref}_{50}$
	$E'^{ref}_{ur} = 2(1+\nu'_{ur})G^{ref}_{ur}$
	$C_s \approx \frac{(1+\nu'_{ur})(1-2\nu'_{ur})}{E'^{ref}_{ur}(1-\nu'_{ur})}(1+e_0)\frac{p^{ref}}{K_0}\ln 10$
E'^{ref}_{oed}	$C_c \approx \frac{1}{E'^{ref}_{oed}}(1+e_0)p^{ref}\ln 10$
K_{0nc}	$K_{0nc} \approx 1 - \sin\phi'$

5.10.2.1 Initialization of State Parameters

The Hardening Soil model requires an input for the isotropic over-consolidation ratio (OCR) which is defined as:

$$OCR = \frac{p'_{p,max}}{p'_{p,i}} \qquad \text{Equation 161}$$

where $p'_{p,max}$ is the past maximum value of the equivalent isotropic stress and $p'_{p,i}$ is the current, or initial, equivalent isotropic stress (Figure 31).

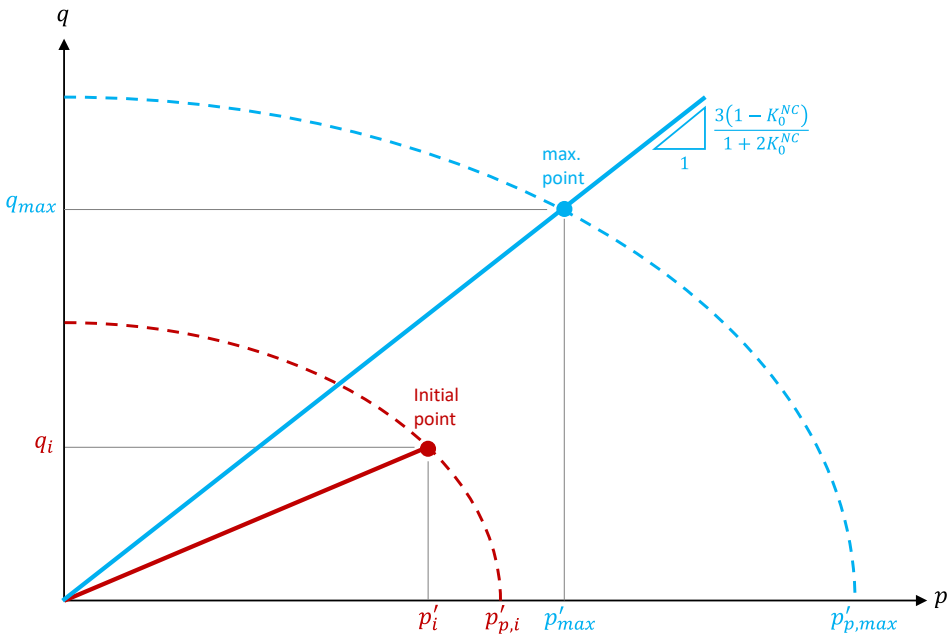

Figure 31. Initial and maximum equivalent isotropic pre-consolidation stresses.

The initial equivalent isotropic stress $p'_{p,i}$ is given in terms of initial invariants using Equation 150:

$$p'_{p,i} = \sqrt{\frac{q_i^2}{M^2 g^2(\theta_i)} + p'^2_i} \qquad \text{Equation 162}$$

The past maximum value of the equivalent isotropic stress is then calculated as:

$$p'_{p,max} = OCR\, p'_{p,i} \qquad \text{Equation 163}$$

The state parameter γ^p must be initialized from Equation 140. An additional assumption is therefore required about the stress history of the soil if the soil is over-consolidated. Assuming that the soil experienced an axially symmetric, one-dimensional, loading-unloading history, the stress invariants are linked by (Figure 31):

$$q_{max} = \eta_{nc} p'_{max} = \frac{3(1-K_0^{nc})}{1+2K_0^{nc}} p'_{max} \qquad \text{Equation 164}$$

where η_{nc} is the 1D normal compression stress ratio and K_0^{nc} is the earth pressure coefficient for the normally compressed state. Sustituting q_{max} from Equation 164 into Equation 150, after considering a Lode angle θ corresponding to one-dimensional normal compression (i.e., $g\left(-\frac{\pi}{6}\right) = 1$) and solving for past maximum mean effective stress:

$$p'_{max} = \frac{p'_{p,max}}{\sqrt{1 + \left(\frac{\eta_{nc}}{M}\right)^2}}$$ Equation 165

In both Equation 162 and Equation 165, the square of the cap's aspect ratio M^2 is required. The parameter M is a secondary model parameter that is calculated from the other model parameters:

$$M^2 = \frac{3\eta_{nc}\left[\frac{P'^{ref}_{ur}}{E'^{ref}_{oed}} - 1\right]}{2\left[\frac{P'^{ref}_{ur}}{E'^{ref}_{oed}} - \frac{1(1+\nu'_{ur})}{3(1-2\nu'_{ur})}\eta_{nc}\right]}$$ Equation 166

where η_{nc} is the 1D normal compression stress ratio (see Equation 164), and P'^{ref}_{ur} is the P-wave modulus or the constrained modulus defined as:

$$P'^{ref}_{ur} = \frac{E'^{ref}_{ur}(1-\nu'_{ur})}{(1+\nu'_{ur})(1-2\nu'_{ur})}$$ Equation 167

5.10.3 Conceptual Response

Section 5.1 describes the approach being taken here to explore some of most important aspects of the Hardening Soil model. As noted, the reader is directed to the example files and the literature for a more complete discourse on the assumptions and/or limitations of any particular constitutive model. The comparable explorations of the Hyperbolic $E-B$ model (Section 5.7.3), Mohr-Coulomb model (Section 5.8.3), and H/S Mohr-Coulomb model (Section 5.9.3) should be consulted before reading this section in order to gain additional insights into the stress-strain response of this model.

Figure 22 depicts the conceptualized simulated results of a conventional drained triaxial test on a dilative material $(\psi > 0)$ represented by the Hardening Soil model. The exponent m was assumed equal to 1.0 so that the expanding shear yield loci conveniently plot as straight lines in the $p' - q$ stress plane (Figure 32a). The peak friction ϕ' was assumed non-zero while the cohesion was assumed zero; consequently, the shear yield loci pass through the origin. As with the drained triaxial test discussed in Section 5.8.3 and Section 5.9.3, it is assumed that the increments start from stress state P lying on the p' axis and at a point in the $V - p'$ compression plane associated with url R. The initial shear and cap yield loci pass through point P $(OCR = 1)$; the shear surface is aligned with the p' axis while the cap yield surface (not shown until loading initiates) has its initial tip stress at point P. The response of the Hardening Soil model at the onset of loading is independent of the initial state in the compression plane; consequently, it is rather paradoxical to display an unloading-reloading line and isotropic normal compression line in Figure 18b. The paradox is ostensibly worsened by having the initial shear and cap yield loci pass through point P, suggesting normal compression, while having the initial void ratio

located on an unloading-reloading line instead of the isotropic normal compression line (Figure 22b). The reason for the curious initial state in the $V - p'$ compression plane, and the display of an unloading-reloading and normal compression line, is to assist with the interpretation of the models conceptual stress-strain response.

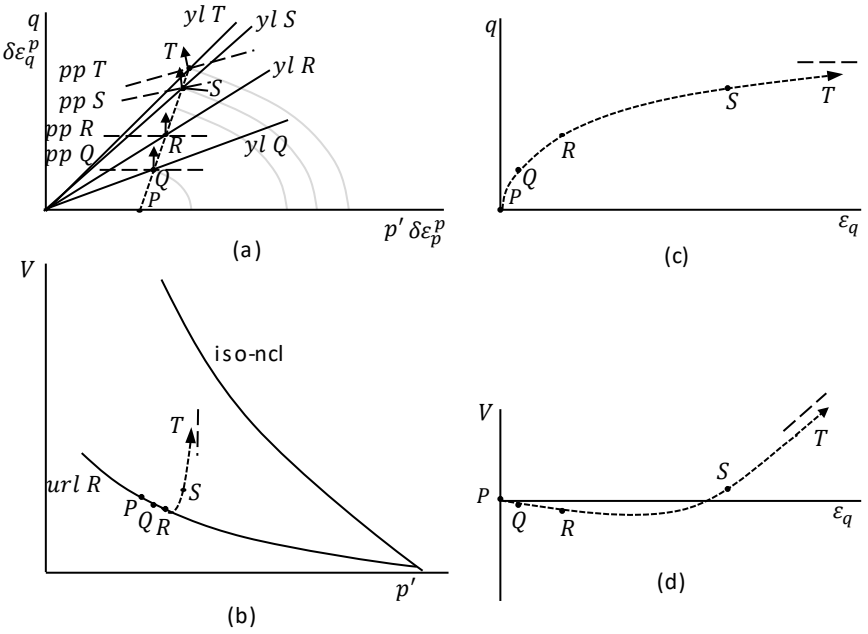

Figure 32. Conventional drained triaxial compression test on a soil described by the Hardening Soil model: (a) $p' - q$ effective stress plane (with increments of plastic volumetric and deviatoric strain); (b) $V - p'$ compression plane; (c) $q - \varepsilon_q$ stress-strain plot; (d) $V - \varepsilon_q$ volume-strain plot.

Point P lies at the tip of the cap yield locus and on the shear yield locus; consequently, as soon as drained compression initiates, both yield loci need to expand to accommodate the new stress states. Plastic deviatoric strains develop from the start of the drained compression. The plastic potential passing through Q and R is horizontal ($\psi_m = 0$; Equation 146) and the direction of the plastic strain increment vector is vertical (Figure 32a), indicating that plastic shear deformation is occurring without plastic change in volume. The soil therefore exhibits a continuous curved stress-strain $q{-}\varepsilon_q$ response (Figure 32c) that is expected of primary loading, but a stiff elastic response in the $V - p'$ compression plane (Figure 32b). It should now be clear why the initial state P, and states Q and R, were located on an unloading-reloading line (Figure 32b).

At R, it is assumed that $\sin\phi'_m \geq (3/4)\sin\phi'$ and that the mobilized friction angle ϕ'_m (Equation 149) is equal to the critical state friction angle ϕ'_{cs}, causing the mobilized dilation angle to be calculated according to Equation 147 (Figure 32a). The yield locus at R therefore represents the critical state line in the $p' - q$ effective stress plane. The progress RST is associated with a plastic strain increment vector on the plastic potentials (e.g. pp S and pp T) that points increasingly to the left (Figure 32a), indicating that that if a continued increase in shear strain is to occur, with plastic shear strains of the same sign as the preceding elastic shear strains (i.e. positive), then negative plastic volumetric strain must occur; that is, plastic volumetric expansion. The mobilized dilation angle initiates at zero at point R and increases to

the peak value ($\psi_m = \psi$) at T, where the mobilized friction angle equals the peak friction angle (${\phi'}_m = \phi'$; see Figure 27). The gradual transition in the mobilized dilation angle from zero to peak is reflected in the similar gradual transition from compression to expansion in the volume-strain $V - \varepsilon_q$ curve (Figure 32d). At some point after S, the mobilized dilation angle is nearing the peak value, causing the $V - \varepsilon_q$ response to become nearly linear in the volume-strain $V - \varepsilon_q$ plot (Figure 32d) and nearly vertical in the $V - p'$ compression plane (Figure 32b). In the absence of a dilatational cut-off, plastic volumetric expansion will continue indefinitely with continued shearing, causing the void ratio to track vertical upwards in the $V - p'$ compression plane (Figure 32b).

Figure 32a shows the evolution of the cap shear surface – and plastic potential given the assumption of associated plasticity – as it expands to pass through the current stress state. The cap yield surface, does not, however, affect the stress-strain response. As noted in Section 5.10.1.2, the stress path would have to track back inside the expanded elastic zone, and then reengage the cap yield surface in a compression dominated loading path, in order for compression hardening to dominate the response.

5.11 Ubiquitous Joint Model

The ubiquitous joint model accounts for the presence of an oriented weak plane, that is, a joint set, embedded in a Sigma/W Mohr-Coulomb material model (sections 5.8 and 5.9). This model is useful for modelling materials with closely spaced joints or bedding planes. The strength criterion of the weak plane is governed by a simple Coulomb criterion with a tension cut-off. A non-associated flow rule is used for joint shear failure and an associated flow rule for joint tension failure.

The Coulomb criterion and plastic potential for the joint material are:

$$f_{js}(\sigma_n, \tau) = \tau - \sigma_n tan\phi'_j - c'_j \qquad \text{Equation 168}$$

$$g_{js}(\sigma_n, \tau) = \tau - \sigma_n tan\psi_j \qquad \text{Equation 169}$$

The tension criterion and plastic potential for the joint material are:

$$f_{jt}(\sigma_n) = \sigma_{jt} - \sigma_n \qquad \text{Equation 170}$$

$$g_{jt}(\sigma_n) = -\sigma_n \qquad \text{Equation 171}$$

Table 10 lists the weak plane strength parameters. This model has two variations: a perfectly plastic version and a hardening/softening version. In the hardening/softening version of this material model, the strength parameters can be made to vary as a function of accumulated plastic strain (Equation 136). In addition to the strength parameters, the weak plane orientation must be specified with a normal vector to the weak plane in the Sigma/W UI. σ_n and τ above are the normal and shear stresses acting on the weak plane.

Table 10. Weak Plane (the joint) Strength Properties.

Parameter	Symbol	Unit
Effective angle of shear resistance as a function of ε_q^p	ϕ_j'	°
Effective cohesion as a function of ε_q^p	c_j'	kPa
Angle of dilation as a function of ε_q^p	ψ_j	°
Tensile strength (a positive value) as a function of $\left\|\varepsilon_3^p\right\|$	σ_{jt}	kPa

The ubiquitous joint model requires two sets of properties to be specified: 1) those of the Mohr-Coulomb matrix (Table 7) and 2) those of the weak plane (Table 10). The model operates in two steps. Stresses are first corrected for the Mohr-Coulomb matrix. These corrected stresses are then resolved into normal and shear stresses acting on the weak plane and they are further adjusted according to the weak plane constitutive equations above.

5.12 Generalized Hoek-Brown Model

The Hoek-Brown criterion (Hoek et al., 2002) is a widely accepted failure criterion for rock masses. The generalized Hoek-Brown criterion is expressed as

$$\sigma_1' = \sigma_3' + \sigma_{ci}\left(m_b\frac{\sigma_3'}{\sigma_{ci}} + s\right)^a \qquad \text{Equation 172}$$

where m_b, s, a are material constants, σ_1' and σ_3' are the maximum and minimum principal effective stresses, respectively, and σ_{ci} is the unconfined compressive strength of the intact rock.

The implementation of Hoek-Brown in Sigma/W is derived directly from the Mohr-Coulomb model (see section 5.8) and includes dilation angle and an optional tensile yield criterion. The non-linear yield surface described by Equation 172 is approximated by the Mohr-Coulomb tangent at the current stress level at σ_3'. In the tensile domain the Mohr-Coulomb tangent at $\sigma_3' = 0$ is used. The implementation does not allow hardening or softening of material strength parameters. User specified strength parameters are listed in Table 11. The model uses a non-associated flow rule for the Mohr-Coulomb approximation to the Hoek-Brown surface and an associated flow rule for the tensile yield surface.

In the implementation, the Hoek-Brown model checks the user input dilation angle against the calculated instantaneous friction angle calculated from the tangent to the Hoek-Brown surface. Dilation for the current calculation step is clamped to the minimum of friction and user specified dilation. If dilation is set to 89 degrees, associated flow can be simulated where friction equals dilation. If you set dilation to 5 degrees and instantaneous friction was 10 degrees then dilation would remain at 5 degrees for this calculation step.

Table 11. Hoek-Brown Strength Properties

Parameter	Symbol	Unit
Unconfined compressive strength of the intact rock	σ_{ci}	kPa
Hoek-Brown parameters	m_b, s, a	
Angle of dilation	ψ	°
Tensile strength (a positive value)	σ_t	kPa

5.13 Modified Cam Clay Model

The Modified Cam Clay (MCC) model (Roscoe and Burland, 1968; Schofield and Wroth, 1968; Roscoe and Schofield, 1963), was one of the first critical state constitutive models for soils to be developed within the generalized elastic-plastic framework (Section 3.4). The model simulates hardening or softening behaviour and the associated volumetric response (i.e. compression or expansion) when plastic straining is occurring. The simulated response is dependent on the overconsolidation state of the soil and the stress path to which the soil is being subjected. Despite its deficiencies, the continued use of the model in practice and research endeavors is a testament to its mathematical elegance, easy parameterization, and insightful simulated responses. The most successful applications of the MCC model involved clay deposits comprising normally compressed to lightly overconsolidated clays. The model is generally understood to overestimate the peak shear capacity of heavily overconsolidated soils (see Section 5.13.3).

5.13.1 Formulation

The modified Cam Clay model adopts an associated flow rule, meaning that the yield function, F, and the potential function, P, are identical. The function can be written as:

$$F(\{\sigma'\},\{k\}) = P(\{\sigma'\},\{m\}) = \left(\frac{q}{p'M}\right)^2 - \left(\frac{{p'}_0}{p'} - 1\right) \qquad \text{Equation 173}$$

where ${p'}_0$ is the equivalent isotropic pre-consolidation stress that defines the size of the current yield locus and therefore defines the hardening parameter $k = m$. The slope of the critical state line in $q - p'$ stress space M is given as:

$$M = \frac{6\sin\phi'}{3 - \sin\phi'} \qquad \text{Equation 174}$$

where ϕ' is the critical state friction angle.

Figure 33 shows the ellipsoidal yield surface of the modified Cam clay model in principal stress space. The size of the ellipsoid is described by the vertex on the major axis; that is, the intersection of the ellipsoid with the space diagonal. This value is essentially the state parameter k of the model, which can

be calculated from the maximum past effective stress to which the soil was subjected, and is comparable to ξ in Figure 2.

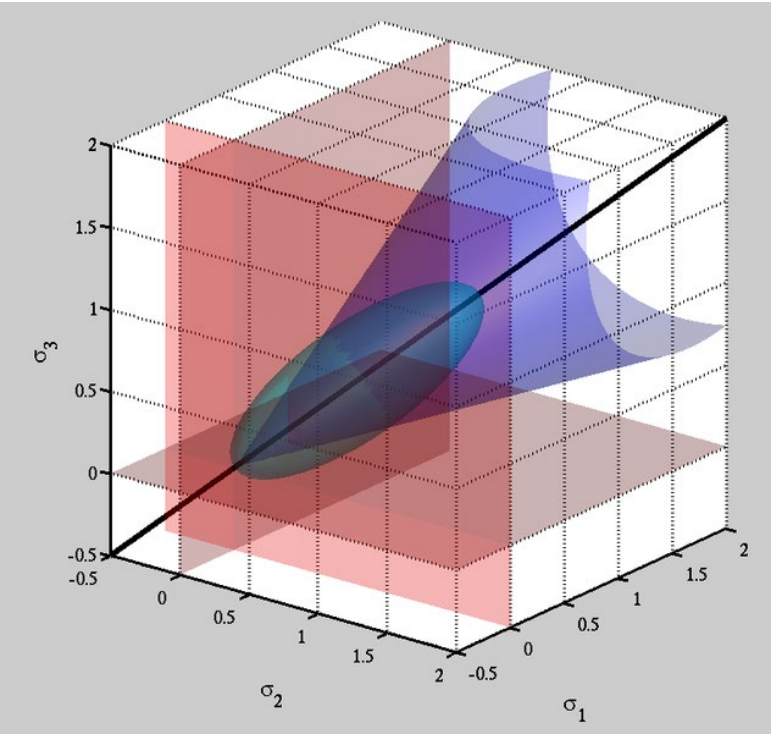

Figure 34a shows the elliptical yield locus of the MCC model in the $p' - q$ effective stress plane (Equation 173). This view of the yield locus can be conceptualized as a cross-section through the yield surface in principal stress space (Figure 33) that runs along the space diagonal. Only one side of the resulting ellipse is shown in Figure 34 because q (Equation 15) is always positive. The size of the yield locus is controlled by the equivalent isotropic preconsolidation stress p'_0 and the shape of the yield locus is controlled by the slope of the critical state failure line M. Equation 174 corresponds to a Drucker-Prager circular circumscription of the irregular Mohr-Coulomb hexagon failure surface at $\theta = -\pi/6$ in the deviatoric plane (i.e. triaxial compression; Figure 15). Figure 33 also shows the Drucker-Prager conical failure surface that that controls the shape of the ellipsoid (i.e. the size of the minor axis).

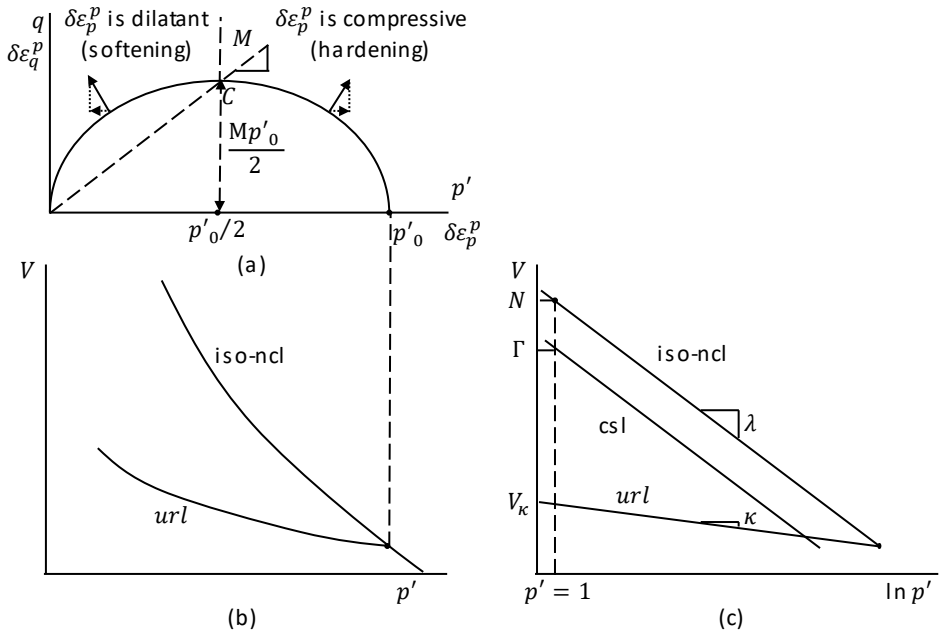

Figure 34. Elliptical yield locus for modified Cam clay model in $p' - q$ effective stress plane (with increments of plastic volumetric and deviatoric strain); (b) $V - p'$ compression plane; (c) $V - ln\ p'$ compression plane.

An inherent assumption of the modified Cam clay model is that the isotropic normal compression line and unloading-reloading lines (Figure 34b) can be assumed linear if the mean effective stress axis is plotted with a natural logarithmic scale (Figure 34c). The equation of the isotropic normal compression line (ncl) is given by:

$$V = N - \lambda \ln p'_0 \qquad \text{Equation 175}$$

and the equation of any particular unloading-reloading line (url) corresponding to an equivalent isotropic preconsolidation stress p'_0 is given by:

$$V = V_\kappa - \kappa \ln p' \qquad \text{Equation 176}$$

where V is specific volume, N and V_κ are intercepts at $p' = 1$, λ the slope of the isotropic normal compression line, and κ the slope of the unloading-reloading line in the $V - \ln p'$ compression plane (Figure 34c). The intercepts N and Γ locate the isotropic normal compression and critical state lines in the $V - \ln p'$compression plane (Figure 34c). These parameters are not used to form the elastic-plastic stiffness matrix, rather they are secondary quantities that can be calculated from the primary model parameters and initial state of the soil.

Stress paths tracking inside the yield surface $F(\{\delta\sigma'\},\{k\}) < 0$ are associated with purely elastic behaviour. The recoverable changes in volume are linked to changes in mean effective stress p' through the incremental form of Equation 176:

$$\delta\varepsilon_p^e = \frac{\kappa}{V}\frac{\delta p'}{p'} \qquad \text{Equation 177}$$

From Equation 177, the effective bulk modulus is deduced as:

$$K' = \frac{Vp'}{\kappa} \qquad \text{Equation 178}$$

Assuming a constant value of Poisson's ratio ν' implies a non-linear effective elastic modulus given by:

$$E' = 3K'^{(1-2\nu')} \qquad \text{Equation 179}$$

and a corresponding elastic shear modulus that is given by:

$$G = \frac{3(1-2\nu')}{2(1+\nu')}K' \qquad \text{Equation 180}$$

Equation 180 indicates that the elastic shear modulus is a non-linear function of mean effectives stress and void ratio. The deviatoric strain increment $\delta\varepsilon_q^e$ is linked to changes in deviatoric stress by Equation 29 by means of Equation 180.

Stress paths that engage the yield locus are associated with plastic straining (i.e. $F(\{\delta\sigma'\},\{k\}) = 0$). The equations of the isotropic normal compression and unloading-reloading lines can be used to calculate the plastic volumetric strain as (Wood, 1990):

$$\delta\varepsilon_p^p = (\lambda-\kappa)\frac{\delta p'_0}{Vp'_0} \qquad \text{Equation 181}$$

Equation 181 is a hardening law that links the changing size of the yield locus $\delta p'_0$ to the plastic volumetric strain increment $\delta\varepsilon_p^p$.

The outward normal to the plastic potential defines the relative magnitudes of the plastic volumetric strain $\delta\varepsilon_p^p$ and the plastic deviatoric strain $\delta\varepsilon_q^p$ (Section 3.4). The plastic potential function of the MCC model has the same mathematical form as the yield function and is therefore also represented by the ellipse in Figure 34a. Soils that yield with a stress state to the right of C (Figure 34a) are associated with incremental plastic volumetric strains $\delta\varepsilon_p^p$ that are positive (i.e. compression) and expansion (i.e. hardening) of the yield locus (i.e. positive $\delta p'_0$; Equation 181). Soils that yield with a stress state to the left of C (Figure 34a) are associated with incremental plastic volumetric strains that are negative (i.e. dilative/expansive) and collapse (i.e. softening) of the yield locus (i.e. negative $\delta p'_0$; Equation 181). Regardless of the scenario, continued shearing will eventually result in the stress path reaching the top of the yield locus C, where the normal to the plastic potential is vertical, indicating zero incremental plastic volumetric strain. At failure, any further shearing is associated with a critical state condition: the yield locus is stationary and there are no further changes in volume. The specific volume of the soil

resides on the critical state line (csl) in the $V - \ln p'$compression plane (Figure 34c) once the critical state has been reached.

5.13.2 Material Parameters

The MCC model simulates hardening or softening behaviour in a natural way and does so using only five material parameters: the slopes of the isotropic normal compression line λ and unloading-reloading line κ in the $V - \ln p'$compression plane (Figure 34c), the slope of the failure line M in the $p' - q$ effective stress plane (via ϕ'; Equation 174), and two elastic constants E' and ν'_{ur}. Table 12 provides a summary of the required parameters. Parameterization of the elastic response requires an input for Poisson's ratio ν'_{ur} that is commensurate with unloading-reloading (i.e. a purely elastic response, hence the subscript ur). Initialization of the model also requires definition of the initial overconsolidation state (OCR) and initial void ratio $e_0 = V_0 - 1$ of the soil.

Table 12. Parameters for the modified Cam clay model

Parameter	Symbol	Unit
Effective angle of shear resistance	ϕ'	°
Slope of normal compression line	λ	
Slope of the unloading-reloading line	κ	
Poisson's ratio	ν'_{ur}	
Isotropic over-consolidation ratio	$OCR = p'_{0,max}/p'_{0,i}$	
Coefficient of earth pressure for the overconsolidated state*	K_0^{oc}	
Initial void ratio	e	

*The coefficient of earth pressure for the over-consolidated state K_0^{oc} is an optional parameter for establishing the initial stresses by means of a Gravity Activation analysis in combination with the K_0-procedure (Section 4.1.2).

Table 13 provides a number of common relationships to assist with conversion between commonly measured material parameters and those required by the MCC model. Interpretation of Table 13 requires consideration of the following notes:

1. A compressibility parameter has a unit of inverse pressure (e.g. kPa^{-1}) while stiffness (e.g. E'^{ref}_{ur}) is the inverse of compressibility and has units of pressure (e.g. kPa).
2. The reference unloading-reloading elastic stiffness E'^{ref}_{ur} is measured in triaxial compression at a reference confining stress p^{ref} of 100 kPa and is a true elastic property.
3. The reference tangent stiffness E'^{ref}_{oed} is measured in an oedometer loading test during primary compression at a reference confining stress $\sigma'_1 = \sigma'_v = p^{ref}$ of 100 kPa. The stiffness E'^{ref}_{oed} is the inverse coefficient of volume compressibility m_v; that is, $E'^{ref}_{oed} = 1/m_v$.
4. The slopes of the unloading-reloading and normal compression lines in the $V - \ln p'$ compression plane can be approximated from the conventional compression index C_c and swelling index C_s measured in the $V - \log \sigma'_v$ compression plane.

Table 13. Relationships between modified Cam clay material parameters and other commonly measured quantities.

Parameter	Relationship
κ	$\kappa \approx \frac{C_s}{\ln 10}$
	$C_s \approx \frac{(1+\nu'_{ur})(1-2\nu'_{ur})}{E'^{ref}_{ur}(1-\nu'_{ur})}(1+e_0)\frac{p^{ref}}{K_0}\ln 10$
λ	$\lambda \approx \frac{C_c}{\ln 10}$
	$C_c \approx \frac{1}{E'^{ref}_{oed}}(1+e_0)p^{ref}\ln 10$

5.13.2.1 Initialization of State Parameters

The modified Cam clay soil model requires an input for the isotropic over-consolidation ratio (OCR) which is defined as:

$$OCR = \frac{p'_{0,max}}{p'_{0,i}} \qquad \text{Equation 182}$$

where $p'_{0,max}$ is the past maximum value of the equivalent isotropic stress and $p'_{0,i}$ is the current, or initial, equivalent isotropic stress (Figure 35).

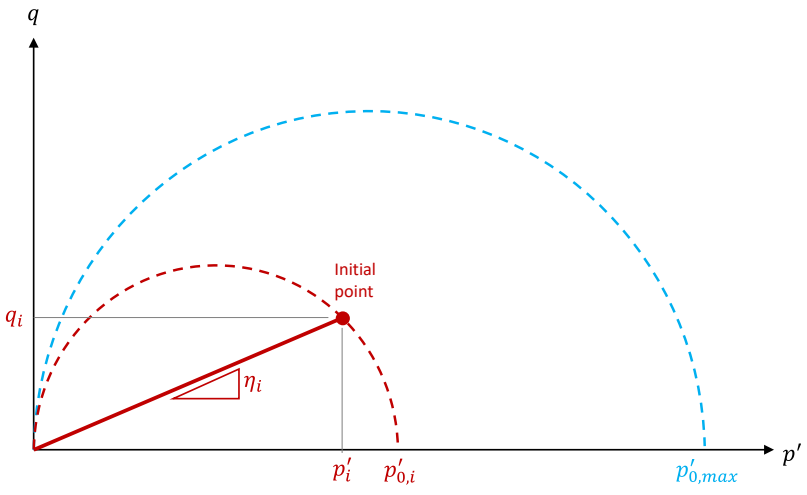

Figure 35. Initial and maximum equivalent isotropic pre-consolidation stresses.

The initial equivalent isotropic stress $p'_{0,i}$ is given in terms of initial invariants using Equation 173:

$$p'_{0,i} = p'_i \left[1 + \left(\frac{q_i}{p'_i M} \right)^2 \right] \qquad \text{Equation 183}$$

The past maximum value of the equivalent isotropic stress is then calculated as:

$$p'_{0,max} = (OCR) p'_{0,i} \qquad \text{Equation 184}$$

5.13.3 Conceptual Response

Section 5.1 describes the approach being taken here to explore some of most important aspects of the modified Cam clay model. As noted, the reader is directed to the example files and the literature for a more complete discourse on the assumptions and/or limitations of any particular constitutive model. Wood (1990) provides an eloquent and insightful exploration of the modified Cam clay model in both drained and undrained triaxial compression. Wood's (1990) discourse on the drained response of the modified Cam clay model forms the basis of the information presented herein and was a template for the comparable explorations of the other material models. The presentations of those models should be consulted before reading this section in order to gain additional insights into the stress-strain response of this model.

Figure 36 depicts the conceptualized simulated results of a conventional drained triaxial test on a lightly overconsolidated material represented by the modified Cam clay model. Parameterization of the modified Cam clay model requires specification of the initial void ratio and OCR. These inputs are used in combination with initial stresses to initialize the state of the soil (point A) in the $V - p'$ compression plane and in the $p' - q$ stress plane relative to the initial yield surface (Section 5.13.2.1). The soil could have been subjected to isotropic normal compression to $p' = p'_{0B}$ and then unloaded isotropically to A. Alternatively, the soil could have been compressed and then unloaded under conditions of one-dimensional axisymmetry, resulting in the same yield locus with tip pressure p'_{0B} and associated elastic-unloading-reloading line url B ending at $p' = p'_{0B}$ on the isotopic normal compression line (Figure 36b). The stress history cannot be deduced from A alone because it is embodied in the initial conditions, the initial void ratio, and the OCR.

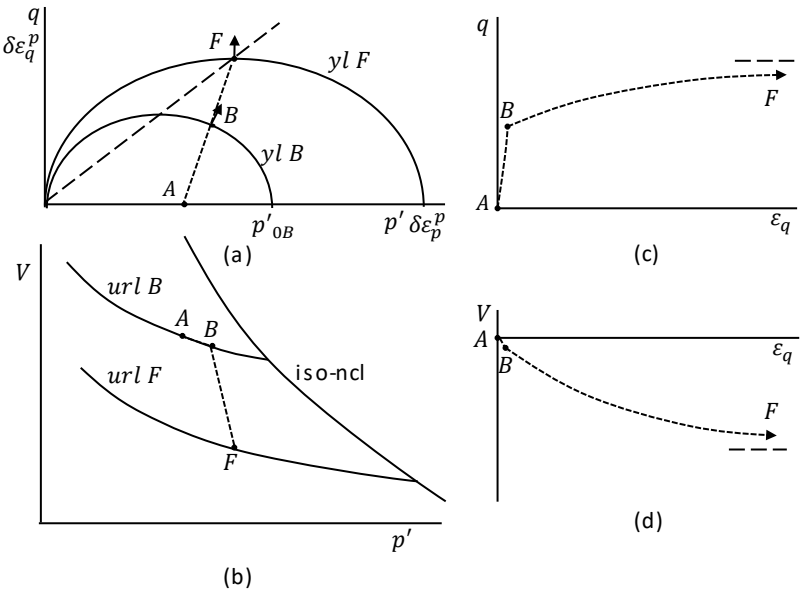

Figure 36. Conventional drained triaxial compression test on lightly overconsolidated soil as described by the modified Cam clay model: $p' - q$ effective stress plane (with increments of plastic volumetric and deviatoric strain); (b) $V - p'$ compression plane; (c) $q - \varepsilon_q$ stress-strain plot; (d) $V - \varepsilon_q$ volume-strain plot (after Wood, 1990).

The drained compression from A to B involves a stress change inside the yield locus; consequently, the response is purely elastic (Figure 36). The soil shows a stiff elastic response on drained compression from A to B, with both points residing on the unloading-reloading line url B. The elastic volumetric strain increment could be calculated by numerical integration of Equation 177 (Figure 36b). The tangent derivative at any point on the stress-strain curve $q-\varepsilon_q$ from A to B is equal to $3G$ (Equation 180 via Equation 178; Figure 36c). The stress-strain curve $q-\varepsilon_q$ shows a sharp drop in stiffness when the soil yields at B because plastic strains start to develop.

The direction of the outward normal to the yield locus yl B at B indicates that the plastic deviatoric strain is accompanied by plastic volumetric compression. Wood (1990) notes that the volume-strain curve $V-\varepsilon_q$ also shows a break at B; however, the sharpness of the break depends on the soil parameters κ, λ, M (Equation 174), and G (Equation 180) and on the stress ratio η at which yield occurs at B (Figure 36d). Wood (1990) goes on to note that it would possible for the ratio of elastic volumetric and deviatoric strain increments just before yield at B to be the same as the ratio of elastic plus plastic volumetric and deviatoric strain increments just after yielding at B.

Additional increments of drained compression BF are associated with progressive enlargement of the yield locus, a phenomenon referred to as hardening. The direction of the outward normal to the yield locus also changes progressively, initially pointing to the right (i.e. plastic volumetric compression) but eventually becoming parallel to the q axis at the crest of the yield locus F, where the ratio of plastic deviatoric strain to plastic volumetric strain is infinite (Figure 36a). At F, the stress ratio $\eta = q/p'$ is equal to the slope of the critical state line M and the mean effective stress $p' = p'_{0F}/2$. At this point, unlimited plastic deviatoric strains will continue to develop with no plastic volumetric strain, which means that the yield locus becomes stationary (i.e. $\delta p'_0 = 0$). Once the stress path intersects the failure

surface, plastic shearing continues at constant effective stresses, meaning that loading can proceed no further. The mathematical formulation of the MCC model inherently produces $\delta\varepsilon_p^p/\delta p' = 0$ and $\delta\varepsilon_q^p/\delta q = \infty$.

The progress of the drained compression BF can also be described with reference to the $V - p'$ compression plane (Figure 36b) and stress-strain $q{-}\varepsilon_q$ curve (Figure 36c). Starting at B, the change in volume is dominated by the irrecoverable plastic deformations, which gradually approach zero as the stress ratio $\eta = q/p'$ increases towards M. At F, the plastic volumetric strain goes to zero and the effective stresses remain constant, which means that the elastic volumetric strain also goes to zero and there is no further change in volume. The slopes $\delta q/\delta\varepsilon_q$ and $\delta V/\delta\varepsilon_q$ decreases steadily towards zero as η increases towards M. The information in Figure 36b, c can be combined to show how the volume changes with deviatoric strain (Figure 36d). The modified Cam clay model produces a ratio of plastic strains $\delta\varepsilon_p^p/\delta\varepsilon_q^p$ that decreases steadily towards zero as η increases towards M, which, when combined with zero elastic volumetric strain (i.e. constant effective stresses) means that the slope $\delta V/\delta\varepsilon_q$ must also steadily decrease towards zero (Figure 36d).

As noted in Section 5.13, the most successful applications of modified Cam clay have involved lightly to normally compressed soils. Having stated that, it remains instructive to consider the response of a heavily overconsolidated soil (Figure 37) and to compare this response to that of the H/S Mohr-Coulomb (Section 5.9.3). On drained compression, the response would be elastic until the yield locus yl Q was reached at a point Q lying to the left of the critical state line (Figure 37a). Wood (1990) notes that the plastic strain increment vector points to the left at Q, indicating that if a continued increase in deviatoric strain is to occur, with plastic deviatoric strain of the same sign as the preceding elastic deviatoric strains, then this must be associated with negative plastic volumetric strain; that is, plastic volumetric expansion.

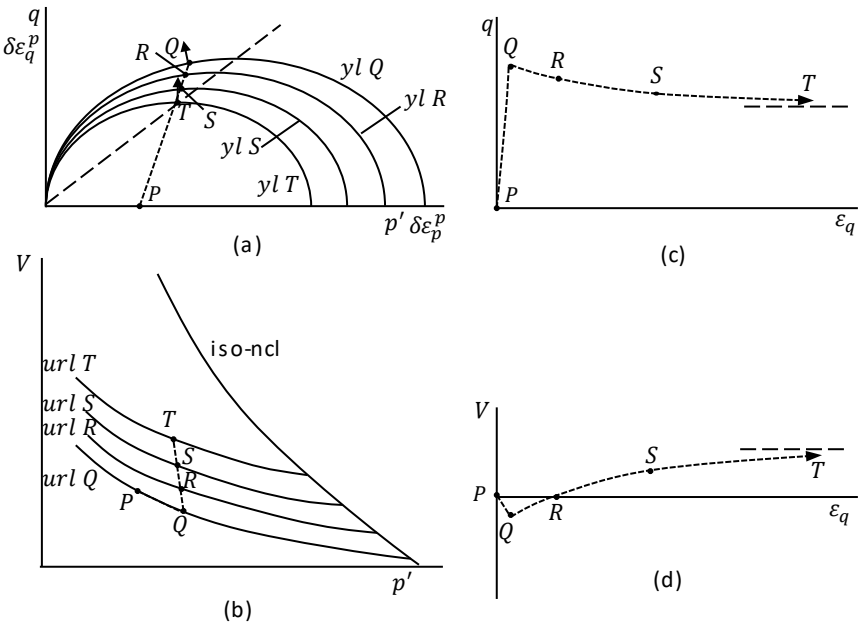

Figure 37. Conventional drained triaxial compression test on heavily overconsolidated soil as described by the modified Cam clay model: $p' - q$ effective stress plane (with increments of plastic volumetric and deviatoric strain); (b) $V - p'$ compression plane; (c) $q - \varepsilon_q$ stress-strain plot; (d) $V - \varepsilon_q$ volume-strain plot (after Wood, 1990).

The plastic volumetric expansion that initiates at Q is associated with a decrement in the size of the yield locus $\delta p'_0 < 0$; a process referred to as softening. The effective stress path retreats towards P with continued shearing. The progress of the test is deduced in the compression plane (Figure 37b) by projecting the points R, S, and T in the stress plane (Figure 37a) from their yield loci yl R, yl S, and yl T down to the corresponding unloading-reloading lines url R, url S, and url T (Wood, 1990). As before, the direction of the plastic strain increment vector gradually approaches the vertical at T where $\eta = M$. At that point, plastic deviatoric strains can continue without plastic volume changes. The progress of the drained compression Q, R, S, T can also be described with reference to the $V - p'$ compression plane (Figure 37b) and stress-strain $q - \varepsilon_q$ curve (Figure 37c). The sharp break at Q corresponds to the onset of plastic volumetric expansion (Figure 37b and d). The initial elastic rise in q and decrease in volume (PQ) is followed by a drop in q and increase in V towards the limiting values corresponding to T.

The main deficiency of the modified Cam clay model is primarily rooted in the potential overestimation of the peak deviatoric stress corresponding to Q. Point Q might correspond to a peak mobilized friction angle that is theoretically unjustified. The user has no direct control over the mobilized friction angle and magnitude of dilatational strains, which are controlled indirectly by means of the material parameters κ, λ, and ϕ'. This contrasts sharply with the H/S Mohr-Coulomb model (Section 5.9), where the mobilized friction angle and dilation angle are functionally related to the plastic deviatoric strain, but bears similarity to the Hardening Soil model (Schanz et al. 1999) that prescribes the dilatancy relationship by linking the dilation angle to the mobilized friction angle. In other words, the dilatancy relationship is also prescribed by the modified Cam clay model formulation.

5.14 SANICLAY model

SANICLAY is a soil model that is suitable for simulating the behaviour of anisotropic clayey materials. Soils that are uniformly deposited over a larger area are generally subjected to a one-dimensional loading history. The ratio of horizontal to vertical effective stresses in such soils is referred to as the coefficient of earth pressure at rest K_0. The stress history of such soils can be reproduced in a conventional triaxial apparatus. Such tests often demonstrate a yield surface that is characterized by a rotated ellipse. Dafalias (1986) proposed a simple extension of the Modified Cam Clay (MCC) model that captures the anisotropic nature of the yield surface. Dafalias *et al.* (2006) further developed the model to capture the softening response of clays under drained and undrained loading following K_0 consolidation. Dafalias and Taiebat (2013) proposed a new rotational hardening rule for this model to capture a unique critical state line in e-p space. The model is called Simple Anisotropic Clay (SANICLAY). The main features of the model are: (1) a non-associated flow rule, (2) rotational hardening rules which leads to the evolving of the yield and plastic potential surfaces, (3) isotropic hardening of the yield surface stress plane.

5.14.1 Formulation

Figure 38 illustrates the elliptical yield surface and plastic potential surface of the SANICLAY model in the triaxial space $p' - q$. As shown in Figure 38, the slope α is the stress ratio q/p' that introduces anisotropy to the plastic potential surface. Similarly, the anisotropy of the yield surface is introduced by the slope β. The slope of the critical state line is denoted by *M*. It is worth noting that the deviatoric stress at the top of the yield surface corresponds to the stress ratio N, a model parameter. The isotropic hardening variable p_0 is the value of p at $\eta = \beta$. The slope of the yield and plastic potential surfaces are assumed to be identical (i.e., $\alpha = \beta$) in Dafalias and Taiebat (2013).

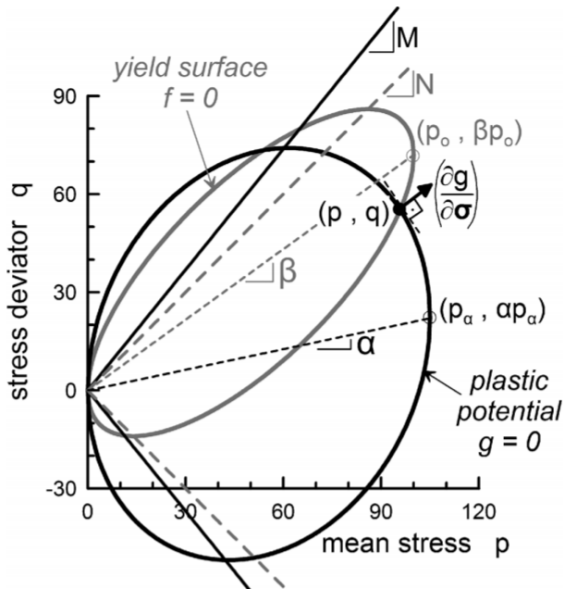

Figure 38. SANICLAY yield and plastic potential surfaces in triaxial stress space (after Dafalias *et al.*, 2006).

Appendix III provides a thorough description of SANICLAY's formulation in generalized stress space. The model is more easily conceptualized by considering its formulation for triaxial stress space. SANICLAY's

formulation reuses some of Modified Cam Clay's foundation components, while adding crucial elements to account for anisotropy. As such, the yield surface, expressed in triaxial space, takes the following form:

$$f = (q - p\beta)^2 - (N^2 - \beta^2)p(p_0 - p) = 0 \qquad \text{Equation 185}$$

If β is taken as zero and N is set equal to the critical state ratio M, Modified Cam Clay's yield surface is obtained. The novel β and N parameters allow anisotropy and softening to occur. Similarly, the plastic potential surface, expressed for the triaxial space, is given as:

$$g = (q - p\alpha)^2 - (M^2 - \alpha^2)p(p_\alpha - p) = 0 \qquad \text{Equation 186}$$

By setting α to zero and taking p_α as equal to p_0, the plastic potential surface becomes equivalent to the yield surface and Modified Cam Clay's associated flow rule is recovered.

5.14.2 Material parameters

Dafalias et al. (2006) and Dafalias and Taiebat (2013) present two different rotational hardening rules for the SANICLAY model, both of which are implemented in the software. Table 14 presents the general model parameters and the unique parameters associated with the rotational hardening (RH) rule. The model parameters can be calibrated from conventional laboratory tests.

Table 14. Parameters for the SANICLAY model.

Parameter	RH (2006)	RH (2013)
Critical stress ratio in compression	M_c	M_c
Critical stress ratio in extension	M_e	M_e
Slope of normal compression line	λ	λ
Slope of the unloading-reloading line	κ	κ
Effective Poisson's ratio	ν	ν
Yield surface shape in compression	N	N_c
Yield surface shape in extension	$= N$	N_e
Saturation limit of anisotropy	x	$-$
Rotational hardening parameter	$-$	s
Rotational hardening parameter	$-$	z
Rotational hardening parameter	$-$	ξ
Rate of evolution of anisotropy	C	C
Overconsolidation ratio	OCR	OCR
Coefficient of earth pressure for the normally compressed state	K_0^{nc}	K_0^{nc}
Initial void ratio	e	e

In SANICLAY, the overconsolidation ratio OCR is defined as the maximum vertical stress experienced by the soil in the past, divided by the current vertical stress.

Table 15 presents the state parameters and stress ratio (η/M) that can be graphed and contoured to interpret the responses simulated by the SANICLAY model. The gradient of the yield and plastic potential surfaces (Table 15) are scalar representations of the tensors used to formulate and implement the model (Appendix III).

Table 15. Material state parameters definition for SANICLAY when drawing graphs.

Parameter name	Corresponding parameter
Gradient of the yield surface	β
Gradient of the plastic potential surface	α
Size of the yield surface	p_0
eta / M (mobilized strength)	η/M

5.14.2.1 Initialization of the state parameters

The SANICLAY model requires an input for the overconsolidation ratio OCR (Equation 105) and coefficient of earth pressure for the normally compressed state K_{0nc}. These inputs are used to establish

the maximum vertical and horizontal effective stresses and thus to establish the past maximum stress tensor.

The past maximum stress tensor is in turn used to calculate the initial rotation of the yield surface and the initial rotation of the plastic potential surface. In the model with the 2006 hardening rule, the initial values of the tensors $\boldsymbol{\beta}$ and $\boldsymbol{\alpha}$ are estimated as follows:

$$\boldsymbol{\alpha} = \frac{\mathbf{r}}{x} \; ; \; \boldsymbol{\beta} = \mathbf{r} \qquad \text{Equation 187}$$

While this estimation for the model with the 2013 hardening rule is:

$$\boldsymbol{\alpha} = \boldsymbol{\beta} = \boldsymbol{\alpha}_b \qquad \text{Equation 188}$$

In Equation 187 and Equation 188, $\mathbf{r}$ is the deviatoric stress-ratio tensor of the past maximum stress state and $\boldsymbol{\alpha}_b$ is the bounding deviatoric stress tensor. The past maximum stress tensor is also used to define the corresponding deviatoric stress tensor, $\mathbf{s}$. Having $\mathbf{s}$ and the inital $\boldsymbol{\beta}$ allows the equivalent isotropic hardening variable (i.e., p_0) to be calculated from the yield function.

It is worth noting that, for heavily over-consolidated soils, where the initial stress state may be located outside the estimated past yield surface, it is required to consider a rotation for the yield surface. This modification on the estimated past yield surface can be taken into account by updating the initial estimations of the deviatoric tensors $\boldsymbol{\alpha}$ and $\boldsymbol{\beta}$ based on the initial stress state of the element.

5.14.3 Conceptual response

SANICLAY's strength and uniqueness comes from its ability to account for soil anisotropy as consolidation and deformations occurs. At its core lies the elliptical yield surface of the Modified Cam Clay (MCC) model. As shown in Figure 39, during isotropic consolidation, from point A to point B, SANICLAY's yield surface develops as a symmetrical ellipse. At this point, the only thing separating SANICLAY from MCC is the use of the parameter N to size and shape the yield surface instead of the critical state ratio M in MCC.

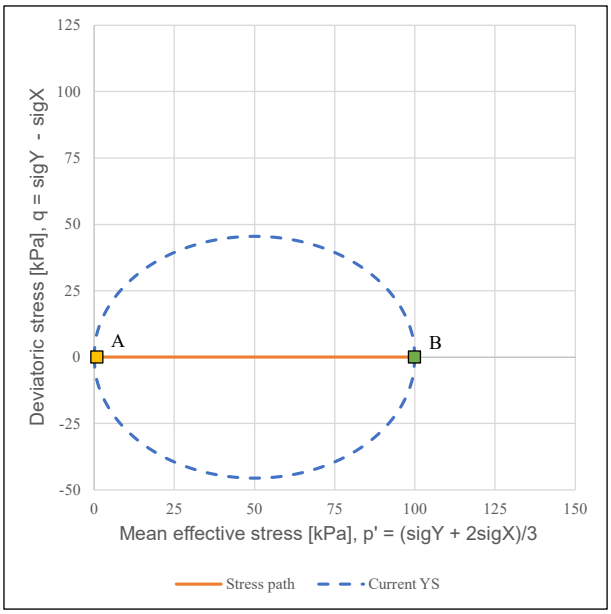

Figure 39. SANICLAY yield surface (YS) after isotropic consolidation.

To see SANICLAY's specificity in action, the stress path must depart from the isotropic axis, as shown in Figure 40, from point B to point C. This part of the stress path involves loading at constant mean effective stress. In doing so, the yield surface changes (expansion and rotation) from its isotropic shape (ellipse centered around $q = 0\ kPa$, dashed light grey curve) to an anisotropic one (inclined ellipse, dashed blue curve). This yield surface evolution is driven by plastic strains, which in turn influence p_0 (size of the yield surface) and β (inclination of the yield surface). Similarly, plastic strains will also influence α and change the size and shape of the plastic potential surface (not displayed in Figure 40).

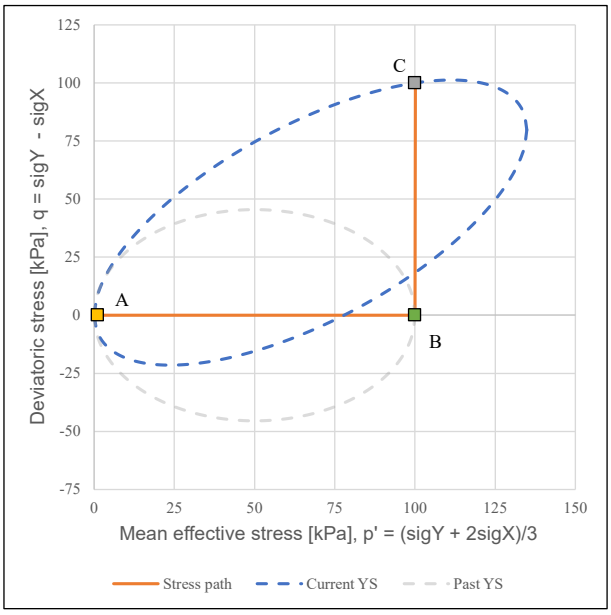

Figure 40. SANICLAY's yield surface (YS) after constant p' loading.

Unloading at constant mean stress is shown in Figure 41, essentially retracing the previous loading stress path, from point C to point E (which coincides with point B). From point C to point D, only elastic strains would be produced, because the stress state lies inside the yield surface (dashed light red curve), and internal state parameters (α, β and p_0) remain constant. Upon hitting the lower part of the yield surface at point D, plastic strains are produced which affects the state parameters and thus changes the yield surface's size and orientation. When unloading ends at point E, the yield surface changed from the dashed light red curve to the dashed blue curve, showcasing the effect of hitting the lower part of the yield surface during unloading, and associated hardening.

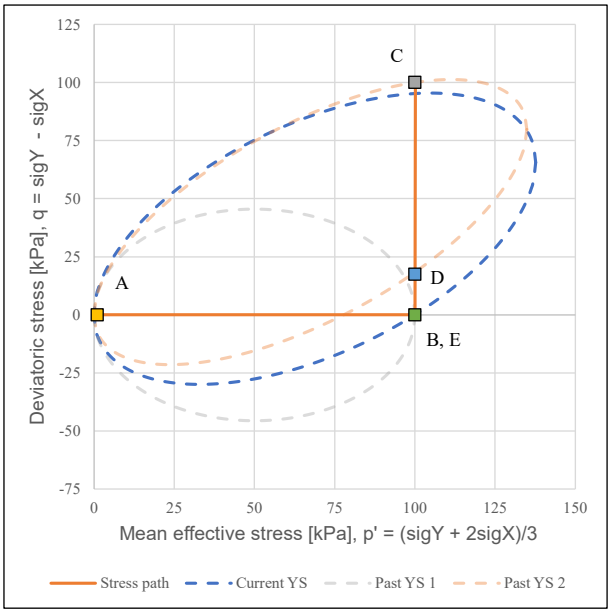

Figure 41. SANICLAY's yield surface (YS) after constant p' unloading.

Also, it is interesting to note on Figure 41 how the yield surface retains its anisotropic shape developed through a past loading phase which involved deviatoric stresses. Although the stress state at point E is isotropic, the yield surface is inclined, showcasing how SANICLAY exhibits anisotropy through past loadings, which is like how real soils behave.

5.15 NorSand Model

NorSand is a soil model based on critical state soil mechanics. While the basic ideas behind the Cam Clay models are also part of NorSand, some important differences make the latter a much more capable soil model, especially for sand behaviour modelling. Having a good understanding of the former will help users better understand the latter.

NorSand was developed during the 80's and 90's based on experience acquired with the construction of structures built on, or even made of, loose sands. The analysis of occurrences of static liquefaction during the construction of these structures contributed to the development of the model by Jefferies (1993). Many iterations of the model have since been proposed. The version built into SIGMA/W is primarily based on Jefferies & Been (2015), but also on Jefferies et al. (2015).

As its name implies, NorSand was mainly developed to model the behaviour of sands, loose and dense, in drained and undrained conditions. The model can successfully predict behaviours ranging from static liquefaction to very strong dilation with a constant set of input parameters, with only initial densities varying. In addition to its excellent performance for sand modelling, NorSand can also perform well for other soil gradations such as silts and tailings. And while there is no published data of the model being used to model clay behaviour, there is no reason why NorSand wouldn't be adequate for such task (Jefferies et al., 2015), given its Cam Clay roots.

5.15.1 Formulation

A brief summary of the model's formulation is presented in the following sections. Jefferies & Been (2015) provide a thorough description of model's formulation and parameters.

5.15.1.1 Elasticity

NorSand considers isotropic elasticity, assuming a constant Poisson's ratio (ν). The elastic shear (G) and bulk (K) moduli are calculated using the following equations, where p_{ref} is a reference stress generally taken as 100kPa, G_{ref} is the reference shear modulus at the reference stress and m is a material constant. The elastic shear modulus can optionally vary via $F_{(e)}$ as a function of the current void ratio if the material constant a is defined. This modifier function accounts for the shape of the soil's grains. Various shapes of grains will impact how the shear modulus varies with regards to the void ratio. The constant a will generally be equal to 2.97 for angular grains and 2.17 for round grains. Other values are also possible.

$$G = G_{ref}\, F_{(e)} \left(\frac{p'}{p_{ref}}\right)^m, \qquad F_{(e)} = \frac{(a-e)^2}{1+e} \tag{Equation 189}$$

$$K = \frac{2(1+\nu)}{3(1-2\nu)} G \tag{Equation 190}$$

Note that m takes values between 0 and 1. A value of $m = 0$ corresponds to a constant elastic shear modulus ($G = G_{ref}$), while $m = 1$ corresponds to an elastic shear modulus that is directly proportional to the current mean stress. Any value of m in between these two extremes is also valid.

The elastic strain increments are calculated as follows:

$$d\varepsilon_v^e = \frac{dp'}{K} \tag{Equation 191}$$

$$d\varepsilon_q^e = \frac{dq}{3G} \tag{Equation 192}$$

5.15.1.2 Critical state

The concept of critical state is cornerstone to NorSand's formulation. There are two axioms to critical state: 1) for a given soil, a unique critical state exists; 2) soils will move toward their critical state when

sheared. For critical state to have been reached, dilation (the ratio of volumetric to deviatoric strain increments) must be zero and the rate of change of dilation must also be zero.

The critical state line is most often defined by a straight line in a semi-ln space ($e - \ln(p')$) as:

$$e_c = \Gamma - \lambda \ln(p') \quad \text{Equation 193}$$

where Γ is the void ratio of the critical state line at p'=1kPa and λ is the slope of the critical state line. Another idealization for the shape of the critical state line is:

$$e_c = C_a - C_b \left(\frac{p'}{p_{ref}}\right)^{C_c} \quad \text{Equation 194}$$

where C_a, C_b and C_c are material parameters. When critical state is reached, the stress ratio $\eta = q/p'$ will reach the critical state ratio M, which is defined based on the Van Eekelen's (1980) formulation as:

$$M = M_c \left(\frac{1 + \beta \sin 3\theta}{1 + \beta}\right)^n \quad \text{Equation 195}$$

where

$$n = -0.229 \quad \text{Equation 196}$$

$$\beta = \frac{1 - k^{\frac{1}{n}}}{1 + k^{\frac{1}{n}}} \quad \text{Equation 197}$$

$$k = \frac{3}{3 + M_c} \quad \text{Equation 198}$$

and where M_c is the critical state ratio for triaxial compression condition and θ is Lode angle (Van Eekelen, 1980).

5.15.1.3 State parameter

An important concept underlying the NorSand model is the state parameter ψ (Been & Jefferies, 1985), defined as the distance between a soil's void ratio and the projected void ratio on its critical state line, at the same mean stress:

$$\psi = e - e_c \quad \text{Equation 199}$$

The state parameter is a dual measure of density and stress level, built into one single parameter. A positive state parameter indicates a looser soil that will generally contract when sheared. A negative state parameter indicates a denser soil that will generally dilate when sheared.

5.15.1.4 Yield surface

In the same way Cam Clay uses the critical state ratio M and the preconsolidation stress p_0' to control the shape and size of its yield surface, NorSand uses the critical state ratio and mean stress at image condition, M_i and p_i' (the image condition is described below), to define its yield surface:

$$F = \eta - M_i \left[1 - \ln\left(\frac{p'}{p_i'}\right)\right] \qquad \text{Equation 200}$$

In the $p' - q$ plane, NorSand's yield surface adopts a teardrop shape, like the original Cam Clay model (Figure 42) where the top of the yield surface is positioned according to the critical state ratio at the image condition M_i. The position of the internal cap (not treated as part of the yield surface in SIGMA/W) is linked to the limiting stress ratio η_L, as defined further on, and controls the maximum allowable dilatancy. Figure 43 shows yield surface in three-dimensional stress space and a cross-section taken in the π-plane, which highlights its dependency on the Lode angle value.

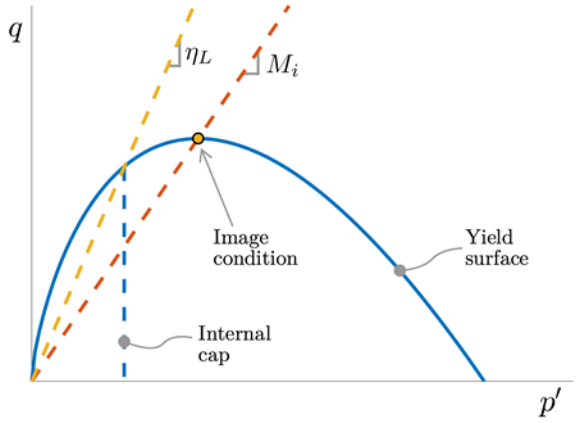

Figure 42. NorSand's yield surface in the p' – q plane.

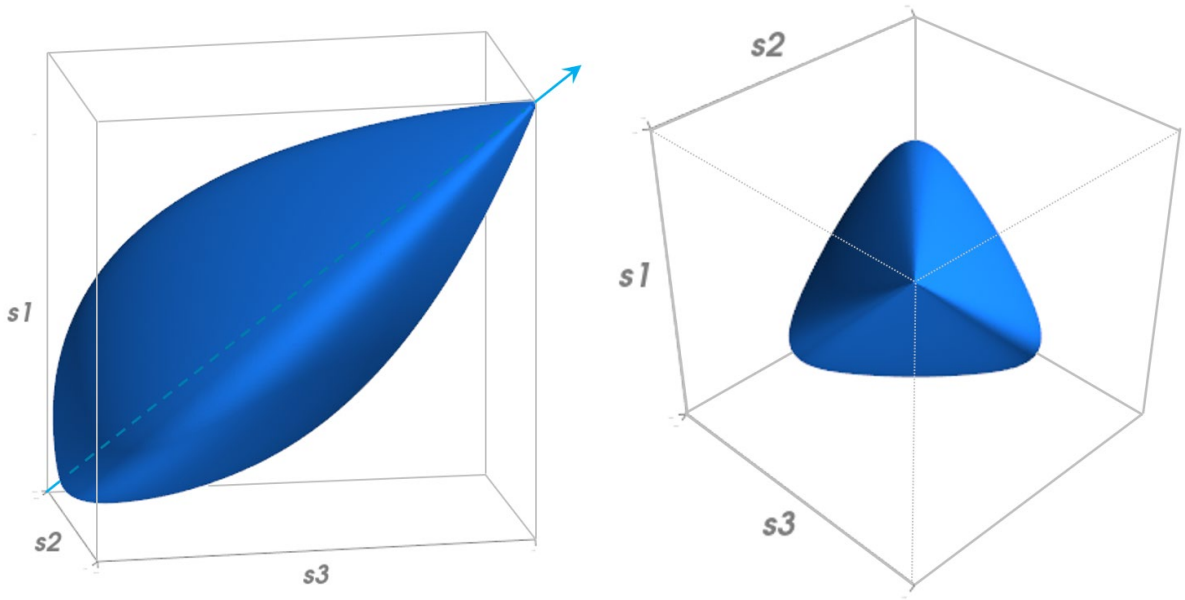

Figure 43. NorSand's yield surface in three-dimensional space and in the π-plane.

5.15.1.5 Image condition

The image condition is used throughout NorSand's formulation as a reference condition towards which many parameters are projected. The image condition refers to a specific point during loading where one of the two requirements to have reached the critical state is met, but not the other. Specifically, when dilation is zero but the rate of change of dilation is not. For example, the image condition arises exactly at the point where a dense sand transitions from contraction to dilation during shearing. The image condition occurs exactly at the top of NorSand's yield surface, where plastic dilatancy is zero, by definition (see Figure 42).

The mean stress at image condition (p_i') is defined using the yield surface definition, as:

$$p_i' = p' \exp\left(\frac{\eta}{M_i} - 1\right) \qquad \text{Equation 201}$$

The state parameter at image condition (ψ_i) is in turn defined using the mean stress at image condition. For the semi-log idealization of the critical state line, the definition would be:

$$\psi_i = e - [\Gamma - \lambda \ln(p_i')] \qquad \text{Equation 202}$$

Finally, the critical state ratio at image condition (M_i) is defined as follows, where N is the volumetric coupling coefficient and χ_i is defined below:

$$M_i = M\left(1 - \frac{N\chi_i|\psi_i|}{M_c}\right)$$ Equation 203

As suggested by Jefferies & Been (2015), Equation 203 only applies to dense soils and $M_i = M$ for loose soils (when $\psi > 0$).

The state-dilatancy parameter χ_c is an important NorSand parameter which relates the maximum dilatancy allowable to the current state. Its triaxial condition value is used as a reference to calculate the state-dilatancy parameter at image condition (χ_i):

$$\chi_i = \frac{\chi_c}{1 - \frac{\chi_c \lambda}{M_c}}$$ Equation 204

5.15.1.6 Hardening rule

Once a soil's state lies on the yield surface and further plastic strains are induced, the yield surface must harden to accommodate the new stress state. NorSand's hardening rule is expressed as follows:

$$\frac{dp_i'}{p_i'} = \left(X_{Hard} + X_{Soft}\right)d\varepsilon_q^p$$ Equation 205

The first term (i.e., X_{Hard}) is the original NorSand hardening rule, where the difference between the maximum allowable dilatancy and the current yield surface position is used to scale the intensity of the hardening:

$$X_{Hard} = H\frac{M_i}{M_{i,c}}\left(\frac{p'}{p_i'}\right)^2\left[\left(\frac{p_i'}{p'}\right)_{max} - \frac{p_i'}{p'}\right]$$ Equation 206

Equation 206 is scaled by the plastic hardening modulus H

$$H = H_0 - H_y\psi$$ Equation 207

where H_0 is the basic plastic hardening modulus and H_y is an optional parameter to induce a dependency on H towards the state parameter ψ.
The maximum allowable dilatancy, which also positions the yield surface's internal cap, is calculated as:

$$\left(\frac{p_i'}{p'}\right)_{max} = \exp\left(-\frac{\chi_i\psi_i}{M_{i,c}}\right)$$ Equation 208

Where $M_{i,c}$ is the image stress ratio at Triaxial compression condition.
The second term of NorSand's hardening rule (i.e., X_{Soft}) brings additional softening that can be scaled by the index S (where $S = 0$ turns the feature completely off, which is the default value):

$$X_{Soft} = S\frac{-1}{\frac{\chi_i \lambda}{M_{i,c}} + 1} D^p \left(\frac{K}{p}\right)\left(\frac{\eta}{\eta_L}\right)$$ Equation 209

This additional softening is appropriate for undrained loading of loose soils, as such it is internally shut off for any drained or dense undrained NorSand material ($\psi < 0$). Values of S between 0 and 1 should be used.

In Equation 209, D^p is the plastic dilatancy and η_L is the limiting stress ratio, corresponding to the junction between NorSand's yield surface and its internal cap (see Figure 42):

$$D^p = \frac{d\varepsilon_v^p}{d\varepsilon_q^p} = M_i - \eta$$ Equation 210

$$\eta_L = M_i\left(1 - \frac{\chi_i \psi_i}{M_{i,c}}\right)$$ Equation 211

5.15.1.7 Failure

SIGMA/W offers the possibility of identifying which elements are failed within any simulation (via the "Draw Plastic States" tool). For non-linear elasto-plastic constitutive models such as NorSand, the concept of failure is not as easily defined as for Mohr-Coulomb for example (where an element is either failed or not, nothing in between). The critical state could represent that failure condition, however, reaching critical state exactly is most often not numerically feasible. As such, a custom failure condition was defined for NorSand which tries to identify when an element is sufficiently close to its critical state so that it can be considered failed. Similar to the actual critical state condition, two distinct conditions must be simultaneously met for an element to be considered failed:

a) $|\psi| < 0.001$
b) $|\eta - M_i| < 0.1$

This custom failure condition is solely used as a visual aid to graphically identify which elements are failed and which aren't in any given simulation. The failure condition does not affect the calculated response in any way.

5.15.2 Material parameters

NorSand being a relatively simple soil model, the number of model parameters required for simulation is also relatively modest, as shown in Table 16. At minimum, NorSand requires eight parameters to function, only three of which are specific to NorSand: two for elasticity (G_{ref} and ν, setting m at either 0 for constant G or 1 for stress-dependant G), two for the critical state locus (Γ and λ) and four for plasticity (M_c, χ_c, N and H_0).

The other model parameters shown in Table 16 can be used to tailor NorSand for specific needs: m and a to better fit elastic behaviour measures, $C_a, C_b\ and\ C_c$ to define the critical state locus by a curve. In

addition, H_y to infer a dependence on H towards ψ and finally S to provide additional softening for undrained loading of loose soils.

Input parameters needed for NorSand can be calibrated using standard drained and undrained triaxial compression tests (three tests of each type will generally provide a reasonable calibration). NorSand's easy calibration represents one of the core qualities of the model.

Table 16 includes the initial condition parameters required to initialize the model: the initial void ratio e (or initial state parameter) and overconsolidation ratio OCR. In the NorSand model, the OCR is used to find the past maximum size of the yield surface (i.e., $p'_{i,max}$):

$$p'_{i,max} = (OCR)p'_{i,0} \qquad \text{Equation 212}$$

where $p'_{i,0}$ is the size of the yield locus passing through the current stresses. From Equation 200:

$$p'_{i,0} = p'_0 \exp\left(\frac{q_0}{M_i p'_0} - 1\right) \qquad \text{Equation 213}$$

where p'_0 and q_0 in Equation 213 are initial values of mean effective stress and deviatoric stress, respectively.

Table 16. Parameters for the NorSand model.

Model parameters		Symbol	Unit
Elastic shear modulus at reference stress		G_{ref}	kPa
Reference stress (default value=100kPa)		p_{ref}	kPa
Elastic exponent		m	
Constant to relate the elastic shear modulus to the void ratio (optional)		a	
Effective Poisson's ratio		ν	
Semi-Ln critical state locus	Altitude of critical state line at $p' = 1kPa$	Γ	
	Slope of critical state line (base e)	λ	
Curved critical state locus	Critical state coefficient	C_a	
	Critical state coefficient	C_b	
	Critical state coefficient	C_c	
Critical state ratio, referenced for triaxial compression conditions		M_c	
State-dilatancy parameter, reference for triaxial compression conditions		χ_c	
Volumetric coupling coefficient		N	
Plastic hardening modulus		H_0	
Evolution hardening modulus		H_y	
Additional softening parameter		S	
Initial conditions			
Initial void ratio OR Initial state parameter		e or ψ	
Overconsolidation ratio		OCR	

Table 17 presents the state parameters and stress ratio (η/M) that can be graphed and contoured to interpret the responses simulated by the NorSand model.

Table 17. Material state parameters definition for NorSand when drawing graphs.

Parameter name	Corresponding parameter
Size of the yield surface	p_i
Critical state ratio at image condition	M_i
State parameter	ψ
eta / M (mobilized strength)	η/M

5.15.3 Conceptual response

NorSand's constitutive equations were presented in Section 5.15.1, where focus was put on formulation rather than conceptualization. Some examples are provided in this section to help users better understand how the model functions.

A drained triaxial compression test simulated with NorSand is shown in Figure 44 for a hypothetical dense sand ($\psi_0 < 0$). Some points of interest in the test are identified with letters in the figure. At the start of the test (point A), the sample is overconsolidated, as the stress point lies inside the yield surface (red curve, Figure 44b, note that on this part of the figure, the stress path is denoted by the blue line, while yield surfaces associated to various loading points are denoted by colored curves). The loading is thus elastic from point A to point B, with little deformations being produced (Figure 44c). As the stress state touches the yield surface (point B), the loading becomes elasto-plastic, which pushes the yield surface to harden. The loading will then proceed to push the yield surface further to accommodate stress states that would lie outside of its boundaries. The sample being dense, dilation is initially positive (Figure 44d), which will produce positive volumetric strains (volumetric contraction, Figure 44c). At point C, the loading passes the image condition (where D^p is momentarily zero, Figure 44d, with the stress point lying exactly on top of the yield surface, yellow curve in Figure 44d). The image condition sparks a new trend in volumetric behaviour, as the sample will now on dilate. At point D, the sample reaches its peak strength (highest deviatoric stress q, Figure 44a, largest yield surface, purple curve in Figure 44b), which corresponds to the maximum negative dilation reached (Figure 44d). As the sample moves closer to its critical state (approximately reached at point E, green yield surface, Figure 44b), dilation will approach zero (Figure 44d) and no further volumetric strains will be produced (Figure 44c).

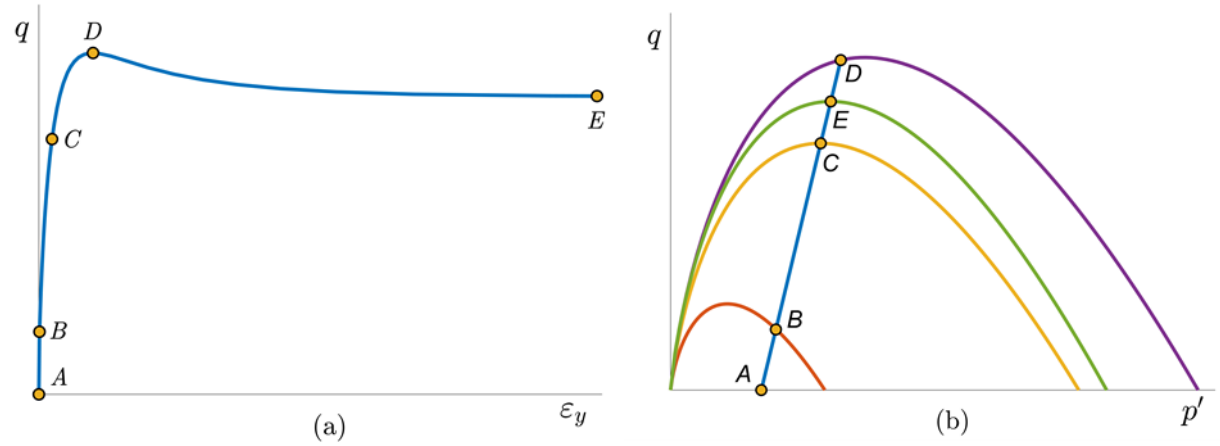

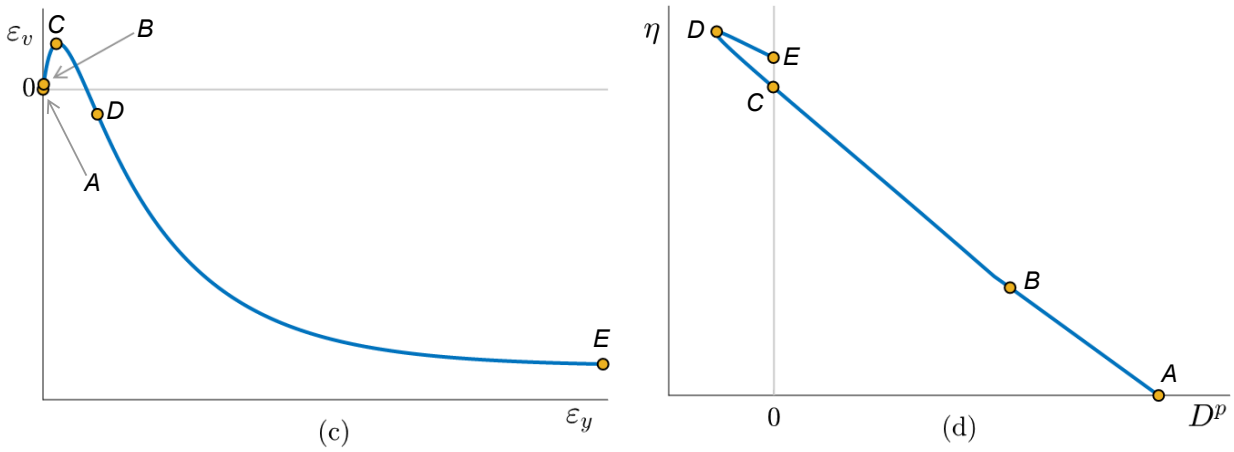

Figure 44. Drained triaxial compression as described by the NorSand model: (a) stress – strain plot; (b) stress path plot with associated yield surfaces; (c) volumetric strain plot; (d) stress ratio – plastic dilation plot.

In another example, three different hypothetical undrained triaxial compression tests modelled with NorSand are shown in Figure 45, again with various points of interest being identified via letters. All tests shown are normally consolidated. The blue line refers to a dense sample ($\psi_0 < 0$), which starts its loading at point A. Similar to the results shown in Figure 44, the dense sample initially contracts (diminution of state parameter value, Figure 45d, augmentation of pore water pressure, Figure 45c) until the image condition is reached at point B. Onwards, plastic dilation will be negative and pore water pressure will decrease (Figure 45c), which will bring the sample's stress state towards higher values of effective stresses (Figure 45b). The sample will reach its critical state at large deformations (Figure 45a), approximately at point C.

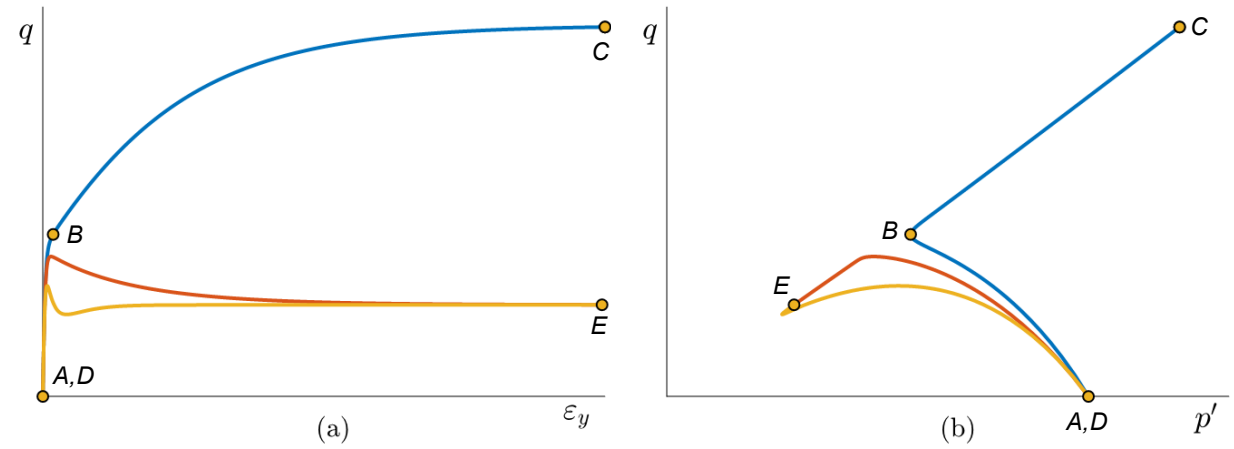

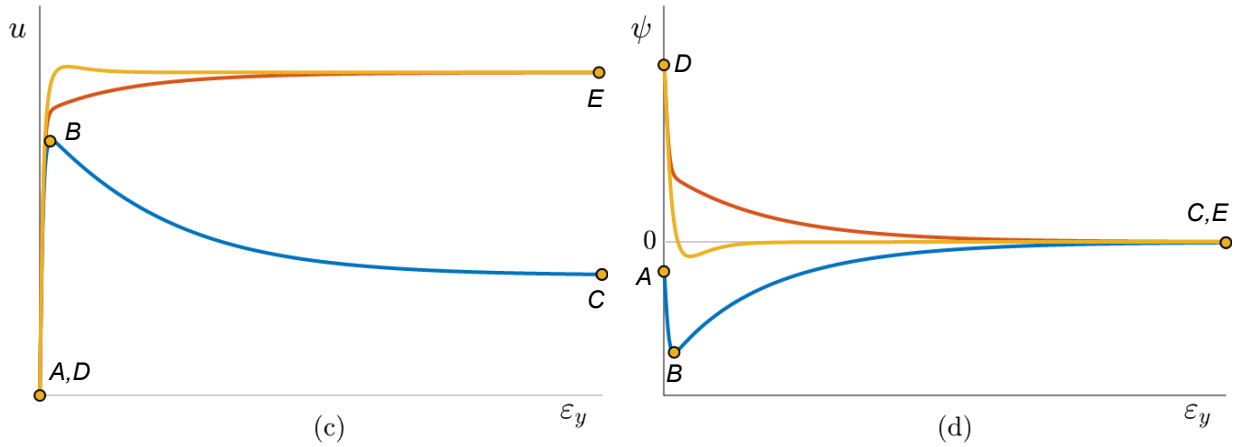

Figure 45. Undrained triaxial compression as described by the NorSand model: dense sample (blue curve), loose sample with $S = 0$ (red curve) and $S = 1$ (yellow curve); (a) stress – strain plot; (b) stress path plot; (c) excess pore pressure – strain plot; (d) state parameter – strain plot.

The red and yellow curves shown in Figure 45 relate to a hypothetical loose sample ($\psi_0 > 0$) being sheared, with the additional softening turned off (red curve, $S = 0$) and on (yellow curve, $S = 1$). Both samples start loading at point D (same state parameter, Figure 45d) and end at point E. The additional softening available in NorSand (Equation 209) for loadings of undrained loose soil causes the yellow sample to generate excess pore water pressure quickly (Figure 45c) and lowers the peak resistance developed (Figure 45a). At large deformations, both samples will reach the same deviatoric stress (Figure 45a) and pore water pressure (Figure 45c), which makes their stress paths coincide on point E. As critical state is nearing, all samples, loose and dense, will see their state parameter tend to zero (points C and E in Figure 45d).

As was demonstrated with the examples presented herein, NorSand is effectively capable of modelling diverse stress-strain behaviours of sands, which range from very dilative (Figure 44, blue curve in Figure 45) to very contractive (red and yellow curves in Figure 45). Those seeking to understand the role each parameter plays within the model are encouraged to simulate the response of hypothetical soils under simple loading conditions (triaxial compression is suggested for such purpose).

5.16 Soft Soil Model

The Soft Soil model was primarily developed for simulating the response of highly compressible soils such as normally consolidated clays and clayey silts (PLAXIS 2017). This constitutive model is formulated within the generalized elastic-plastic framework (Section 3.4) and takes advantage of some features of the Modified Cam Clay model (Section 5.13).

Numerous modifications have been proposed to the Modified Cam Clay model since its inception. Many of these modifications have been concerned with the overestimation of failure stresses on the supercritical (dry) side of the elliptical yield surface. Zienkiewicz and Naylor (1973), for example, adopted a linear Hvorslev surface on the supercritical side that passed through the peak of the elliptical yield surface. Di Maggio and Sandler (1971) and Sandler et al. (1976) proposed 'Cap models' in which the

elliptical yield surface hardened with plastic volumetric strain while the failure surface remained fixed. The Soft Soil model implemented in SIGMA/W is similarly formulated to deal with stresses in the supercritical region of the yield surface.

5.16.1 Formulation

The Soft Soil model includes an elliptical yield surface with a horizontal major axis (Figure 46). The flow rule is assumed to be associated and the failure criterion is the van Eekelen (1980) extension of the Mohr-Coulomb failure criterion.

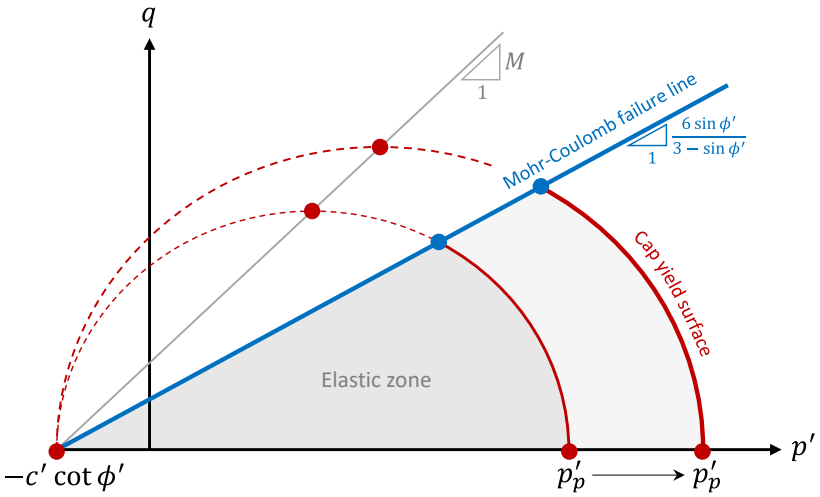

Figure 46. Yield surface and failure line in the Soft Soil model

5.16.1.1 Isotropic behaviour

The soil behaviour during isotropic unloading and reloading is assumed to be elastic based on Hooke's law. The unloading-reloading bulk modulus K_s is defined as:

$$K_s = \frac{p'_p + c' \cot \phi'}{\kappa^*} \qquad \text{Equation 214}$$

where p'_p represents the isotropic effective stress, c' and ϕ' are the effective cohesion and the effective friction angle, respectively, and the parameter κ^* is the modified swelling index. A similar linear stress dependency is also assumed for the elastic-plastic bulk modulus K_c, so that:

$$K_c = \frac{p'_p + c' \cot \phi'}{\lambda^*} \qquad \text{Equation 215}$$

where the parameter λ^* is the modified compression index. The linear behavior of the sample in the semi-log stress-strain space is shown in Figure 47.

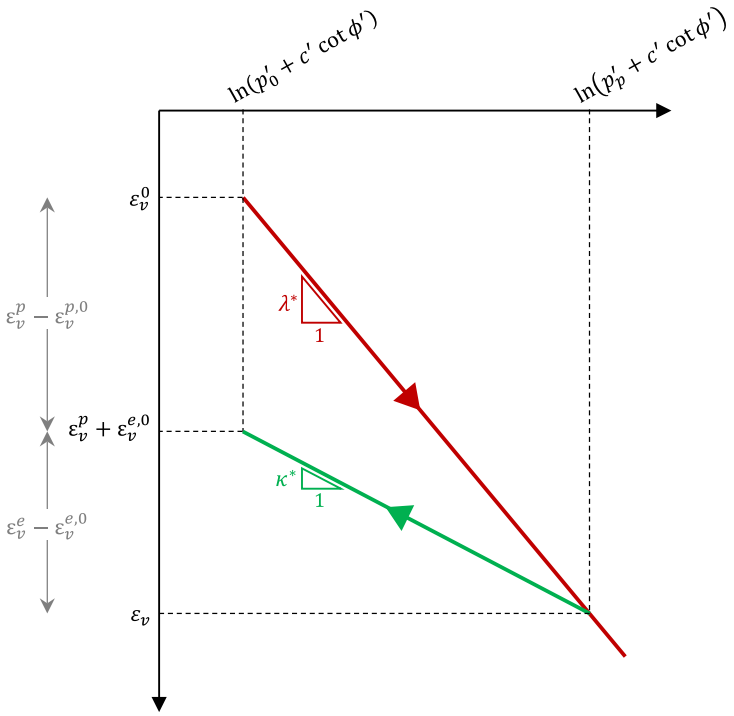

Figure 47. Logarithmic relation between volumetric strain and isotropic effective stress

The plastic bulk modulus of the sample (i.e., H) is expressed in the Soft Soil model in terms of the elastic and elastic-plastic bulk moduli:

$$\frac{1}{H} = \frac{1}{K_c} - \frac{1}{K_s} \qquad \text{Equation 216}$$

which conceptually represents the elastic-plastic stiffness of the sample (K_c) as an equivalent spring stiffness resulting from the elastic (K_c) and plastic (H) springs in series. Substitution of Equation 214 and Equation 215 into Equation 216 gives:

$$H = \frac{K_c}{K_s - K_c} K_s = \frac{p'_p + c' \cot\phi'}{\lambda^* - \kappa^*} \qquad \text{Equation 217}$$

5.16.1.2 Failure law

The failure criterion adopted by the Soft Soil model is the van Eekelen (1980) extension of the Mohr-Coulomb failure law:

$$F = q - g(\theta) \frac{6 \sin\phi'}{3 - \sin\phi'} \left(p' + c' \cot\phi'\right) = 0 \qquad \text{Equation 218}$$

where q and p' are generalized stress invariants (Section 3.2), θ is the Lode angle, and $g(\theta)$ represents the van Eekelen function (see Equation 151).

5.16.1.3 Cap yield function

The cap yield surface is described by the equation of an ellipse when written in terms of stress invariants (see Figure 46):

$$f = \frac{q^2}{M^2 g^2(\theta)\left(p' + c' \cot \phi'\right)} + p' - p'_p \qquad \text{Equation 219}$$

where M is a constant that determines the aspect ratio of the ellipse. The plastic potential function is obtained by assuming associated flow rule; therefore, the plastic potential function is also identical to the yield function given by Equation 219. The parameter M is derived in terms of the other model constants:

$$M = 3\sqrt{\left(\frac{1 - K_0^{NC}}{1 + 2K_0^{NC}}\right)^2 + \frac{\lambda^* - \kappa^*}{\frac{1 + 2K_0^{NC}}{1 - K_0^{NC}}\lambda^* - \frac{1 + \nu'}{1 - 2\nu'}\kappa^*}} \qquad \text{Equation 220}$$

where K_0^{NC} represents the coefficient of lateral pressure in a one-dimensional compression loading on a normally consolidated soil, and ν' is the Poisson's ratio in unloading-reloading.

5.16.1.4 Initialization of State Parameters

The Soft Soil model, like the modified Cam clay and Hardening Soil models, requires an input for the isotropic over-consolidation ratio (OCR), which is defined as:

$$OCR = \frac{p'_{p,max}}{p'_{p,i}} \qquad \text{Equation 221}$$

where $p'_{p,max}$ is the past maximum value of the equivalent isotropic stress and $p'_{p,i}$ is the current, or initial, equivalent isotropic stress (refer to Figure 35, noting the difference in the subscripts). The initial equivalent isotropic stress $p'_{p,i}$ is given in terms of initial invariants using Equation 219:

$$p'_{p,i} = \sqrt{\frac{q_i^2}{M^2 g^2(\theta_i)\left(p'_i + c' \cot \phi'\right)} + {p'}_i^2} \qquad \text{Equation 222}$$

The past maximum value of the equivalent isotropic stress is then calculated as:

$$p'_{p,max} = (OCR) p'_{p,i} \qquad \text{Equation 223}$$

5.16.2 Material Parameters

Table 18 provides a summary of the required parameters for the Soft Soil model.

Table 18. Parameters for the Soft Soil Model

Parameter	Symbol	Unit
Effective friction angle	ϕ'	°
Effective cohesion	c'	kPa
Angle of dilation	ψ	°
Over consolidation ratio	OCR	
Coefficient of earth pressure for the normally compressed state	K_0^{NC}	
Poisson's ratio	ν'	
Modified swelling index	κ^*	
Modified compression index	λ^*	

Table 19 provides relationships to assist with conversion between the modified swelling and compression indices and their original counterparts from the modified Cam Clay model. Approximate relationships are also included to relate to the compression index (see Table 13 for important notes regarding the latter).

Table 19. Relationships between modified Cam clay material parameters and other commonly measured quantities.

Parameter	Relationship
κ^*	$\kappa^* = \frac{\kappa}{1+e}$
	$\kappa^* \approx \frac{2C_c}{(1+e)\ln 10}$
λ^*	$\lambda^* = \frac{\lambda}{1+e}$
	$\lambda^* = \frac{C_c}{(1+e)\ln 10}$

Conceptual Response

The key aspects of the Soft Soil model formulation and its parameters were presented in Sections 5.16.1 and 5.16.2. In this section, the main features of the Soft Soil model are explored by considering triaxial test simulations.

Figure 48 depicts the conceptualized simulated results of a conventional drained triaxial test on an overconsolidated material represented by the Soft Soil model. Point S represents the state of the

sample at the start of shearing. As shown in Figure 48a, the soil behavior is assumed to be linear elastic as long as the stress state is located inside the elliptical yield surface. The modified swelling index (i.e., κ^*) determines the stiffness of the sample during this elastic loading stage (Figure 48c). The elastic-plastic non-linear response begins when the stress path intersections the yield surface at point Y (Figure 48b). The simulated response during this stage of loading corresponds to that of a normally consolidated soil. The elliptical (cap) yield surface expands as the stress path progresses towards the failure surface (Figure 48a). Failure occurs at point F where the stress state reaches the Mohr-Coulomb failure line. The axial strain continues after failure occurs in a constant-volume manner (Figure 48b and Figure 48d).

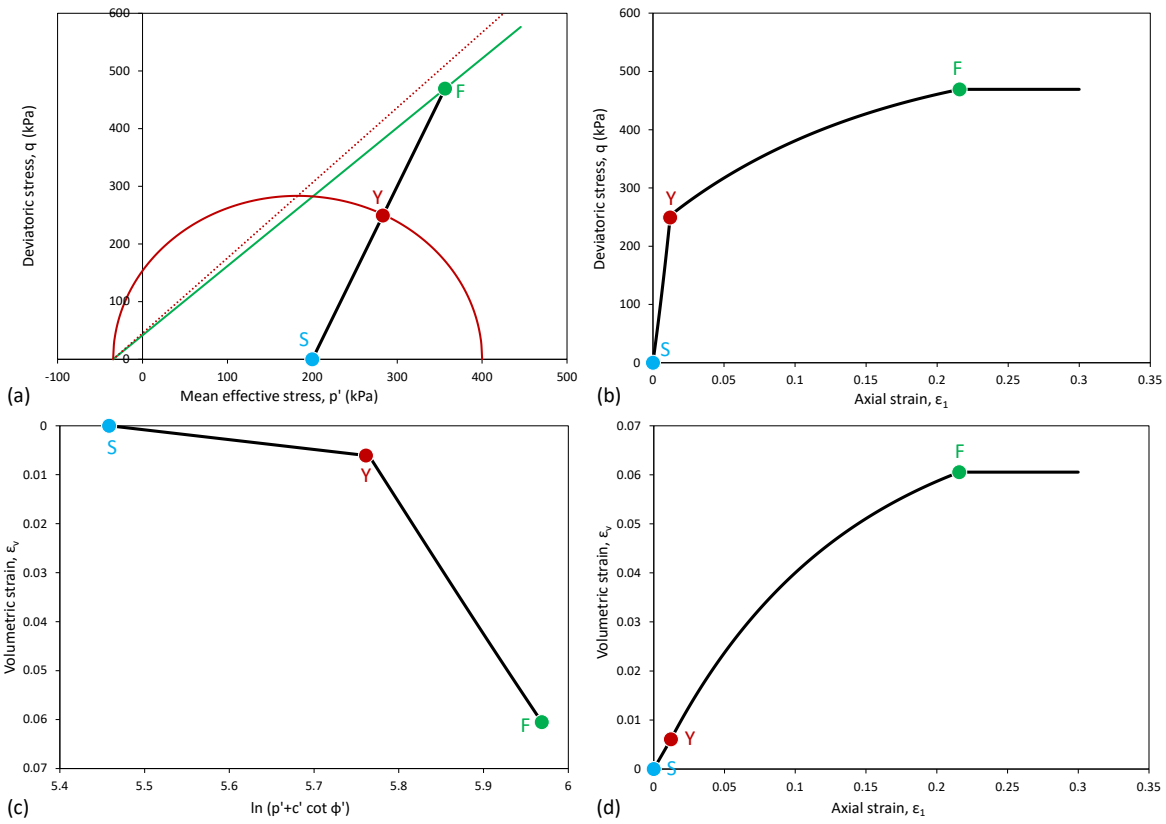

Figure 48. Conventional drained triaxial compression test on an over-consolidated soil described by the Soft Soil model: (a) $p' - q$ effective stress plane; (b) $q - \varepsilon_1$ stress-strain plot; (c) $\varepsilon_v - \ln(p' + c' \cot\phi')$ compression plane; (d) $\varepsilon_v - \varepsilon_1$ volume-strain plot.

Figure 49 depicts the conceptualized simulated results of a conventional drained triaxial test on a normally compressed material represented by the Soft Soil model. The stress state at the start (S) of the loading (Point S) is located on the yield surface (Point Y). During drained triaxial loading, the yield surface expands, and the non-linear response lasts until the stress path touches the Mohr-Coulomb failure line at point F (Figure 49a).

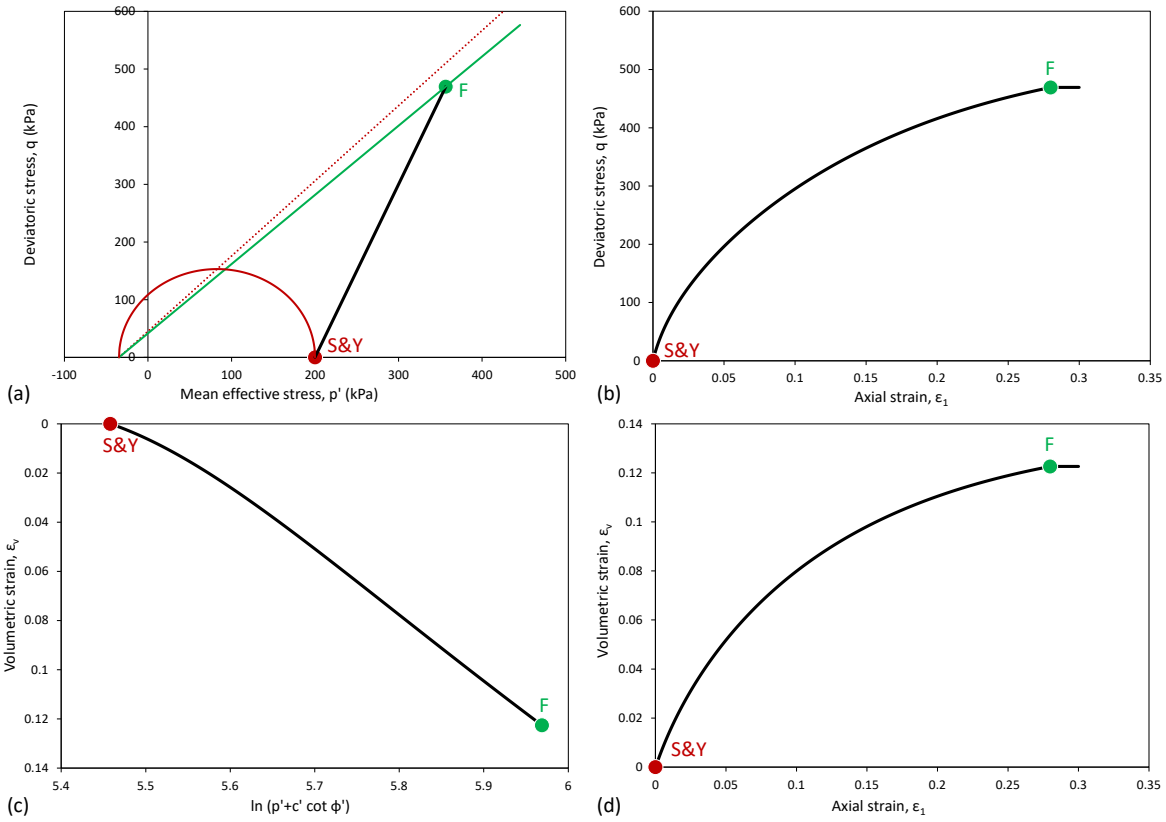

Figure 49. Conventional drained triaxial compression test on a normally consolidated soil described by the Soft Soil model: (a) $p' - q$ effective stress plane; (b) $q - \varepsilon_1$ stress-strain plot; (c) $\varepsilon_v - \ln(p' + c' \cot \phi')$ compression plane; (d) $\varepsilon_v - \varepsilon_1$ volume-strain plot.

Figure 50 depicts the conceptualized simulated results of a conventional undrained triaxial test on an overconsolidated material represented by the Soft Soil model. During the first stage of loading – that is, from point S to yield at point Y – the size of the yield surface is fixed, and the stress path is located entirely within the elastic zone (Figure 50a). The changes in pore pressure are equal to the change in mean total stress (Figure 50c); consequently, the mean effective stress does not change, and the stress path tracks vertically (Figure 50a). The slope from S to Y in Figure 50b is equal to $3G$, where the shear modulus can be related to the bulk modulus (Equation 214) by Equation 26 and Equation 28. There is a sharp decrease in stiffness when yielding begins at point Y (Figure 50b) because of the addition of plastic strains. The additional tendency for plastic volumetric compression produces an addition component to the pore pressure increase, causing the stress path to turn to the left (Figure 50a). In addition, there is a kink in the pore pressure vs mean effective stress and axial strain plots (see Figure 50c and Figure 50d). These trends continue until the critical state is reached; that is, when failure occurs at point F.

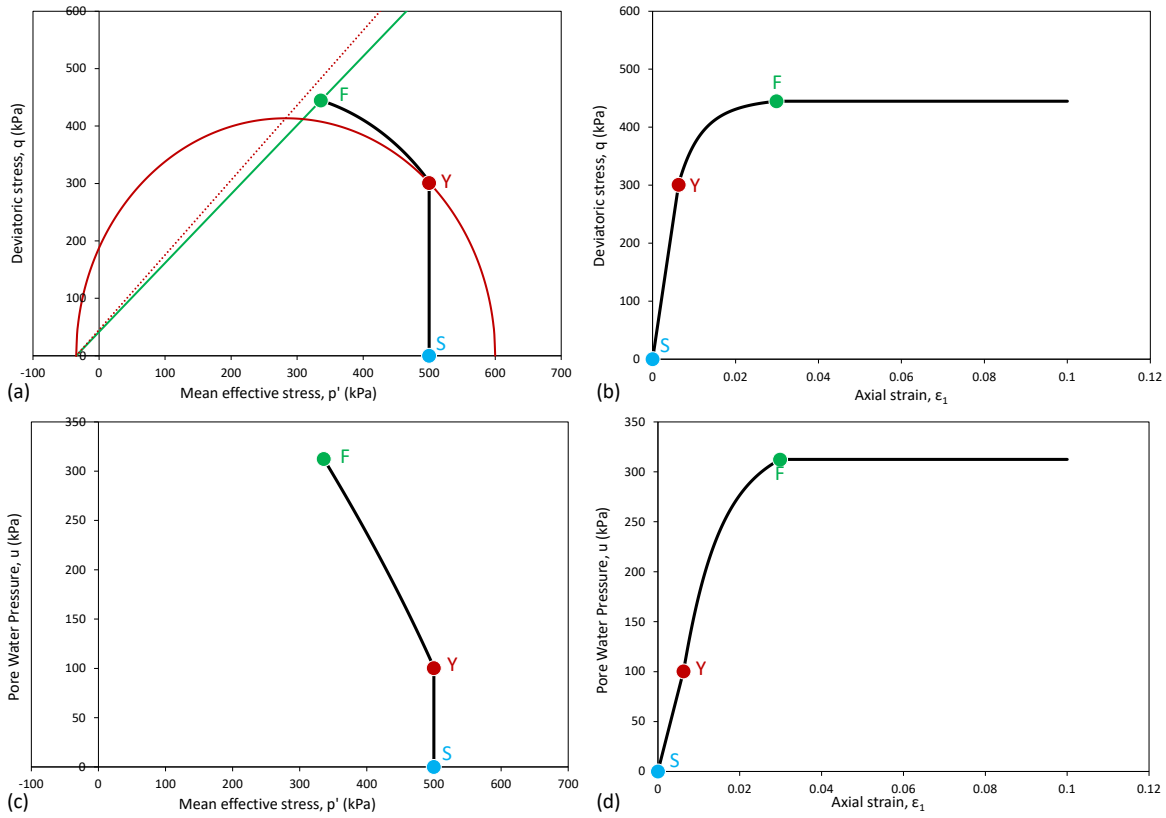

Figure 50. Conventional undrained triaxial compression test on an over-consolidated soil described by the Soft Soil model: (a) $p' - q$ effective stress plane; (b) $q - \varepsilon_1$ stress-strain plot; (c) $u - p'$ pore pressure-stress plot; (d) $u - \varepsilon_1$ pore pressure-strain plot.

The Soft soil model simulates the same undrained response in normally consolidated soils, except that there is no elastic stage in the response of normally consolidated samples (Figure 51). In other words, the stress state is located on the yield surface when deviatoric loading initiates.

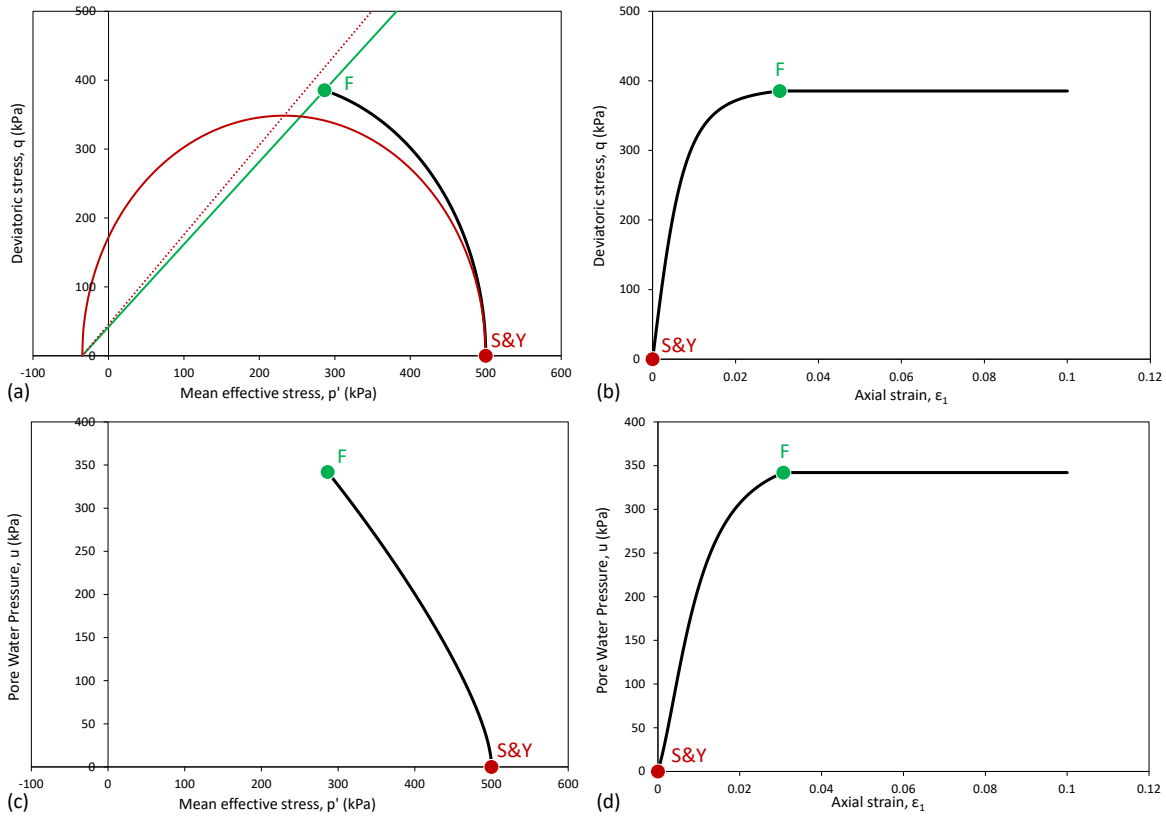

Figure 51. Conventional undrained triaxial compression test on a normally consolidated soil described by the Soft Soil model: (a) $p' - q$ effective stress plane; (b) $q - \varepsilon_1$ stress-strain plot; (c) $u - p'$ pore pressure-stress plot; (d) $u - \varepsilon_1$ pore pressure-strain plot.

6 Structural Components

Section 3.8 provides a brief overview of the key concepts pertaining to the formulation of structural elements. The following sections define the constitutive law that relates the strain increments to the element forces and, in some instances, bending moments for each structural component. The constitutive law reveals the properties required to parameterize the response of the structure in a stress-strain analysis.

6.1 Pin-Ended Bar

A pin-ended bar can be used to represent structures such as a prop, the free length of an anchor, or an end bearing pile. The pin-ended bar can be conceptualized as a spring between two nodes; hence it is sometimes referred to as a node-to-node anchor. A pin-ended bar is applied to a line, forming a one-dimensional structure within a two-dimensional domain. The constitutive law for a pin-ended bar in a 2D plane strain simulation is given as:

$$\delta N_1 = [EA]\{\delta\varepsilon_1\} \qquad \text{Equation 224}$$

where δN_1 and $\delta \varepsilon_1$ are the axial force and axial strain increments, respectively. Table 20 presents the inputs for a pin-ended bar. The spacing is the out-out-plane installation distance.

Table 20. Parameters for pin-end bar.

Parameter	Symbol	Unit
Spacing	s	m
Elastic Modulus	E	kPa
Cross-sectional Area	A	m^2
Pre-Axial Force		kN

6.1.1 Prestressed Bar

SIGMA/W assumes that a structural bar is prestressed if the pre-axial force input is non-zero. Prestressing results in a force boundary condition applied at the end-points of a structural bar. Prestress forces are applied on the first load/time step of an analysis. A bar should not be prestressed if other loads are applied to the domain, including via region activation or deactivation.

6.2 Beam

The beam element is formulated based on Timoshenko beam theory, which considers the shear deformations and rotational bending effects. Taking into account the added mechanism of deformation effectively lowers the stiffness of the beam, which results in a larger deflection under a static load when compared to an element formulated based on Euler-Bernoulli beam theory. Timoshenko beam theory converges towards Euler-Bernoulli beam theory if the shear modulus approaches infinity, making the beam rigid in shear. The maximum deflection of a cantilevered beam with a single load can be simulated in accordance with ordinary beam theory by artificially increasing the axial stiffness, and therefore the shear resistance.

A beam is used in a plane strain (2D) analysis to model structures that have axial stiffness, resistance to shear and bending. A beam is applied to a line, forming a one-dimensional element within a two-dimensional domain. The constitutive law is given as:

$$\begin{Bmatrix} \delta N_1 \\ \delta F_{12} \\ \delta M_3 \end{Bmatrix} = \begin{bmatrix} EA & 0 & 0 \\ \square & kGA & \square \\ \square & \square & EI_{\square} \end{bmatrix} \begin{Bmatrix} \delta \varepsilon_1 \\ \delta \gamma_{12} \\ \delta \kappa_3 \end{Bmatrix} \qquad \text{Equation 225}$$

where ΔF_{12} is the shear force, γ_{12} the shear strain, and M_3 and κ_3 are the bending moment and bending

strain, respectively. Beams cannot be used in axisymmetric analyses. Table 21 presents the inputs required for a beam. The stiffness and capacity values are normalized by spacing at solve-time in the same manner as a bar.

Table 21. Parameters for a beam.

Parameter	Symbol	Unit
Spacing	s	m
Elastic Modulus	E	kPa
Cross-sectional Area	A	m^2
Moment of Inertia	I	m^4

7 Boundary Conditions

The solution of the finite element equations is constrained by boundary conditions (Appendix I). The fundamental boundary conditions for a stress-strain analysis are force and displacement. Displacement boundary conditions must be applied to the domain in a manner that limits rigid body deformation of the entire finite element mesh. If these conditions are not satisfied, the global stiffness matrix will be singular and the equations cannot be solved. Stated another way, sufficient displacement boundary conditions must be applied to maintain equilibrium of the system.

For a three-dimensional analysis, there are three degrees-of-freedom at every node with the displacements given as:

$$\{\delta u\}^T = \{\delta u_x \quad \delta u_y \quad \delta u_z\} \qquad \text{Equation 226}$$

and the nodal forces given by:

$$\{\delta F\}^T = \{\delta F_x \quad \delta F_y \quad \delta F_z\} \qquad \text{Equation 227}$$

Stress-strain constitutive relationships (Equation 10) link infinitesimal changes in stress and strain. Accordingly, the displacement and force boundary conditions are incremental. The basic boundary conditions are generally self explanatory and the means of defining them are described in the example files and tutorials. However, the more complex boundary conditions merit further discussion and are described in the following sections.

7.1 Prescribed Displacements

A displacement boundary condition imposes the movement of a node for the various degrees-of-freedom. A constant displacement boundary condition is applied on each load step and time step for Load-Deformation and Consolidation analyses, respectively. A step function must therefore be defined if the displacement is to be applied on the first step of an analysis with multiple load-steps. Displacement boundary conditions can be applied to points, lines, and regions.

7.2 Boundary Stresses

Stress boundary conditions are converted to equivalent nodal forces via formal numerical integration over the area of an element. Consider for example the normal stress and shear stress boundary conditions applied to the line segments in Figure 52. Integration of the normal stress will result in an apportioning of a y-force to each node under the generalized stress distribution (edge 1-5). Similarly, numerical integration of the shear stress will produce an x-force at each node along edge 5-6. Stress boundary conditions are useful for modelling external loads on the system that do not need to be represented by a region. Stress boundary conditions can be applied to lines and regions. Finally, a stress boundary function must be used for Load-Deformation and Coupled Consolidation analyses if the load is to be applied on the first step only.

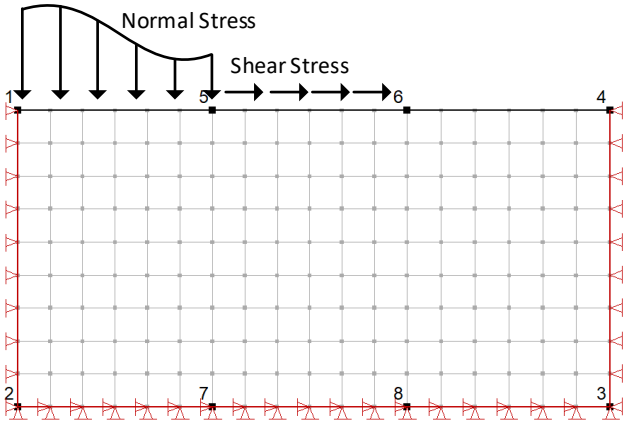

Figure 52. Example of stress boundary conditions.

7.2.1 Hydrostatic Pressure

The presence of a fluid surcharge load on the ground surface increases the total stress within the domain (Figure 53). This condition is handled in SIGMA/W through the use of a hydrostatic pressure boundary condition. The inputs include the elevation of the fluid surface and the unit weight of the fluid. SIGMA/W automatically applies the stress boundary normal to the ground surface. The fluid elevation can be defined as a function of time for a Coupled Consolidation analysis.

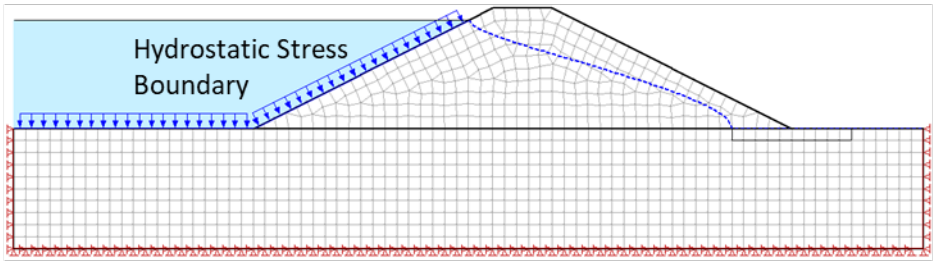

Figure 53. Example of a hydrostatic boundary condition.

7.3 Construction and Excavation

Many geotechnical problems involve placing new material or removing existing material. For example, building an embankment or backfilling behind a retaining wall both involve placing material on a pre-existing geometry. Similarly, material is removed for the construction of a deep foundation or tunnel. These two scenarios are handled in SIGMA/W through material activation and deactivation.

Material activation is similar to the Gravity Activation analysis described in Section 4.1.2. The activation of a new material is manifest in a body force boundary condition for regions that become active for the first time. Consider, for example, the embankment construction problem shown in Figure 54. The embankment construction is sub-divided into five stages. The geometry and elements representing the embankment are present in the original (i.e. Parent) SIGMA/W analysis, but a material has not been applied to these regions. The application of a material to a region produces a body force boundary condition for the load step. In a subsequent analysis, a new layer becomes active while the first layer is now fully present in the analysis

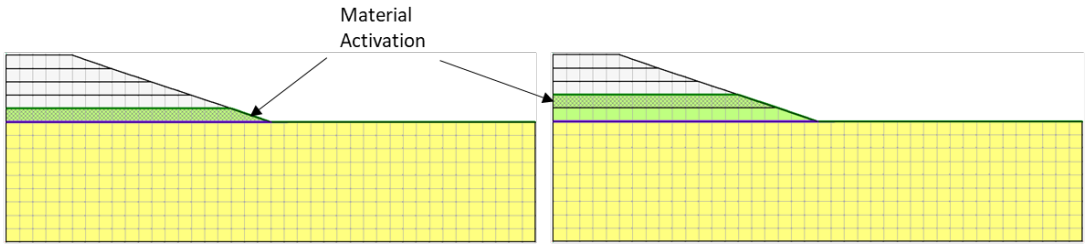

Figure 54. An example of material activation.

Material deactivation involves determining the reaction forces acting on boundaries of regions that are to be deactivated (excavated). When a region becomes deactivated, opposing reaction forces are applied as boundary conditions to the adjacent active region boundaries. Material deactivation requires the finite element mesh to be present and active in the original (i.e. Parent) SIGMA/W analysis.

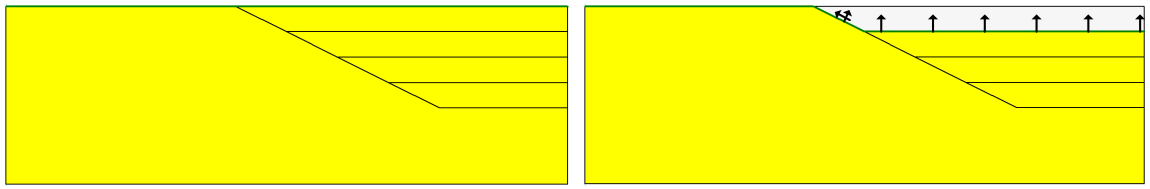

Figure 55. An example of material deactivation.

The material activation and deactivation procedure for modeling construction and excavation is summarized as follows:

1. The geometry must include all regions for the construction and/or excavation sequence;
2. The activation boundary condition is automatically assembled when a material is applied to a region that was previously inactive;
    a. The activation boundary condition calculates the body force load in the same manner as a Gravity Activation analysis;
3. The deactivation boundary condition is automatically applied when a material is removed from a region that was previously active;
    a. The deactivation boundary condition calculates a traction force that is based on the existing stresses at the excavation boundary;
4. The displacements of nodes connected to inactive elements are zeroed until the element becomes active; and,
5. The activation/deactivation procedure is applicable to Load-Deformation and Coupled Consolidation analysis types.

7.3.1 Submerged Construction

Submerged fill placement is a common class of problem in geotechnical engineering. The material activation procedure described above is used for analysing this scenario. In a load-deformation analysis, SIGMA/W automatically determines if the pore-water pressure at the ground surface of a newly activated region is positive. The buoyant unit weight is subsequently used to form the activation boundary condition. This procedure is not relevant in a consolidation analysis because the final pore-water pressure condition is unknown, meaning that the submergence condition cannot be detected *a priori*.

7.3.2 Submerged Excavation

In contrast to submerged construction (Section 7.3.1), submergence is not automatically detected when a material is deactivated. Deactivation of a region removes the total unit weight of the material, making it necessary to apply a hydrostatic pressure boundary condition so that the net effect is commensurate with removing the buoyant unit weight of the material (Figure 56).

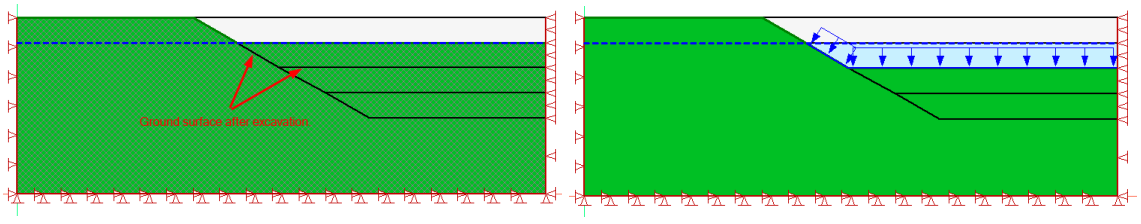

Figure 56. Hydrostatic pressure boundary applied to the new ground surface to model a submerged excavation (right).

7.4 Pore-water Pressure Changes

Pore-water pressure changes specified in a Load-Deformation analysis are accommodated by means of nodal force boundary condition, which is calculated as:

$$\boldsymbol{R} = \sum_{m} \int_{V^{(m)}} S_e \boldsymbol{B}^{(\boldsymbol{m})\boldsymbol{T}} \{m\} \delta u_w dV^{(\boldsymbol{m})} \qquad \text{Equation 228}$$

where $\{m\}^T = \{1 \quad 1 \quad 1 \quad 0 \quad 0 \quad 0\}$ and S_e is the effective degree of saturation (Equation 88). The following should be noted:

1. In an *In Situ* analysis, the pore-water pressure change δu_w is equal to the final pore-water pressures because the initial pore-water pressure is inherently zero for activated regions.
2. In a Load-Deformation analysis, the pore-water pressure change δu_w is calculated as the difference between the final and initial values. The pore-water pressure increment is ignored if the Response Type is Undrained (Section 3.6.1).
3. The effective degree of saturation (Equation 88) is calculated by numerically integrating the volumetric water content function over the change in negative pore-water pressure.
4. In an *In Situ* or Load-Deformation analysis, an increment or decrement in the pore-water pressure is fully realized ($\alpha = S_e = 1.0$; Equation 88) if a volumetric water content function is not defined (Equation 52).
5. A pore-water pressure increment could be negative or positive. The former leads to an increase in effective stress, while the latter produces a decrease in effective stress.

8 References

Atkinson, J.H. and Bransby, P.L., 1978. The mechanics of soils: an introduction to critical state soil mechanics. McGraw-Hill, London.

Atkinson, J.H., 2007. The mechanics of soils and foundations, 2d edition: Taylor & Francis, London.

Bathe, K.J., 2006. Finite element procedures. Prentice Hall, Pearson Education, Inc. U.S.

Been, K. and Jefferies, M.G., 1985. A state parameter for sands. Géotechnique, 35(2), pp.99-112.

Biot, M.A., 1941. General theory of three-dimensional consolidation. Journal of applied physics, 12(2), pp.155-164.

Britto, A.M. and Gunn, M.J., 1987. Critical state soil mechanics via finite elements. John Wiley & Sons, New York.

Budhu, M., 2011. Soil mechanics and foundations, 3rd edition. John Wiley & Sons Inc., New York.

Cudny, M. and Truty, A., 2020. Refinement of the Hardening Soil model within the small strain range. Acta Geotechnica, 15, pp.2031-2051.

Dafalias, Y.F., 1986. An anisotropic critical state soil plasticity model. Mechanics research communications, 13(6), pp.341-347.

Dafalias, Y.F., Manzari, M.T. and Papadimitriou, A.G., 2006. SANICLAY: simple anisotropic clay plasticity model. International Journal for Numerical and Analytical Methods in Geomechanics, 30(12), pp.1231-1257.

Dafalias, Y.F. and Taiebat, M., 2013. Anatomy of rotational hardening in clay plasticity. Géotechnique, 63(16), pp.1406-1418.

Dakshanamurthy, V., Fredlund, D.G. and Rahardjo, H., 1984, Coupled three-dimensional consolidation theory of unsaturated porous media. In Proceedings of the fifth international conference on expansive soils, Adelaide, Australia. pp. 99-103.

Day, R.A., 1990. Finite element analysis of sheet pile retaining walls. PhD thesis, Imperial College, University of London.

DiMaggio, F.L. and Sandler, I.S., 1971. Material model for granular soils. Journal of the Engineering mechanics Division, 97(3), pp.935-950.

Domenico, P.A. and Schwartz, F.W., 1998. Physical and chemical hydrogeology, 2nd Edition. John Wiley & Sons Inc., New York.

Duncan, J. M., Byrne, P. M., Wong, K. S., and Mabry, P., 1980. Strength, stress-strain and bulk modulus parameters for finite element analyses of stresses and movements in soil masses. Report No. UCB/GT/80-01., Univ. of Calif., Berkeley.

Frank, R., Bauduin, C., Driscoll, R., Kavvadas, M., Krebs Ovesen, N., Orr, T. and Schuppener, B. 2004. Designers' guide to EN 1997-1 Eurocode 7: Geotechnical design-General rules. Thomas Telford, London.

Fredlund, D.G. and Morgenstern, N.R., 1976. Constitutive relations for volume change in unsaturated soils. Canadian Geotechnical Journal, 13(3), pp.261-276.

Fredlund, D.G. and Rahardjo, H., 1993. Soil mechanics for unsaturated soils. John Wiley & Sons.

Hoek, E., Carranza-Torres, C. and Corkum, B., 2002. Hoek-Brown failure criterion-2002 edition. Proceedings of the fifth North American symposium, NARMS-TAC, Toronto, Ontario, Canada.

Janbu, N., 1963. Soil compressibility as determined by odometer and triaxial tests. Proceedings of the European Conference on Soil Mechanics and Foundation Engineering, Wissbaden, Germany, Vol. 1. pp.19-25.

Jefferies, M.G., 1993. Nor-Sand: a simple critical state model for sand. Géotechnique, 43(1), pp.91-103.

Jefferies, M. and Been, K., 2016. Soil liquefaction: a critical state approach. CRC press.

Jefferies, M., Shuttle, D. and Been, K., 2015. Principal stress rotation as cause of cyclic mobility. Geotechnical Research, 2(2), pp.66-96.

Kondner, R.L. and Zelasko, J.S. 1963. A hyperbolic stress-strain formulation for sands. Proceedings of the 2nd Pan-American Conference on Soil Mechanics and Foundation Engineering, Brazil, Vol. 1, pp.289-324.

Kondner, R.L., 1963. Hyperbolic stress-strain response: cohesive soils. Journal of the Soil Mechanics and Foundations Division, 89(1), pp.115-143.

Meyerhof, G.G., 1976. Bearing capacity and settlement of pile foundations. Journal of the Geotechnical Engineering Division, 102(3), pp.197-228.

Mitchell, J.K. and Soga, K., 1993. Fundamentals of Soil Behavior. John Wiley & Sons, Inc. New York.

Naylor, D.J., 1974. Stresses in nearly incompressible materials by finite elements with application to the calculation of excess pore pressures. International journal for numerical methods in engineering, 8(3), pp.443-460.

Pickering, D.J., 1970. Anisotropic elastic parameters for soil. Geotechnique, 20(3), pp.271-276.

PLAXIS., 2017. Material Models Manual, pp. 93-102.

Potts, D.M. and Zdravković, L., 1999. Finite Element Analysis in Geotechnical Engineering: Theory. Thomas Telford Ltd. London.

Potts, D.M. and Zdravkovic, L., 2012. Accounting for partial material factors in numerical analysis. Géotechnique, 62(12), pp.1053-1065.

Roscoe, K. and Burland, J.B., 1968. On the generalized stress-strain behaviour of wet clay. In J. Heyman and F.A Leckie (eds.), Engineering Plasticity (Cambridge: Cambridge University Press), pp.535-609.

Roscoe, K.H. and Schofield, A.N., 1963. Mechanical behaviour of an idealized 'wet' clay. Proceeding of the third European Conference on Soil Mechanics and Foundation Engineering. Wiesbaden, Germany, pp.47-54.

Rowe, P.W., 1962. The stress-dilatancy relation for static equilibrium of an assembly of particles in contact. Proceedings of the Royal Society of London. Series A. Mathematical and Physical Sciences, 269, pp.500-527.

Rowe, P.W., 1971. Theoretical meaning and observed values of deformation parameters for soils. Proceedings of the Roscoe Memorial Symposium, R. H. G. Parry, ed., Foulis, Henley on Thames, U.K., pp.143–194.

Sandler, I.S., Baladi, G.Y. and DiMaggio, F.L., 1976. Generalized cap model for geological materials. Journal of the Geotechnical Engineering Division, 102(7), pp.683-699.

Schanz, T., Vermeer, P.A. and Bonnier, P.G., 1999. The hardening soil model: formulation and verification. In Beyond 2000 in computational geotechnics, Balkema, Rotterdam, pp. 281-296.

Schmidt, B., 1966. Earth pressures at rest related to stress history. Canadian Geotechnical Journal, 3(4), pp.239-242.

Sheng, D., Gens, A., Fredlund, D.G. and Sloan, S.W., 2008. Unsaturated soils: from constitutive modelling to numerical algorithms. Computers and Geotechnics, 35(6), pp.810-824.

Schofield, A.N. and Wroth, P., 1968. Critical state soil mechanics, McGraw-Hill, New York.

Taylor, D.W., 1948. Fundamentals of Soil Mechanics: John Wiley and Sons. Inc., New York.

Tschuchnigg, F., Schweiger, H.F., Sloan, S.W., Lyamin, A.V. and Raissakis, I., 2015a. Comparison of finite-element limit analysis and strength reduction techniques. Géotechnique, 65(4), pp.249-257.

Tschuchnigg, F., Schweiger, H.F. and Sloan, S.W., 2015b. Slope stability analysis by means of finite element limit analysis and finite element strength reduction techniques. Part I: Numerical studies considering non-associated plasticity. Computers and Geotechnics, 70, pp.169-177.

Van Eekelen, H.A.M., 1980. Isotropic yield surfaces in three dimensions for use in soil mechanics. International Journal for Numerical and Analytical Methods in Geomechanics, 4(1), pp.89-101.

Vermeer, P.A. and De Borst, R., 1984. Non-associated plasticity for soils, concrete and rock. HERON, 29 (3), pp.1-64.

Wong, T.T., Fredlund, D.G. and Krahn, J., 1998. A numerical study of coupled consolidation in unsaturated soils. Canadian Geotechnical Journal, 35(6), pp.926-937.

Wood, D.M., 1990. Soil behaviour and critical state soil mechanics. Cambridge university press, Cambridge.

Wood, D.M., 2004. Geotechnical Modelling. Taylor & Francis Group, London.

Zienkiewicz, O.C. and Cormeau, I.C., 1974. Visco-plasticity—plasticity and creep in elastic solids—a unified numerical solution approach. International Journal for Numerical Methods in Engineering, 8(4), pp.821-845.

Zienkiewicz, O.C. and Naylor, D.J., 1973. Finite element studies of soils and porous media. Lect. Finite elements in continuum mechanics, pp.459-493.

Appendix I Formulation Fundamentals

There have been many thorough textbooks written on the subject of the finite element method (e.g. Bathe, 2006; Zienkiewicz and Taylor, 1989). The method is mathematically elegant and generalized; however, the details of the derivations and implementation strategies can be overwhelming. As such, the objective of this appendix is to provide a basic overview of the method with the goal being to provide a framework for discussing other topics such as discretization, the need for a constitutive model, and boundary conditions.

An analytical or closed-form solution of a physical problem always involves a few common steps. First, a set of mathematical equations must be derived to describe the physical process under consideration; commonly this takes the form of a partial differential equation (PDE) expressed in terms of some dependent variable. Next, the temporal and spatial limits of the problem (the domain over which the solution is sought) is defined and the appropriate boundary conditions which constrain the solution are defined. All parameters within the PDE must then be defined, including material properties used to characterize a particular material behavior. The solution of the PDE over the domain, given the specified material properties and subject to the selected boundary conditions, is the value of the dependent variable(s) as a function of position and time (in the case of a transient problem).

A similar solution pattern is applied in the case of the FEM. A conceptual model of a physical system is developed, the relevant physics (PDE) are selected, and the domain for the solution is defined. Just as in the analytical solution, the material properties across the domain must be specified and boundary conditions must be applied to constrain the solution. The FEM is selected as a solution method, rather than an analytical solution, likely due to complexities in geometry or material behavior. In order to overcome these complexities, the FEM, essentially, 'solves' the governing equation over smaller 'finite elements' which have well defined geometry and have a pre-selected shape to the distribution of the dependent variable across the element. The PDE across an individual element is then described in terms of the values of the dependent variable at the element nodes (fixed positions within the domain). Solving for the common set of nodal values for all elements at the same time then results in the solution of the dependent variable across the domain (i.e. in space and time).

As a consequence, the finite element method involves the following general steps:

1. Discretization of the domain into finite elements;
2. Selection of a function to describe how the primary variable(s) varies within an element;
3. Definition of a constitutive relationship;
4. Derivation of element equations;
5. Assembly of the global equations and modification for boundary conditions; and,
6. Solution of the global equations.

The solution of the global equations, which is a solution to a partial differential equation, provides a spatial and temporal description of the primary variable (e.g. temperature or displacement) within the domain.

I.1 Governing Equation

The governing partial differential equations for the stress-strain (Section 3.1) and water transfer (Section 3.7) formulations are derived from the requirement for energy or mass conservation, respectively. The governing equation for the stress-strain formulation is fundamentally an energy (work) conservation statement that is conveniently interpreted as statement of equilibrium. The governing equation for the water the transfer formulation, which is required for a coupled consolidation analysis, states that the total mass of a system is conserved and that the mass in a system can only change if mass crosses its boundaries.

I.2 Domain Discretization

The essence of the finite element method is embodied by discretization. Discretization is the process of subdividing a complex system into a number of finite elements. Figure 57 shows an 8-node quadrilateral and 6-node triangular element. Subdivision of the system into finite elements makes it possible to solve the governing equation by writing equations for each individual finite element. The term discretization implies approximation because the finite element method solves for the independent variable(s) at discrete points (the element nodes) within the domain. This produces a piece-wise approximation of a variable, which in reality is continuously distributed (e.g., x-displacement increment).

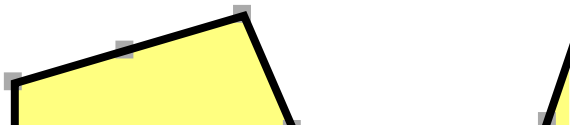

Figure 57. Examples of finite elements.

I.3 Primary Variable Approximation

A primary variable is calculated only at the element nodes. Thus, a shape or interpolation function is required to generate a continuously distributed approximation of the primary variable across the element. The interpolation function describes the spatial variation of the primary variable within the element and is used to estimate its value between the known data points (i.e., the nodes). Interpolation of a primary variable is given by:

$$u = \sum_{i=1}^{q} h_i u_i$$ Equation 229

where u is the is the primary value anywhere within the element, u_i is the value at nodal points, and h_i is the interpolating function for that particular node. A function of this form is written for all primary variables, if there are more than 1 (e.g., displacement in the direction of the three primary coordinates).

The mathematical descriptions of the interpolating functions are irrelevant to this discussion. The key concept is that the primary variable anywhere within the element is described based on nodal values.

I.4 Element Equations

The solution of a partial differential equation by the finite element method ultimately produces an equation for each element. Bathe (2006) provides an insightful and generalized derivation of the finite element equation for a static stress-strain problem, which can be written using matrix notation as:

$$\boldsymbol{K}^{(m)}\boldsymbol{U}^{(m)} = \boldsymbol{R}^{(m)} \qquad \text{Equation 230}$$

where $\boldsymbol{K}^{(m)}$ is the element characteristic (stiffness) matrix, $\boldsymbol{U}^{(m)}$ is the matrix of nodal unknowns, $\boldsymbol{R}^{(m)}$ is the nodal load vector for the element, which is sometimes called the forcing vector or the resultant vector. The matrix notation represents a set of simultaneous algebraic equations that can be solved using several techniques. The element characteristic matrix comprises several terms, including the constitutive matrix, $\boldsymbol{D}^{(m)}$, that is populated with the material properties. The finite element equation for a dynamic stress-strain problem takes the form:

$$\boldsymbol{M}^{(m)}\ddot{\boldsymbol{U}}^{(m)} + \boldsymbol{C}^{(m)}\dot{\boldsymbol{U}}^{(m)} + \boldsymbol{K}^{(m)}\boldsymbol{U}^{(m)} = \boldsymbol{R}^{(m)} \qquad \text{Equation 231}$$

The over dot indicates a time derivative of the primary variable (i.e. velocity), the double over dot indicates a second time derivative of the primary variable (i.e. acceleration), $\boldsymbol{M}^{(m)}$ is the element mass matrix, and $\boldsymbol{C}^{(m)}$ is the damping matrix. The mass matrix is calculated from the density of the material and the damping matrix can be calculated from the mass and stiffness matrix by means of Rayleigh damping assumptions. The first- and second-time derivative of the primary variable is related to the primary variable by means of direction integration methods (Bathe, 1996).

Although not revealed by this basic discourse, and regardless of the complexity of the final form of the equation, the element equation is in fact a perfect reflection of the conservation statement on which it was derived. In other words, it is possible to inspect the mathematical operations and recover the conservation statement, which in the case of a stress-strain analysis is static equilibrium (even if at discrete time intervals and including the effects of inertia and damping forces). Desai (1979) provides a more elementary derivation that lends clarity to the idea that the element equation is a perfect reflection of the conservation statement.

I.5 Global Equations

One of the most elegant aspects of the finite element method lies in Step 5: assembly of the global finite element equation. The element equations (Equation 231) are generated recursively for every element in the domain and then added to the global finite element equation:

$$\boldsymbol{K}\boldsymbol{U} = \boldsymbol{R} \qquad \text{Equation 232}$$

where $\boldsymbol{K}$ is the global characteristic matrix, $\boldsymbol{U}$ is the global assemblage of nodal unknowns, and $\boldsymbol{R}$ is the global load vector.

The assembly process is based on the law of compatibility or continuity. The assembly process can also be considered the final step required to obey the governing partial differential equation, which applies to the entire domain (i.e., not just one element). The global finite element equation satisfies the governing partial differential equation because it is the result of assembling the individual equations for a single element that were formulated to satisfy the governing PDE. The assembly procedure is analogous to the method of sections used to analyze the static equilibrium of a truss. Equilibrium of the entire system is ensured by satisfying static equilibrium for each member of the structure.

Assembly of the finite element equations requires material property and element geometry definitions. Conveniently, the discretization process produces a collection of elements and nodes with defined geometry, namely the Cartesian coordinates of all the nodes.

It is important to note that the global finite element equation shown above is essentially a set of 'n' equations where n is the number of nodes multiplied by the degrees of freedom. The $\boldsymbol{U}$ vector represents the 'n' primary variables and the $\boldsymbol{R}$ vector represents the nodal load vector. Consequently, the only way a solution can be sought for this set of linear equations is to have no more than 'n' unknowns; consequently, a value of the primary variable or the nodal load must be known (specified) at every node. The final step of the finite element procedure (Step 6) is specification of the physical constraints to the solution at all nodes (i.e., boundary conditions) in order to solve the global equations to obtain a spatial description of the primary variable(s).

Consider, for example, a simple domain in which the primary unknown is specified uniquely at two nodes on the left side and two nodes on the right side of the domain (Figure 58). Solution of Equation 231 subject to these boundary conditions produces the primary variable at all nodes at which the primary variable is unknown. Since the left and right-side nodes had a specified value of the dependent variable, the forces at these nodes is unknown; while, in the interior nodes the value of the dependent variable is unknown; however, to satisfy the conservation of energy (i.e. static equilibrium), the net of the forces (in all coordinate directions) at these nodes is zero. Subsequent assembly of Equation 232 produces the nodal forces at all nodes. The forces at the boundary nodes are non-zero because there is no adjacent element that apportions a forces with equal magnitude and opposite sign to cause cancellation.

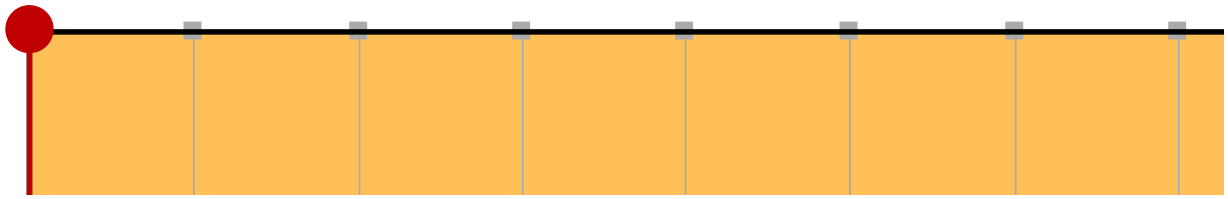

Figure 58. A simple finite element domain with boundary conditions on the left and right sides.

In summary, the finite element method is a procedure for solving a partial differential equation, which is a mathematical expression that governs the response of a physical system. Naturally, analysts seek to describe and analyze the behavior of these systems. The key aspects of the finite element method are:

1. The partial differential equation describing the behavior of a physical system can be solved, using the finite element method, by discretizing the domain into finite elements.
2. The process of discretization implies approximation; that is, the solution to the finite element equation provides the approximate spatial distribution of the primary variable at the nodes.
3. The derivation of the finite element equations is based on a single element. The final equation embodies the material properties and element geometry.
4. Using the principle of compatibility, these element equations are written recursively for every element in the domain and assembled into the global finite element equation.
5. The global finite element equation is solved subject to boundary conditions.

I.6 Constitutive Behaviour

A constitutive model links a secondary quantity (e.g., stress) to the primary variable (e.g., displacement). More specifically, problems involving mechanical energy transfer (i.e. static equilibrium) require a constitutive law that links incremental stress changes to incremental strain quantities. The soil models presented in Section 5 and the structural constitutive models presented in Section 6 are examples of constitutive relationships that govern the link between stress and strain increments. The constitutive models often comprise material properties and/or functional relationships (e.g. failure law, yield function and plastic potential) that are a function of the 'state' (i.e. stress and strains) of the material, which are directly or indirectly functions of the primary variable (i.e. displacement increments). The mathematical descriptions embodied by the constitutive model lead to various types of stress-strain behaviours such as linear or non-linear elasticity, elastic-(perfect) plasticity, strain hardening and strain softening.

I.6.1 Functional Relationships

Many of the constitutive models in GeoStudio require a functional relationship between a material property and some other parameter. For example, water hydraulic conductivity can be defined as a function of matric suction and the effective elastic modulus can be made to vary with either minor effective stress or mean effective stress. Functional relationships are defined by a data set that relates the property to a parameter. The software then represents the data by a computed functional relationship, $f(x)$ (e.g., polynomial spline, linear interpolation, step function), which is used by the solver.

The data points defining the functional relationship can be from a measured dataset or generated by published empirical or semi-empirical methods. In some cases, the software provides an estimation routine.

I.6.2 Add-ins

User-defined functional relationships, such as those mentioned in Section I.6.1, can be generated by an Add-In. An Add-In is compiled computer code called by the solver. A material function add-in returns a specific property (e.g., thermal conductivity) at every Gauss point within every element to which the material model is assigned to the solver. The add-in can comprise a functional relationship that is multi-variable, of any mathematical form, and dependent on another variable from the analysis being solved or from another analysis.

SIGMA/W also has the capacity to accept a User Defined Constitutive Model (UDCM). A UDCM add-in essentially must return to the solver a constitutive matrix $\boldsymbol{D}^{(m)}$ for assembling the global stiffness matrix $\boldsymbol{K}$ and the accumulated stresses at the end of an iterative displacement (strain increment). The add-in Software Developer Kit (SDK) provides additional information regarding the development of a UDCM.

I.7 Boundary Conditions

GeoStudio can be used to analyze a variety of field problems in order to define the state variable spatially within the domain. The state variable may be a vector or scalar, where a vector has both magnitude and direction (e.g., forces/stresses in SIGMA/W), while a scalar has only magnitude (e.g., total head in SEEP/W).

In the analysis of field problems, the values of the state variables are generally given on the boundaries. An example would be the total head along the ground surface of a reservoir impoundment or the vertical stress beneath a rigid foundation. Accordingly, these problems are called boundary value problems, where the solution within the domain depends on the conditions along the boundary of the domain (Bathe, 2006). A change in only one boundary value affects the entire solution.

I.7.1 Types

There are fundamentally three types of boundary conditions used in a finite element analysis:

1. First-type or Dirichlet boundary condition;
2. Second-type or Neumann boundary condition; and,
3. Third-type or Robin boundary condition.

Consider the global finite element equation (Equation 232) that comprises the global assemblage of nodal unknowns ($\boldsymbol{U}$) and the global load vector ($\boldsymbol{R}$). A first-type boundary condition specifies the primary unknown at a node and is used to populate the $\boldsymbol{U}$ vector. A second-type boundary condition is the spatial derivative of the primary variable normal to the boundary. In the case of scalar problems, this would be equivalent to applying a flux. Second-type boundary conditions are applied over an area and apportioned to nodes via numerical integration. These boundary values are used to populate the $\boldsymbol{R}$ vector. Finally, a third-type boundary condition specifies a nodal value directly in the global load vector. Table 22 summarizes the fundamental boundary conditions in each GeoStudio product, while Section 7 details boundary conditions unique SIGMA/W.

Table 22. Boundary condition types for each GeoStudio application.

Application	First-type	Second-type	Third-type
SEEP/W	Pore-water Total Head	Water Flux	Water Rate
TEMP/W	Temperature	Heat Flux	Heat Rate
AIR/W	Pore-air Total Head	Air Flux	Air Rate
CTRAN/W	Concentration	Mass Flux	Mass Rate
SIGMA/W	Displacement	Stress	Force
QUAKE/W	Displacement	Stress	Force

Boundary values can be defined as constants or functions. A constant boundary condition implies that the state of the boundary remains the same throughout the analysis. Functions are generally used in transient analyses to define the boundary-type as a function of time, but functions also have an important role in a SIGMA/W Load-Deformation or coupled analysis. Finally, it should be noted that even the most involved boundary conditions, such as the surface energy balance boundary in TEMP/W or the unit gradient boundary in SEEP/W, ultimately reduces to one of the three fundamental types. The surface energy balance boundary condition, for example, is a heat flux (second-type) boundary.

I.7.2 Add-ins

User-defined boundary conditions can be generated by an Add-In. A boundary condition add-in returns a specific value to the solver for every node (First or Third Type) or Gauss point (Second Type) within every element to which the boundary condition is applied. The add-in can comprise a functional relationship that is multi-variable, of any mathematical form, and may be dependent on another variable from the analysis being solved or from a different analysis.

I.8 Convergence

The assemblage of finite element matrices includes a global stiffness matrix $[K]$ that comprises a constitutive law $[D]$ that could vary with stress and/or strain. A commonly used numerical procedure for coping with the non-linearity of the constitutive law involves repeatedly solving the finite element equations subject to a residual load vector:

$$[K]^i\left(\{\Delta d\}^i\right)^j = \{\psi\}^{j-1} \qquad \text{Equation 233}$$

where the subscript j is the iteration number, the subscript i is the load step, $\{\psi\}$ is the vector of residual loads, and $\{\psi\}^0 = \{\Delta R\}$. The residual load vector is calculated as a difference between the externally incremental boundary loads $\{\Delta R\}$ and the incremental nodal forces $\{\Delta F\}$ that are consistent with the incremental stresses $\{\Delta\sigma\}$ calculated by the constitutive law. A difference arises because a constant constitutive stiffness matrix was assumed to assemble and solve the finite element equations, but in actuality the global stiffness matrix varies with stress and/or strain changes over the increment. Iteration continues until the maximum number of iterations is reached or the residual loads and iterative displacements are small. There are two techniques for settings the limits to the maximum allowable sizes of the residual loads and iterative displacements.

I.8.1 Relative Displacements\Residual Loads

A limit can be set on the relative displacements:

$$\frac{\left\|\left(\{\Delta d\}^i\right)^j\right\|}{\|\{\Delta d\}^i\|} < TOL \qquad \text{Equation 234}$$

and on the relative residual loads:

$$\frac{\|\{\psi\}^j\|}{\|\{\psi\}^{j=1}\|} < TOL \qquad \text{Equation 235}$$

where $\left(\{\Delta d\}^i\right)^j$ is the vector of displacement increments for the current iteration j, $\{\Delta d\}^i$ the vector of displacement increments for the load step i, $\{\psi\}^j$ the vector of residual loads for the current iteration j, and $\{\psi\}^{j=1}$ the vector of residual loads from the first iteration. The tolerance (TOL) defines the maximum allowable relative displacements or relative residual loads for a load step. The required tolerance can be dependent on various aspects of the simulation and the size of the domain. A tolerance TOL of 5.0E-06 to 5.0E-05 is generally required to obtain an accurate solution.

I.8.2 Unbalanced Energy

The maximum allowable sizes of the residual loads and iterative displacements can be embodied by a single relative quantity referred to as the relative unbalanced energy:

$$\frac{\left|\left(\{\psi\}^j\right)^T\left(\{\Delta d\}^i\right)^j\right|}{|(\{\psi\}^{j=1})^T\{\Delta d\}^i|} < TOL \qquad \text{Equation 236}$$

where $\left(\{\Delta d\}^i\right)^j$ is the vector of displacement increments for the current iteration j, $\{\Delta d\}^i$ the vector of displacement increments for the load step i, $\{\psi\}^j$ the vector of residual loads for the current iteration j, $\{\psi\}^{j=1}$ the vector of residual loads from the first iteration. The tolerance (TOL) defines the maximum

allowable relative unbalanced energy for a load step. The required tolerance can be dependent on various aspects of the simulation and the size of the domain. A tolerance TOL of 1.0E-06 to 1.0E-05 is generally required to obtain an accurate solution.

I.8.3 Stress Update Algorithm

The residual load vector for each iteration $\{\psi\}^j$ is calculated as the difference between the externally applied incremental boundary loads $\{\Delta R\}^i$ and the incremental nodal forces $\{\Delta F\}^i$ that are consistent with the incremental stresses $\{\Delta\sigma\}^i$ calculated by the constitutive law (refer to Section 3.4). Various strategies are employed to integrate the constitutive equations (Section 5) along an incremental strain path $\left\{\Delta\varepsilon^j\right\}^i$ produced by the iterative nodal displacements $\left(\{\Delta d\}^i\right)^j$ (Potts and Zdravković, 1990). Regardless of the scheme that is employed, the integration is done numerically, resulting in successive estimates of the incremental stresses $\{\Delta\sigma\}$ that must be equal within a tolerance. The local error $\{E\}$ in the successive estimates of the stress increments is calculated as (Potts and Zdravković, 1990):

$$\{E\} = \frac{1}{2}(\{\Delta\sigma_2\} - \{\Delta\sigma_1\}) \qquad \text{Equation 237}$$

where $\{\Delta\sigma_2\}$ and $\{\Delta\sigma_1\}$ are two successive estimates of the stress increments. The relative error is calculated as:

$$R = \frac{\|\{E\}\|}{\|\{\sigma + \Delta\sigma\}\|} \leq STOL \qquad \text{Equation 238}$$

where $STOL$ is a user defined tolerance which is typically in the range of 1.0E-02 to 1.0E-05. The denominator of Equation 238 comprises the accumulate stresses $\{\sigma + \Delta\sigma\}$, which are calculated from the average of two successive estimates of the stress increments $\{\Delta\sigma\}$:

$$\{\Delta\sigma\} = \frac{1}{2}(\{\Delta\sigma_2\} + \{\Delta\sigma_1\}) \qquad \text{Equation 239}$$

The integration schemes adapts the differentials of the strain increment until $R \leq STOL$ or a minimum allowable differential is encountered. In the later case, $R > STOL$ and the $\{\Delta\sigma\}^i$ could be inaccurate. Sensitivity studies can be used to determine if $STOL$ is significantly small enough to obtain an accurate solution without unnecessarily increasing computational time.

I.8.4 Verifying Convergence

The general techniques for verifying convergence include:

1. Plotting graphs of the relative quantities calculated by Equation 236 or Equation 234 and Equation 235 versus the iteration count;

2. Plotting a graph of the number of iterations for each load.
3. Identifying global rupture zones by means of perfectly plastic points and contours of deviatoric strain.

Convergence settings for various types of analyses are illustrated in the example files provided in the Learning Resources.

Appendix II Numerical Modelling Best Practice

Burland (1987), in his seminal Nash Lecture, presented the idea that modelling is an integral part of geotechnical engineering practice (Figure 59). Geotechnical engineering involves defining the geological and hydrogeological system, understanding the constitutive behaviour of the material, and modelling. All three components are interlinked by experience. In the context of this discussion, the most prominent feature of this conceptualization is the fact that modelling is an integral part of the engineering process.

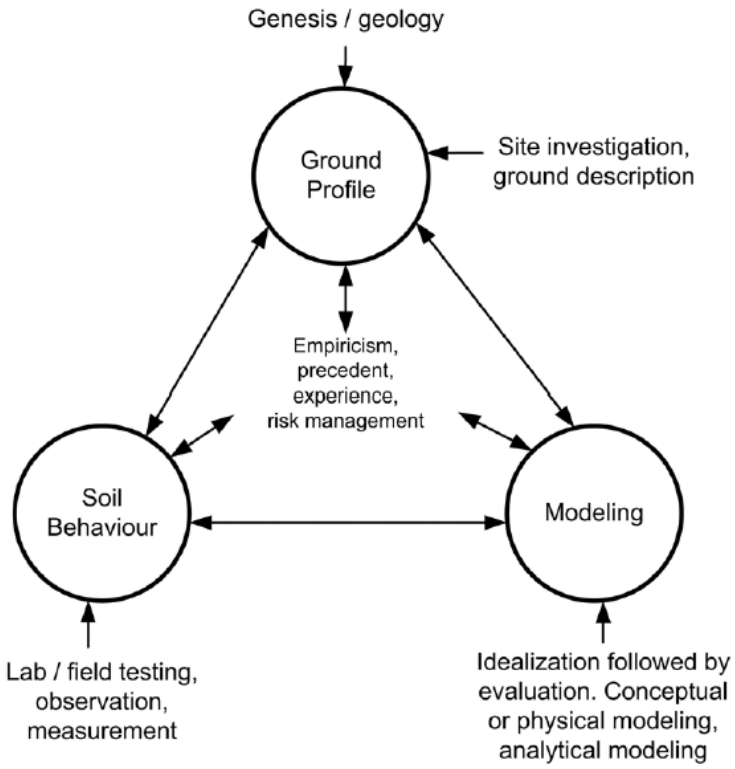

Figure 59. Burland Triangle (Ground Engineering, 1996).

Barbour and Krahn (2004) built upon the ideas of Burland (1996) and defined modelling as "the process by which we extract from a complex physical reality an appropriate mathematical reality on which we can base a design. The role of the numerical model is simply to assist us in developing the appropriate mathematical abstraction." Stated another way, a mathematical model is a simplified representation of a complex reality based on our understanding of the physical system.

This definition of modelling endorses the idea that modelling is about process, not prediction. The greatest strength of modelling is to develop the appropriate mathematical abstraction of a complex physical system. In turn, engineers are able to develop a sound understanding of the physical system and exercise better engineering judgment. The maximum benefit can only be achieved if modelling is incorporated into the entire problem solving process (Figure 59).

A finite element analysis is just one type of numerical model that is less restrictive and complimentary to other types of numerical models, such as analytical and graphical solutions. The primary reason for invoking a finite element analysis is to cope with various complexities, including: a) intricate geological and hydrogeological settings; b) nontrivial physical processes; c) multiple and competing design alternatives and economic implications; and, d) a decision making process that can be made difficult by the need to communicate ideas to regulators and the general public.

Barbour and Krahn (2004) elaborate on some of the intricacies of each of these complexities. It is perhaps worth highlighting that engineering problems involving the earth are particularly complicated because natural systems exhibit extreme spatial variability, complex and sometimes unquantifiable material behavior, incongruent temporal and spatial scales, and in many cases, physical processes that are not fully understood. Barbour and Krahn (2004) illustrate this realization with a poignant case history involving a comparison of various numerical simulations to measured deflections of a structurally supported retaining wall for a deep excavation. None of the predictions of the lateral deflections were accurate, or true to the measurements.

The reasons for the inaccuracies were related in part to the aforementioned complexities and conceptualization errors, and in part to numerical problems. One can conclude that, in general, predicting the exact response of a physical system is not feasible because it is impossible to reproduce all of the detail present in the physical problem in even the most refined mathematical model. Prediction should therefore not be the primary objective of numerical modelling. The encouraging aspect of the case history was that the overall patterns of the physical behaviour were adequately simulated. As such, the numerical solutions provided an appropriate basis for design.

This short discourse brings us back to the key advantage of numerical modelling: the process of numerical modelling enhances engineering judgement and provides a basis for understanding complicated physical processes. The process of modelling is iterative and comprises at least four essential components:

1. Define the modelling objective and develop a conceptual model of the problem;
2. Determine the appropriate theoretical models (i.e., physics) that describe the key physical processes;
3. Develop a mathematical description of these processes and verify that it provides an accurate solution; and,
4. Interpret the results in relation to the observed physical reality.

Defining the modelling objective and developing a conceptual model are the most important steps in the modelling process. Again, this is where numerical modelling can be exceptionally useful, as the process forces the analyst to incorporate information on site geology and hydrogeology, laboratory information, and any other pertinent information (e.g., construction sequencing) into a conceptual model of the problem. The conceptual model must also be linked with the objectives of the modelling exercise.

Determining the appropriate theoretical model involves gaining an understanding of the underlying physics and the constitutive behavior governing material behavior. From the analysts' perspective, this is tantamount to ensuring that the formulation of the numerical model is representative of the physical process being explored. This understanding is manifest in a model's development through the definition of the boundary conditions and material properties. These components often change as the analyst iterates through the modelling process; refining the model as the understanding of the physical system evolves and additional field and laboratory data becomes available.

Eventually, the conceptual and theoretical models are committed to a mathematical solution. In a finite element analysis, the geometry of the problem domain is drawn, material properties are defined, and boundary conditions are applied to the domain. A verification of the solution is completed to ensure convergence, appropriate spatial and temporal discretization, and correct application of physics (perhaps via comparison with an analytical solution). A simple to complex mantra must be adopted, so that the analyst can be confident in the numerical solution.

Finally, the results are interpreted within the context of the physical reality. The most fundamental question that should always be asked is: are the results reasonable? Stated another way, interpretation of the results should be done with a skeptical mind-set. The results of the finite element analysis could be compared with field monitoring data and should always be interpreted in light of the information used to develop the conceptual and theoretical models.

A numerical model will likely evolve repeatedly over the course of the modelling process as the analyst is challenged by interpreting the results. Increasing complexity of the conceptual model may be required; however, speculating on high degrees of complexity in the absence of supporting observations is not just problematic, it makes the remaining parts of the process more difficult or impossible. The best numerical models include just enough complexity for the mathematical abstraction to reasonably approximate the physical reality.

Appendix III SANICLAY Formulation

The SANICLAY model (Dafalias *el al.* 2006) in general stress space is defined by the mean effective stress, p' (Equation 14) and the deviatoric part of the effective stress tensor, $\boldsymbol{s}$, which is defined by:

$$\mathbf{s} = \boldsymbol{\sigma}' - p'\mathbf{I} \qquad \text{Equation 240}$$

where $\boldsymbol{\sigma}'$ is the effective stress tensor and $\mathbf{I}$ is the identity tensor.

The model adopts a non associated flow rule, meaning that the yield function, F, and the plastic potential function, P, are different. The yield function can be written as:

$$F(\{\sigma'\},\{k\}) = \frac{3}{2}(\mathbf{s} - p'\boldsymbol{\beta}):(\mathbf{s} - p'\boldsymbol{\beta}) - \left(N^2 - \frac{3}{2}\boldsymbol{\beta}:\boldsymbol{\beta}\right)p'\left(p'_0 - p'\right) \qquad \text{Equation 241}$$

where p'_0 presents the isotropic hardening variable, that is the value of p' at $\mathbf{s} = p'\boldsymbol{\beta}$. Here $\boldsymbol{\beta}$ is a stress-ratio-type tensor variable defining the rotation of the yield surface, and N defines the shape of yield surface. The symbol : implies the trace of the product of two tensors.

The plastic potential function is expressed by:

$$P(\{\sigma'\},\{m\}) = \frac{3}{2}(\mathbf{s} - p'\boldsymbol{\alpha}):(\mathbf{s} - p'\boldsymbol{\alpha}) - \left(M^2 - \frac{3}{2}\boldsymbol{\alpha}:\boldsymbol{\alpha}\right)p'\left(p'_\alpha - p'\right) \qquad \text{Equation 242}$$

Similar with the yield function, $\boldsymbol{\alpha}$ is a stress-ratio-type tensor variable defining the rotation of the plastic potential surface with p'_α the value of p' at $\mathbf{s} = p'\boldsymbol{\alpha}$.

The critical stress-ratio M in Equation 242 will be interpolated between its values M_c and M_e by means of the Lode angle θ; according to:

$$M = \Theta(\theta, c)M_c; \quad \Theta(\theta, c) = \frac{2c}{(1+c) - (1-c)cos(3\theta)}; \quad c = \frac{M_e}{M_c} \qquad \text{Equation 243}$$

where

$$cos(3\theta) = \sqrt{6}\, trace\, \mathbf{n}^3 \qquad \text{Equation 244}$$

in which $\mathbf{n}$ is the unit vector defined by the tensor $(\mathbf{r} - \boldsymbol{\alpha})$ as:

$$\mathbf{n} = \frac{\mathbf{r} - \boldsymbol{\alpha}}{\|\mathbf{r} - \boldsymbol{\alpha}\|} = \frac{\mathbf{r} - \boldsymbol{\alpha}}{\sqrt{(\mathbf{r} - \boldsymbol{\alpha}):(\mathbf{r} - \boldsymbol{\alpha})}} \qquad \text{Equation 245}$$

where $\mathbf{r}$ indicates the deviatoric stress- ratio tensor as:

$$\mathbf{r} = \mathbf{s}/p' \qquad \text{Equation 246}$$

The basic components of the model proposed by Dafalias and Taiebat (2013) are similar to what was described above in terms of the yield and plastic potential functions, expect that the shape of the yield surface (i.e., N) is not constant in the new version of the model but depends on the direction of the loading through the value of the Lode angle (see Equation 243). In addition, according to Dafalias and Taiebat (2013), the orientation of both yield and plastic potential surfaces is assumed to be identical (i.e., $\boldsymbol{\alpha} = \boldsymbol{\beta}$).

The hardening rule of the SANICLAY model involves the evolution of its state parameters (i.e., p'_0, $\boldsymbol{\alpha}$ and $\boldsymbol{\beta}$). As suggested by Dafalias *el al.* (2006) in a general stress space:

$$\dot{p}'_0 = \langle L \rangle \bar{p}'_0 = \langle L \rangle \left(\frac{1+e}{\lambda-\kappa}\right) p'_0 \operatorname{tr}\left(\frac{\partial g}{\partial \boldsymbol{\sigma}}\right) \qquad \text{Equation 247}$$

$$\dot{\boldsymbol{\alpha}} = \langle L \rangle \bar{\boldsymbol{\alpha}} = \langle L \rangle \left(\frac{1+e}{\lambda-\kappa}\right) C \left(\frac{p'}{p'_0}\right)^2 \left|\operatorname{tr}\left(\frac{\partial g}{\partial \boldsymbol{\sigma}}\right)\right| \left[\frac{3}{2}(\mathbf{r} - x\boldsymbol{\alpha}) : (\mathbf{r} - x\boldsymbol{\alpha})\right]^{\frac{1}{2}} (\boldsymbol{\alpha}_b - \boldsymbol{\alpha}) \qquad \text{Equation 248}$$

$$\dot{\boldsymbol{\beta}} = \langle L \rangle \bar{\boldsymbol{\beta}} = \langle L \rangle \left(\frac{1+e}{\lambda-\kappa}\right) C \left(\frac{p'}{p'_0}\right)^2 \left|\operatorname{tr}\left(\frac{\partial g}{\partial \boldsymbol{\sigma}}\right)\right| \left[\frac{3}{2}(\mathbf{r} - \boldsymbol{\beta}) : (\mathbf{r} - \boldsymbol{\beta})\right]^{\frac{1}{2}} (\boldsymbol{\beta}_b - \boldsymbol{\beta}) \qquad \text{Equation 249}$$

where the scalar multiplier is defined as:

$$L = \frac{3(\mathbf{r} - \boldsymbol{\beta}) : \dot{\mathbf{s}} + \left(N^2 - \frac{3}{2}\mathbf{r} : \mathbf{r}\right)\dot{p}'}{3(\mathbf{s} - p'_0\boldsymbol{\beta}) : \bar{\boldsymbol{\beta}} + \left(N^2 - \frac{3}{2}\boldsymbol{\beta} : \boldsymbol{\beta}\right)\bar{p}'_0} \qquad \text{Equation 250}$$

and the bounding deviatoric tensors are:

$$\boldsymbol{\alpha}_b = \sqrt{2/3} M \mathbf{n}_x; \qquad \mathbf{n}_x = \frac{\mathbf{r}/x - \boldsymbol{\alpha}}{[(\mathbf{r}/x - \boldsymbol{\alpha}) : (\mathbf{r}/x - \boldsymbol{\alpha})]^{\frac{1}{2}}} \qquad \text{Equation 251}$$

$$\boldsymbol{\beta}_b = \sqrt{2/3} N \mathbf{m}; \qquad \mathbf{m} = \frac{\mathbf{r} - \boldsymbol{\beta}}{[(\mathbf{r} - \boldsymbol{\beta}) : (\mathbf{r} - \boldsymbol{\beta})]^{\frac{1}{2}}} \qquad \text{Equation 252}$$

In the new version of the SANICLAY model (Dafalias and Taiebat 2013), the evolution of the size of the yield surface (i.e., p'_0) is the same as Equation 247. The orientation of the yield and plastic potential surfaces, however, changes as follows:

$$\dot{\boldsymbol{\alpha}} = \langle L \rangle c p_{at} \frac{p'}{p'_0} (\boldsymbol{\alpha}_b - \boldsymbol{\alpha}) \qquad \text{Equation 253}$$

where

$$\boldsymbol{\alpha}_b = \sqrt{2/3}\frac{M}{z}\left\{1 - \exp\left[-s\frac{|\eta|}{M}\right]\right\}\mathbf{n}_r; \qquad \mathbf{n}_r = \frac{\mathbf{r}}{[\mathbf{r}:\mathbf{r}]^{\frac{1}{2}}}; \qquad |\eta| = \left[\frac{3}{2}\mathbf{r}:\mathbf{r}\right]^{\frac{1}{2}} \qquad \text{Equation 254}$$

To prevent the excessive rotation of the yield and plastic potential surfaces, Dafalias and Taiebat (2013) propose a remedy on Equation 254 that involves the substitution of $|\eta|$ with $|\eta| - \langle|\eta| - \xi M\rangle$. In this correction procedure, ξ is a model parameter and have a maximum allowable value as follows:

$$\xi \leq -\frac{1}{s}\ln\left[1 - z\frac{\min(M_e, N_e)}{M_c}\right] \qquad \text{Equation 255}$$